University of Oviedo

DOCTORAL THESIS

Ph.D. PROGRAM IN ENERGY AND PROCESS CONTROL

CFD-based optimization of an axial impulse turbine for a twin topology

By

Hosam Mohamed Abdul-hasieb

A thesis Submitted in Fulfillment of the Requirements for the Degree of
Doctor of Philosophy in the
Energy Department, Area of Fluid Mechanics

Supervised by:

Prof. José González Pérez Prof. Bruno Pereiras García

Polytechnic School
Gijon, 2023

Universidad de Oviedo

DOCTORAL THESIS

PROGRAMA DE DOCTORADO EN ENERGÍA Y
CONTROL DE PROCESOS

Optimización de una turbina de impulso axial con topología gemela usando técnicas de simulación numérica

Por

Hosam Mohamed Abdul-hasieb

Una Tesis Presentada en Cumplimiento de los Requisitos para el Título de Doctor en el Departamento de Energía, Área de Mecánica de Fluidos

Directores:

Prof. José González Pérez Prof. Bruno Pereiras García

Escuela Politécnica de Gijón, Asturias. 2023

University of Oviedo

DOCTORAL THESIS

Ph.D. PROGRAM IN ENERGY AND PROCESS CONTROL

CFD-based optimization of an axial impulse turbine for a twin topology

By

Hosam Mohamed Abdul-hasieb

Supervised by:

Prof. José González Pérez Prof. Bruno Pereiras García

2023

Declaration

I hereby declare that the contents and organization of this dissertation constitute my own original work and do not compromise in any way the rights of third parties, including those relating to the security of personal data.

Hosam M. Abdul-hasieb

2023

I would like to dedicate this thesis to those who have an unwavering belief in our ability to overcome challenges and achieve success, even in the face of daunting obstacles. Your unwavering support and belief in our potential have been instrumental in this journey. I am grateful for your faith in our abilities. Together, we have defied the odds and reached new heights. It is with heartfelt gratitude and appreciation that I dedicate this thesis to you.

I would also like to acknowledge and honor the memory of my dear friend,

***Dr. Ahmed Madani**,*

who stood by my side and supported me on the way, both in his presence and even in his absence. His unwavering dedication and friendship will always be remembered and cherished.

Acknowledgment

My greatest debt of gratitude is owed to my supervisors **Prof. José González Pérez** and **Prof. Bruno Pereiras García.** Who gave me the initial stimulus for this study and offered all help that made it possible.

I am deeply grateful to the Arab Academy for Science and Technology and Maritime Transport (AASTMT) for the support. This support is greatly acknowledged.

And my special thanks should be expressed to my professors and colleagues at the AASTMT-Smart Village branch, for their support and help in all my work.

Special thanks should be also expressed to **Dr. Paresh Halder** and **Dr. Khairy Elsayed** for their appreciated help in completing this work.

Last and not least, all thanks, gratefulness, and appreciation should be expressed to my family, as no words can thank their effort, patience, and support in all time. especially to those who set me on the path of life, made me calm, and took care of me until I became old, my **MAMA.**

Abstract

The ocean holds a lot of energy and using it to meet our rising energy needs is a reasonable solution. Despite its widespread availability, wave energy converter commercialization is hampered by insufficient technology of Wave Energy Converters (WEC). The oscillating water column (OWC) is widely used to harness the energy of ocean waves. One essential element of this system is the air turbine, which operates as the power take-off unit (PTO), converting pneumatic power into mechanical energy. The turbine represents the most intricate component within the system and is typically designed in either an axial or radial configuration. To meet the increasing energy requirements of the future, this work is focused on the optimization of a previously designed unidirectional axial turbine for twin systems. An optimization algorithm, based on CFD results, was used to improve the performance of the system. The automated design optimization process was divided into three stages: Design of Experiments, Response Surface and optimization.

A parametric turbine geometry was generated by modifying geometric characteristics to control the design of guide vanes and rotor blades. This approach allowed for greater flexibility in designing and adjusting both the rotating and stationary components.

By altering the values of specific parameters, such as the guide vane radius (R_g), guide vane angle (α_1), rotor tip radius (R_t), pressure side radius on the rotor (R_r), and trailing edge relative angle of the rotor (β_2), the optimized design achieved a remarkable increase in efficiency for a single axial flow impulse turbine. Using the response surface method, an automated optimized analysis was conducted to explore a vast design space consisting of 51 different cases for the turbine geometry. Through this process, the optimal turbine geometry was determined.

In this study, a comprehensive analysis was conducted to evaluate the influence of each parameter on the performance of the turbine. The analysis was carried out systematically,

following a three-step approach. The first step involved performing a steady performance analysis by comparing the torque coefficient, input coefficient, and efficiency of the initial geometry with the optimized geometry. Second, the loss distribution of the fluid flow throughout the entire domain was analyzed for both the initial and optimized geometry, the third step focused on studying the unsteady turbine performance by analyzing the unsteady efficiency and the blocking efficiency. For both the initial and optimized geometry

This study made a notable contribution by demonstrating a 28% improvement in efficiency at low flow coefficients compared to the initial design. Furthermore, it is evident that the optimized geometry, particularly at lower flow coefficients, resulted in a significant reduction in energy losses within the rotor domain. Specifically, at flow coefficients of Ø=0.25 and Ø=0.50, the optimized geometry displayed a reduction in energy losses by approximately 66.2% and 22.3%, respectively. The unsteady performance evaluation optimized the turbine's peak efficiency to be 12% higher than that of the initial turbine peak. The blocking efficiency experienced a modest improvement of approximately 2% across the entire range of flow coefficient amplitudes.

Key words: OWC, Axial turbine, Twin turbines, Design optimization, Efficiency maximization, Computational fluid dynamics.

Table of Contents

List of Figures

List of Tables

Nomenclature

Abbreviations

CCD	Central Composite Design	---------
CFD	Computational Fluid Dynamics	---------
DE	Design Exploration	---------
DOE	Design of Experiments	---------
MOGA	Multi-Objective Genetic Algorithm	---------
OWC	Oscillating Water Column.	---------
RANS	Reynolds-Averaged Navier-Stokes	---------
RMS	Root Mean Squared	---------
RS	Response Surface	---------
RSO	Response Surface Optimization	---------
SMM	Sliding Moving Nesh technique	---------
WEC	Wave Energy Converters	---------

Symbols

A_r	Turbine flow passage area at rR	mm ^{2}
b	Blade height	mm

C_A	Input power coefficient	Dimensionless
C_T	The torque coefficient	Dimensionless
l	Blade chord length	mm
P_{max}	Pressure amplitude of the OWC oscillations	Pa
ΔP	Total pressure drops	Pa
Q_{Total}	Volumetric flow rate	m^3/sec
Q_{max}	Peak flow rate of the OWC oscillations	m^3/sec
R_g	Radius of the guide vane	mm
r_R	Mean radius of the rotor	mm
R_r	Radius of the pressure side on the rotor	mm
R_t	Radius of rotor tip	mm
t	Time of the OWC oscillations	sec
t_{max}	Maximum thickness of the rotor	mm
T	The period of the OWC oscillations	sec
T_o	Torque	N.m
U_r	Blade speed	m/s
V_a	Air velocity at r_R	m/s
z	Number of blades	Dimensionless

Greek Symbols

Ø	Flow coefficient	Dimensionless
α	Absolute flow angle	Degree
β	Relative flow angle	Degree
η	Turbine efficiency	Dimensionless
ρ	Air density	kg/m³
ω	Angular velocity of rotor	rad/sec
Φ	Unsteady flow coefficients	Dimensionless

Subscripts/superscripts Indexes

rot.	Rotor blade
N.S	Non steady
*	Solid blade/guide vane angle

Chapter 1

INTRODUCTION

1.1 Preface

Today, energy is a vital component of our society, powering our cars, homes, and industries. The consumption of energy has a significant effect on the environment. Understanding the various types of energy sources and their applications is of great importance to ensure the availability of the energy needed to meet the world's growing needs. This chapter will provide a brief overview of the field of turbomachines, as the OWC being studied belongs to this category. I will discuss the classification of turbines, the different types of energy sources, and energy consumption patterns.

1.2 Fluid machine

A fluid machine is a mechanical device that transforms the energy contained within a fluid into mechanical energy, or conversely, converts mechanical energy into fluid energy. The energy contained within a fluid mass manifests in different forms, including potential, kinetic, and intermolecular energy. Mechanical energy is usually transmitted by the rotating shaft. Hydraulic machines, on the other hand are those that use liquid. In order to categorize these machines, they can be divided into distinct groups based on two fundamental criteria (Dixon, 2005).

1.2.1 Classification based on direction of energy conversion.

The process of energy conversion in a fluid machine can be classified into two broad categories, namely, turbine and pump. A turbine is a device that converts the kinetic, potential, or intermolecular energy possessed by the fluid into the mechanical energy of a rotating member. On the other hand, a pump, compressor, fan, or blower is a machine that transfers mechanical energy from moving parts to a fluid, resulting in an increase in its stored energy through an increase in either its pressure or velocity.

1.2.2 Classification based on the principle of operation.

Fluid machines can also be classified based on their principle of operation as positive displacement machines or rotodynamic machines. Positive displacement machines function by changing the volume of a specific amount of fluid within the machine. This physical displacement of the boundary of a fluid mass as a closed system is achieved through the reciprocating motion of a piston within a cylinder while entrapping a certain amount of fluid in it. Such machines are commonly known as reciprocating machines, and they can either produce mechanical energy (reciprocating engine) or develop energy in the fluid from mechanical energy (reciprocating pump or reciprocating compressor).

In contrast, rotodynamic machines operate based on the principles of fluid dynamics and require relative motion between the fluid and the moving part of the machine. These machines typically consist of a rotating element, such as a rotor or impeller, made up of several vanes or blades, and a fixed part known as the stator. The impeller is responsible for the change in the

angular momentum of the fluid, which imparts torque to the rotating member, making it the heart of rotodynamic machines(Turbomachines).

1.3 Turbomachinery

Turbomachines are essential devices in many industries that are used for energy conversion in various forms. They facilitate the transfer of energy between a moving fluid and rotating or stationary components of the machine through hydrodynamic forces. These machines engage in dynamic energy exchange between the rapidly moving fluid and one or more rotating elements, leading to alterations in the pressure and momentum of the fluid. This mechanical transfer of energy into or out of the turbomachine enables its operation. Among the different types of turbomachines are centrifugal pumps and compressors, which are capable of generating significant power or creating substantial head/pressure. (Turton, 1984).

Turbomachines consist of main components that enable their functioning. These components include a rotating element with vanes, one or more stationary elements responsible for directing the flow and converting energy, an input/output shaft, and, if applicable, a housing. The rotating element, also referred to as the rotor, runner, or impeller, interacts with the fluid, exchanging momentum to facilitate energy transfer. The stationary element, known as the guide blade or nozzle, may not be present in all turbomachines. Depending on the specific application, the presence of an input shaft, output shaft, or both may be necessary. Power-transmitting turbomachines serve the purpose of transferring power from an input shaft to an output shaft, similar to the function of a clutch-plate gear drive in a car.

Power-absorbing turbomachines encompass a range of devices, including mixed-flow, axial-flow, and centrifugal pumps, fans, and blowers, as well as power-generating devices including steam, gas, and hydraulic turbines. Fluid couplings and torque converters are examples of power-transmitting turbomachines. In the case of turbomachines with housing, it serves to constrain fluid flow, ensuring it follows the desired paths for energy transfer and utilization. However, the housing does not directly participate in the energy conversion process. The presence or absence of a housing distinguishes between enclosed and extended turbomachines. Turbomachines can also be classified based on various characteristics, such as the compressibility of the fluid and the flow path within the machine. In the upcoming section

there will be a discussion on the classification of these turbine types.(Ingram, 2009; Peng, 2008; Venkanna, 2009)

1.3.1 Classification according to the compressibility of the fluid passing through them

Turbomachines can be categorized based on the compressibility of the fluid that flows through them. The two main categories are compressible fluid turbomachines and incompressible fluid turbomachines. Compressible fluid turbomachines experience changes in fluid density with changes in pressure and include gas turbines, steam turbines, and compressors. In contrast, incompressible fluid turbomachines maintain a constant fluid density during the energy exchange process and include pumps and water turbines. (Earl Logan, 1993).

1.3.2 Classification according to the fluid flow path across the blades

The fluid flow path across blades can be used to determine the type of turbines that are suitable for different applications. There are three main types of turbines that are commonly used in the power generation industry: radial, axial, and mixed.

Centrifugal or radial turbines are machines in which the fluid enters the impeller chamber through radial vanes Fig. 1.1, which rotate. As a result, centrifugal forces draw the fluid towards the center, and the energy of the fluid and its pressure increase during this operation.

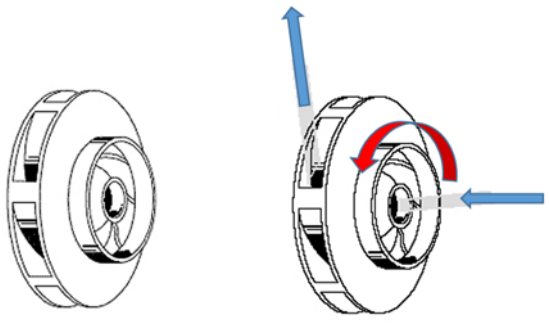

Fig. 1.1: Radial flow impeller. (Engineersedge, 2012a)

Axial turbines are machines in which the fluid path is parallel to the axis of the machine Fig. 1.2. The Kaplan turbine and some water pumps are among these turbomachines.

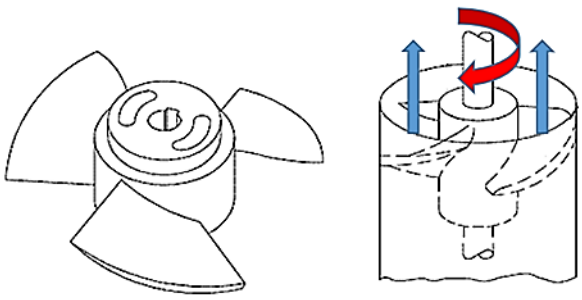

Fig. 1.2: Axial flow impeller. (Engineersedge, 2012b)

Mixed-flow turbines are machines in which the pathway of the fluid contains both radial and axial components Fig. 1.3. For example, the modern Francis turbine and some pumps are of the mixed type.

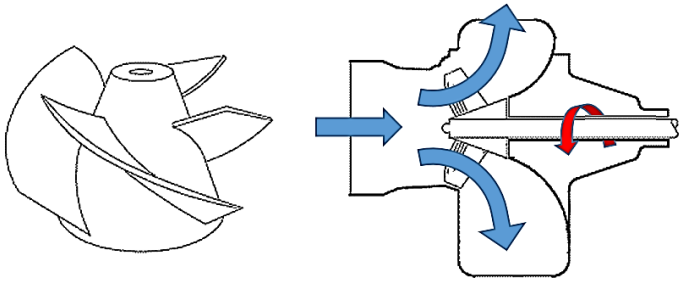

Fig. 1.3 : Mixed flow impeller. (Engineersedge, 2012c)

In addition, the radial and mixed-flow impellers can be classified as open, semi-open, and closed type as shown Fig. 1.4

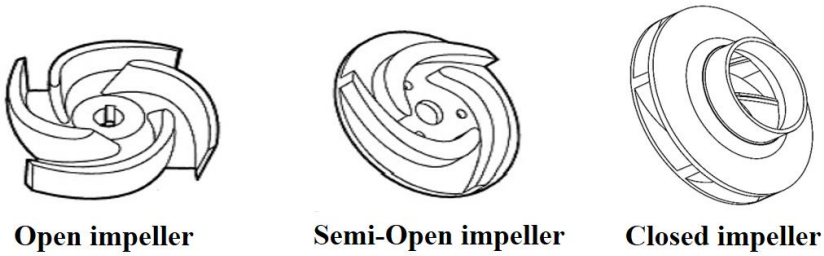

Fig. 1.4 : Types of impeller. (Flexachem, 2020)

1.3.3 Classification according to how the static pressure changes

Based on this criterion, turbomachines are classified into two types: impulse turbines and reaction turbines Fig. 1.5.

a. Reaction Turbines

In reaction turbines, the static pressure of the fluid changes as it passes through the rotor. This means that some of the pressure energy of the fluid is converted into kinetic energy, and some of it is converted into potential energy. The rotor in a reaction turbine is designed to create a force that acts on the fluid, and this force causes a change in the direction of the fluid flow. The change in direction of the fluid flow results in a change in pressure and velocity, which allows for the transfer of energy between the fluid and the rotor.

One example of a reaction turbine is the Kaplan turbine Fig. 1.6. The Kaplan turbine is commonly used for hydroelectric power generation in low-head, high-flow applications. In this type of turbine, the rotor has a series of blades that are adjustable. The fluid enters the turbine and passes over the blades, which are angled to create a force on the fluid. As the fluid passes over the blades, it changes direction, and this causes a change in pressure and velocity. The fluid then leaves the turbine with a lower pressure and a high velocity.

b. Impulse Turbines

In impulse turbines, the static pressure of the fluid remains constant as it passes through the rotor. This means that the pressure energy of the fluid is converted entirely into kinetic energy as it passes through the rotor. The rotor in an impulse turbine is designed to create a jet of fluid that moves in the same direction as the rotor's rotation. The fluid jet impinges on a stationary blade, which redirects the fluid flow by 180 degrees. This results in a change in the direction of the fluid flow, and the fluid leaves the rotor with a high velocity and a low pressure.

One example of an impulse turbine is the Pelton turbine Fig. 1.6. The Pelton turbine is commonly used for hydroelectric power generation. In this type of turbine, a jet of water is directed onto the blades of the rotor, which has a series of cups or buckets. The water jet hits the cups and is redirected, and the momentum of the water causes the rotor to rotate. The

water then leaves the turbine with a lower pressure and a high velocity. The Pelton turbine is efficient because it allows for the transfer of a large amount of energy between the fluid and the rotor.

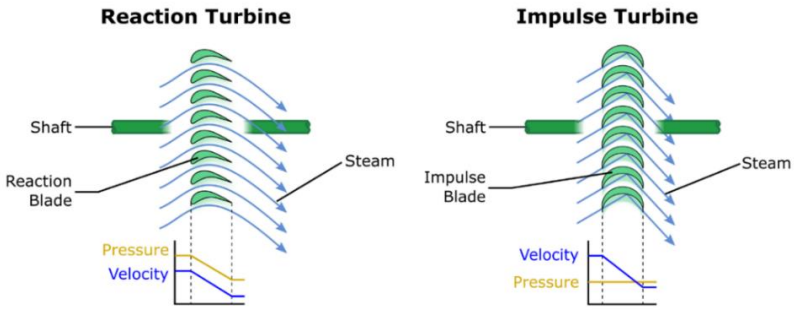

Fig. 1.5 : Reaction and impulse turbines blades. (Savree, 2019)

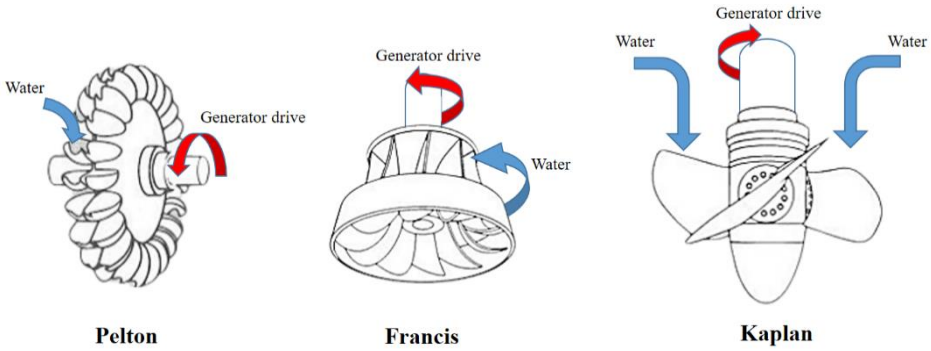

Fig. 1.6 : Types of hydro turbines.

1.3.4 Classification according to the speed at which the rotor rotates

A low-speed machine is a type of turbine that's commonly used in industrial processes such as oil and water pumping. These turbines are capable of operating at rotor speeds below 500 rpm, making them particularly suitable for power generation facilities and refineries. Their simplicity in design and large size contributes to their versatility, rendering them ideal for various of applications.

This type of turbine is ideal for applications that require a high flow rate. However, it's not ideal for those that require high pressure. In addition, they require a huge amount of space and are No suggestions not well-suited for areas with limited room.

Medium-speed machines, characterized by rotor speeds ranging from approximately 500 to 3,000 rpm, and is commonly used in the marine and aviation industries for power generation and propulsion purposes .

Unlike their low-speed counterparts, medium-speed turbines are more complicated in design, necessitating meticulous manufacturing processes. As a result, they tend to be more expensive than low-speed turbines.

High-speed turbines are characterized by rotor speeds greater than 3,000 rpm and are extensively employed in jet and gas turbine engines These machines are known for their complexity and substantial cost. They demand precise manufacturing techniques and are constructed using exceptional materials like nickel and titanium.

They're known to have high efficiency due to their capability to operate at high speeds and handle high temperatures and pressures making them valuable assets in sectors such as chemical manufacturing and petroleum refining. The combination of increased efficiency, compact design, and expanded power output positions high-speed turbines as pivotal components in driving the global adoption of renewable and sustainable energy solutions. (Seppo A. Korpela, 2019)

1.3.5 Classification according to the specific speed

The specific speed of a turbomachine is defined as the speed at which a geometrically similar machine would operate if it had the same specific speed coefficient and the same head coefficient. The specific speed is given by the following formula:

$$n_S = \omega \frac{Q^{1/2}}{(g\ H)^{3/4}} \tag{1.1}$$

where **ω** is the rotational speed, **Q** is the flow rate, and **H** is the head.

Turbomachines can be classified into three main categories based on their specific speed:

Low specific speed turbomachines: These are machines with a specific speed of less than 10. They are generally used for low-flow rate applications, such as small pumps and fans. The impeller diameter of these machines is relatively large compared to the flow rate.

Medium-specific speed turbomachines: These are machines with a specific speed between 10 and 100. They are used for medium flow rate applications, such as centrifugal pumps and compressors. The impeller diameter of these machines is moderate compared to the flow rate.

High-specific speed turbomachines: These are machines with a specific speed greater than 100. They are used for high-flow rate applications, such as propellers and large turbines. The impeller diameter of these machines is relatively small compared to the flow rate.

The specific speed also affects the design of the impeller. Low-specific speed machines require a thicker and wider impeller blade, while high-specific speed machines require a thinner and narrower blade.

Turbomachines may be further classified into additional categories:

1.3.6 Classification according to the working medium

Turbomachines can be classified into the following categories based on the working medium: Gas turbines, Steam turbine, Hydraulic turbines and Wind turbines

1.3.7 Classification according to the position of turbine main shaft

Turbomachinery can also be classified based on the position of the rotating shaft into two types: vertical and horizontal-axis turbines Fig. 1.7.

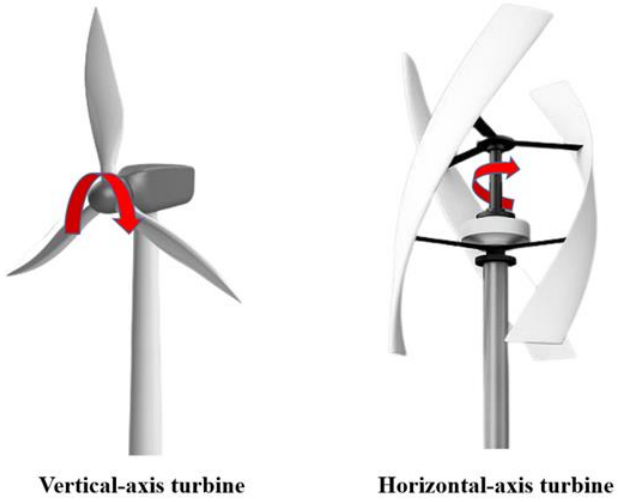

Fig. 1.7 : Orientation of rotation in vertical and horizontal-axis turbines.

1.4 Energy resource and consumption

Energy is one of the most fundamental resources for human survival, development, and progress. As the world population grows and economies expand, the demand for energy increases. Energy resources are sources of power that are used to generate electricity, heat, and perform other essential functions in everyday life. This section will discuss the various types of energy resources, their properties and characteristics, and the advantages and disadvantages of each. (Brown, 2002; Wiser, 2000)

1.4.1 Fossil Fuels

Fossil fuels are the most common type of energy resource used today. These resources are formed from the remains of dead plants and animals that have been buried for millions of years. They include coal, oil, and natural gas. Fossil fuels are non-renewable resources, meaning they are finite and will eventually be depleted. Fossil fuels are also the largest source of greenhouse gas emissions, contributing to global warming and climate change.

- Coal is a black or brownish-black sedimentary rock that is primarily composed of carbon. Coal is mined from the ground and then burned to generate electricity. The burning of coal releases carbon dioxide, sulfur dioxide, and nitrogen oxides into the atmosphere, which contributes to air pollution and climate change. Coal mining can also

have significant environmental impacts, including soil erosion, water pollution, and habitat destruction.

- Oil is a liquid fossil fuel that is extracted from underground reservoirs. Oil is primarily used to produce gasoline and diesel fuel for transportation. Oil spills can devastate the environment, including harm to marine life and damage to ecosystems. The burning of oil also releases greenhouse gases into the atmosphere.

- Natural gas is a gaseous fossil fuel that is primarily composed of methane. Natural gas is often used for heating and cooking, and it is also used to generate electricity. The burning of natural gas produces less greenhouse gases than coal or oil, but it is still a significant contributor to climate change. The extraction of natural gas can also have significant environmental impacts, including the release of methane into the atmosphere and contamination of groundwater.

1.4.2 Renewable Energy Sources

Renewable energy sources are resources that are replenished naturally and can be used indefinitely. These sources include solar, wind, hydroelectric, geothermal, and biomass energy.

- Solar energy is generated from the sun's rays, which are converted into electricity through the use of solar panels. Solar energy is a clean and renewable resource, and it produces no greenhouse gas emissions. However, the production of solar panels can have significant environmental impacts, including the release of greenhouse gases during manufacturing and the use of hazardous materials.

- Wind energy is generated by the movement of air across wind turbines. Wind energy is a clean and renewable resource, and it produces no greenhouse gas emissions. However, wind turbines can have significant impacts on wildlife and their habitats, and they can also be noisy and visually intrusive.

- Hydroelectric energy is generated from the flow of water through turbines. Hydroelectric energy is a clean and renewable resource, and it produces no greenhouse

gas emissions. However, the construction of dams and reservoirs can have significant environmental impacts, including habitat destruction and alteration of waterways.

Although energy consumption is a vital component of growth and development, its impact on the environment and society has significant implications. By understanding how energy is distributed across different sectors, one can gain a deeper understanding of how consumption affects sustainable growth. This section looks into the distribution of energy in different sectors, providing a sector-by-sector analysis of global consumption, as well as the implications of these data.

The International Energy Agency (IEA), noted that by 2050, global energy consumption will increase by almost 50%. The Fig. 1.8 shows an analysis based on the available data for the largest end-uses of energy for nineteen IEA countries including Australia, Austria, Canada, Czech Republic, Finland, France, Germany, Hungary, Japan, Italy, Korea, Luxembourg, New Zealand, Poland, Portugal, Spain, Switzerland, the United Kingdom, and the United States, the analysis in 2019.

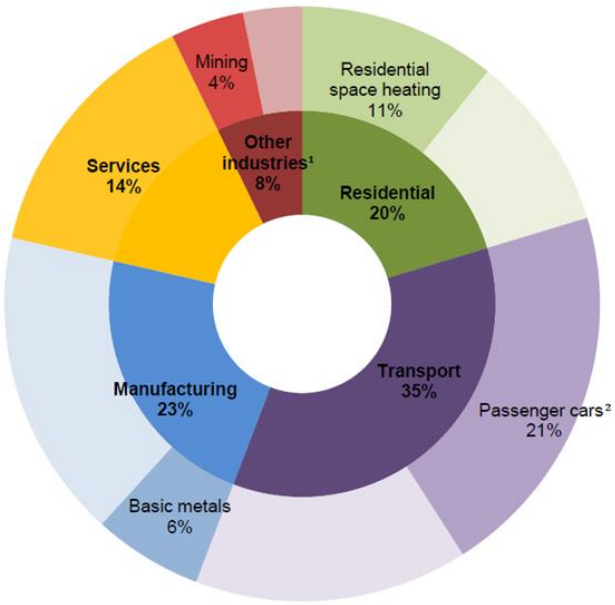

Fig. 1.8 : Global energy consumption. (Energy Agency, 2021)

Over the years, there has been a steady rise in the global demand for energy, making it crucial to comprehend its utilization. This section will explore the proportion of energy dedicated to electricity generation compared to other energy applications on a global scale.

According to the International Energy Agency (IEA), electricity production accounted for 20% of the world's energy consumption in 2020, marking an increase from 15% in 2000. The agency predicts that this percentage will continue to grow due to escalating demand. When contrasted with other energy uses, electricity consumption holds the second-largest share of global energy consumption, trailing only transportation.

In 2020, transportation accounted for 32% of global energy consumption, while industry and buildings each contributed 24%. Additionally, other energy sources made up 5% of the overall energy consumption.

The distribution of energy consumption for electricity generation varies across different regions. For example, in North America and Europe, approximately 40% of energy consumption is attributed to electricity generation. In contrast, in Asia, it constitutes approximately 50% of the overall energy used. This disparity can be attributed to factors such as population density and economic development in each country.

Considering the various energy sources utilized in the generation of electricity in 2020, fossil fuels, including coal, oil, and natural gas, accounted for over 60% of global power generation. Renewables, such as solar, wind, and geothermal energy, followed closely at around 29%, while nuclear power contributed 8%. It's worth noting that the energy mix also differs across regions. Fig. 1.9

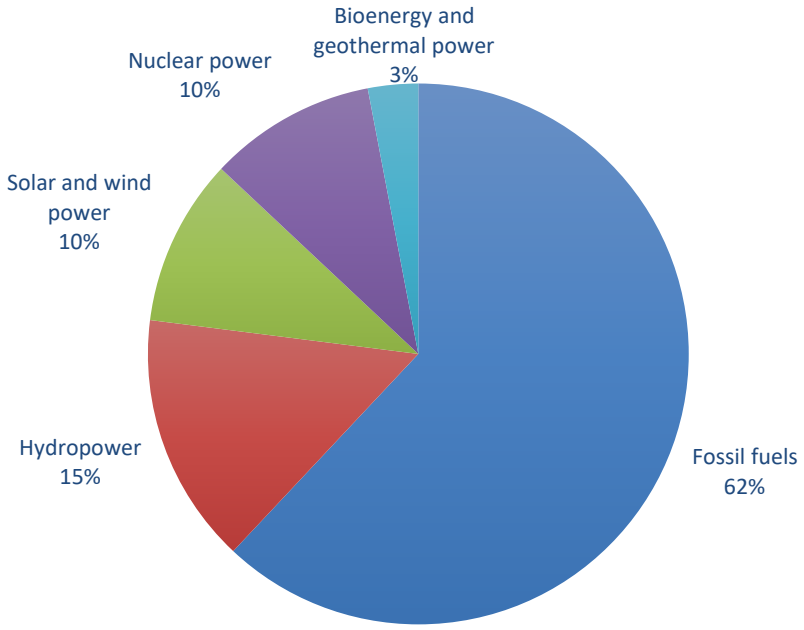

Fig. 1.9 : Global share of renewable energy in electricity generation -2021 (Energy Agency, 2021)

Governments have also implemented various programs aimed at promoting research and development of new technologies for exploiting renewable energy resources such as hydropower, solar, wind, bioenergy and geothermal.

In 2022 (Fig. 1.10), Asia once again dominated the addition of new capacity, accounting for approximately 60% of the total. Their renewable capacity increased by 174.9 GW, reaching 1.63 TW, which represents 48% of the global total. The majority of this increase occurred in China, which saw a surge of 141 GW. Europe and North America also experienced growth with an increase of 57.3 GW (+8.8%) and 29.1 GW (+6.3%), respectively. Meanwhile, Africa steadily expanded with an increase of 2.7 GW (+4.8%), slightly higher than last year. The Oceania region also experienced steady growth, growing by 5.2 GW (+10.6%), mainly due to Australia's expansion experienced growth with an increase of 57.3 GW (+8.8%) and 29.1 GW (+6.3%), respectively. Meanwhile, Africa steadily expanded with an increase of 2.7 GW (+4.8%), slightly higher than last year. The Oceania region also experienced steady growth, growing by 5.2 GW (+10.6%), mainly due to Australia's expansion.

Additionally, South America continued its upward trend with an expansion of 18.2 GW (+7.4%). The Middle East also saw its highest expansion on record, with 3.2 GW of new capacity commissioned in 2022 (+12.8%).

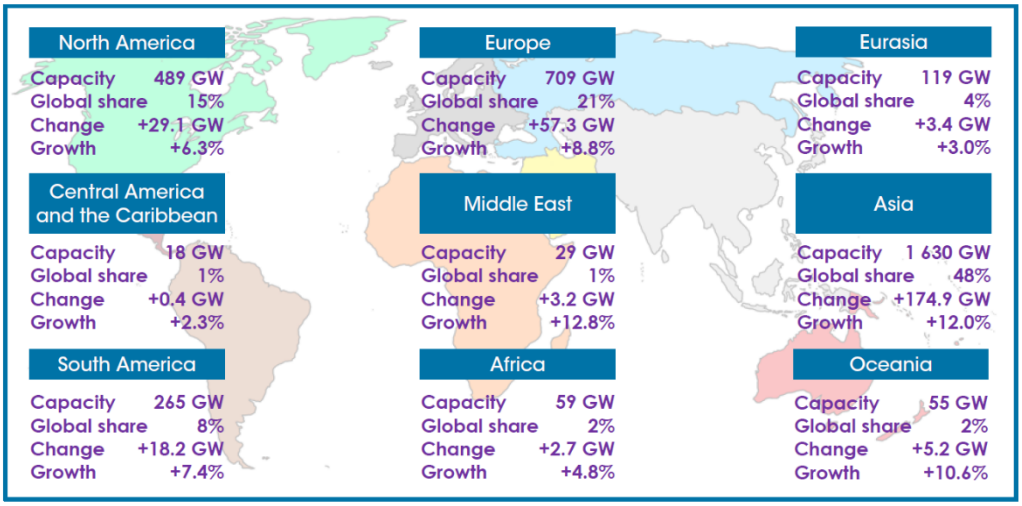

Fig. 1.10 : Renewable generation capacity by region -2022 (IRENA, 2023)

At the end of 2022 (Fig. 1.11), global renewable generation capacity amounted to 3372 GW. Renewable hydropower accounted for the largest share of the global total, with a capacity of 1256 GW. Solar and wind energy accounted for most of the remainder, with total capacities of 1053 GW and 899 GW respectively. Other renewable capacities included 164 GW.

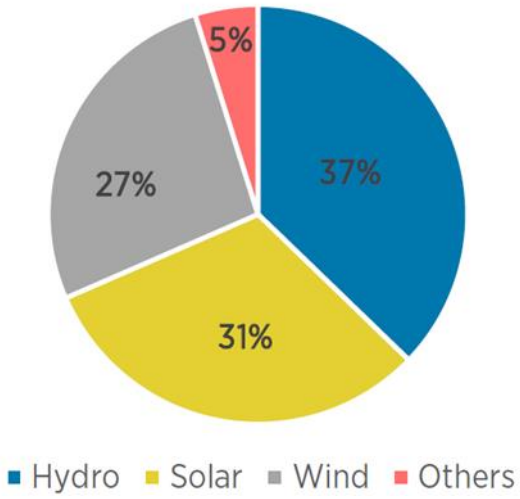

Fig. 1.11 : Renewable generation capacity by energy source -2022 (IRENA, 2023)

One of the sources of hydropower is ocean wave energy. The ocean waves are a significant source of green energy, characterized by high power density and ideal for harvesting. When compared to other renewable energy sources, wave power emerges as notably more potent.

Wind waves, seismic disturbance waves, and tsunamis are just a few of the many waves that can be in the water. Wave energy is the energy generated by these sorts of waveforms. The impact of solar power on the Earth's atmosphere drives these powerful winds, which then transfer their energy to the ocean.

In the process of converting solar energy into wind energy, the power density increases. The Sun's power density is around 0.170 kilowatts per square meter. At a location 15^{o} north or south of the Equator, the wind power density is around 0.580 kilowatts per square meter. Wind waves, on the other hand, have a power density of over 8 kilowatts per square meter. Despite the various obstacles that prevent the development of wind waves, their energy potential has been acknowledged for a long time. The first attempts to harness this resource were made during the 18th century. However, technology development only started in 1973 following the oil crisis. (Iglesias & Garcia Novo, 2013)

New patents related to technology continue to emerge. This is due to the increasing number of people who are interested in the development of wave energy. The public and private sectors are also contributing to the research and development of this promising technology. Therefore, the various organizations and individuals involved in the research and development of wave energy must continue to support and promote this process. To ensure that the exploitation of wave energy is carried out in a sustainable way, the environmental impact of its activities must be considered.

1.5 Definitions and background

1.5.1 Wave energy

Oceans and seas occupy two-thirds of Earth's surface, and there are tremendous amounts of energy in various forms (waves, tides, salinity, etc.). Winds blowing across water produce the development of waves. The magnitude of the waves produced by the wind will vary depending on the speed and duration of the movement. Wave-harvesting devices can

subsequently harvest kinetic energy from this motion. Around 2 TW of ocean wave energy is believed to be generated globally (Rodrigues, 2008) In the past few decades, various technological advancements have allowed for the development of new ways to harness this energy.

The potential of wave energy as a renewable energy source with many applications is compelling. Power plants, desalinization plants, and water pumps can all benefit from their use. It was first proposed in 1799 by a French explorer named Edouard Girard to use wave power to tap into the energy of the ocean, (López et al., 2013).

Following the first patent for wave power conversion, thousands of innovations related to this technology were invented. During the 1970s, the oil crisis highlighted the need for new energy sources. Several researchers set out to develop replacement energy sources for powering electronic devices. Masato Masuda is one of the most prominent individuals who has contributed to the development of wave energy technology. He is well known for his work on several systems that provide energy for use in navigation lights. Some of these include the prototype of the KAIMEI, a large barge that served as a testing facility (Falcão & Henriques, 2016).

1.5.2 Advantages and disadvantages of wave energy

Wave energy is a renewable and eco-friendly alternative to fossil fuels that can be used to reduce greenhouse gas emissions. It can also be used to conserve space and avoid the harmful effects of global warming. One of the main advantages of wave energy is that it is renewable, as it can be produced continuously. It can also be used for extended periods than wind and solar power due to its continuous nature. Also, wave farms can be tiny, generating tremendous power. Despite its pure nature, wave energy still has some disadvantages. In addition to being detrimental to the environment, it poses a hazard to the aquatic life nearby. Large equipment is installed near the seafloor to gather wave energy. These platforms can disturb the seafloor and negatively affect the habitats of various sea life.

The locations of wave energy power plants are also important. They must be close to populated areas and coastlines to benefit everyone. However, these areas are also crucial for

commercial and cargo ships. Due to the presence of these facilities in the ocean, people must now consider other locations for them.(Maehlum, 2013)

1.5.3 Wave energy converters (WECs)

WECs is a term that refers to devices that convert the kinetic and potential energy from the waves into useful electrical or mechanical energy. These devices can be used for various applications, such as powering marine vessels and desalination facilities. The following section will discuss the various types of wave energy converters that are now available, in addition to introducing their general principles with some examples.

1.6 WECs classification

There are currently several technologies in the development stage of their exploitation. Although each of these is promising, it's not yet clear which technology will be most prevalent in the future. WECs can be classified according to the following criteria.

1.6.1 Classification according to the installation site

According to this criterion, two types of WECs can be distinguished:

a. *Location of the device to the distance to the coast (Fig. 1.12). (Titah-Benbouzid & Benbouzid, 2015)*

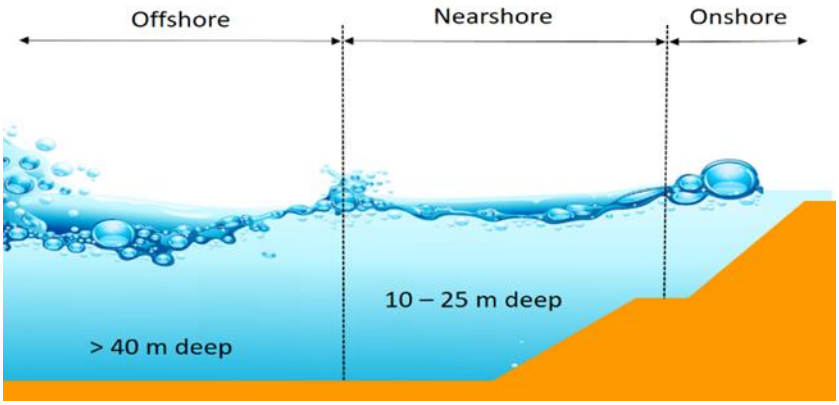

Fig. 1.12: WECs locations.

i. Onshore

Shore-mounted devices are generally easier to maintain and close to the utility network. However, they are disadvantaged due to the waves' reduced power as they travel through shallow water. This makes them less effective at capturing and converting the energy from the waves.

Also, wave energy converters are not ideal for mass production due to their location. Site-specific requirements such as geology and shoreline geometry are also considered to ensure they can operate efficiently.

ii. Nearshore

This device is typically placed in shallow water. They are usually attached to the seabed, which provides a suitable stationary base for their operation. Although nearshore devices can be placed in shallow water, they can't harvest the full potential of the waves due to their limited power.

iii. Offshore

Although offshore devices are commonly placed in deep water, there is still not a clear definition of what deep water is. However, a depth of more than 40m can be defined. An advantage of offshore WECs is that they can harvest more energy from the waves due to the higher energy content they possess. Unfortunately, building and maintaining offshore devices can be very challenging due to their higher energy content. Despite this, it's still believed that deep water offers a more stable and resilient environment for the development of wave energy technology.

b. Position of the device related to the sea level (Fig. 1.13).

i. Floating

One of the main characteristics of offshore WECs is that it floats on the sea surface. This type of device takes advantage of the movement of the waves by using floating components. These components are connected to the platform using rows of floating buoys.

ii. Resting on seabed

Although submerged WECs are relatively less common, their design and maintenance are complex. This makes them an ideal choice when dealing with harsh environmental conditions. Also, since all the equipment is submerged, they can perform maintenance work underwater, which is beneficial when dealing with storms. However, the manufacturing process of this type of device is not as easy due to its size and complexity.

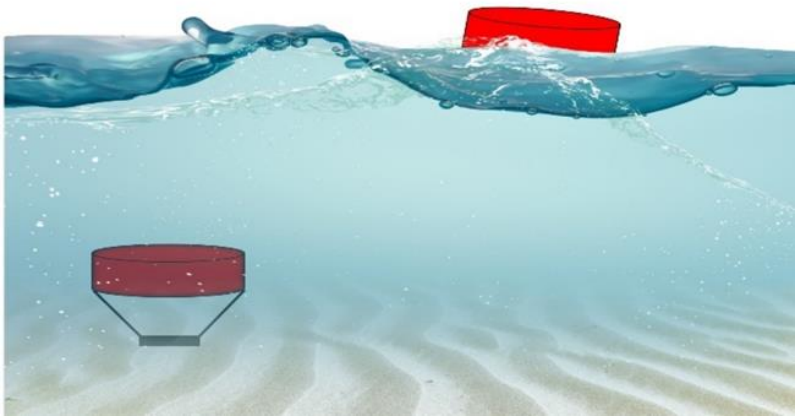

Fig. 1.13: WECs related to the sea level.

1.6.2 Classification according to the energy capture system

Two categories result from this criterion:

a. Devices that fluid drive the turbine –water, oil or air.

b. Devices that use wave energy to move a mechanism (whether linear or rotational)

1.6.3 Classification according to the position of the capture system, relative to the wave direction

This criterion distinguishes between two types of WECs (Lehmann et al., 2017):

a. Point absorbers.

Due to their modest size in relation to the wavelength, these systems perform regardless of wave direction (Fig. 1.14).

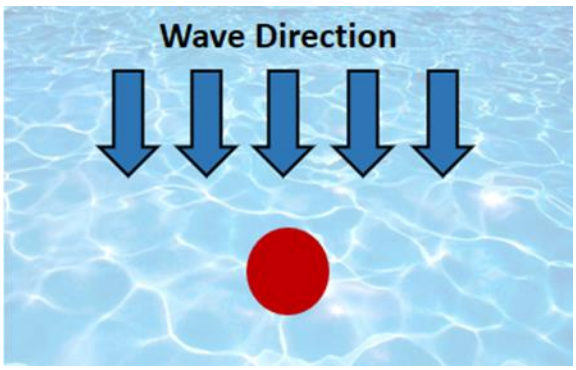

Fig. 1.14: The Point absorbers

b. Line absorbers

i. Attenuator

These systems are designed to capture the energy of the incoming wave by adapting their shape to the wave profile (Fig. 1.15). Since they have a parallel length to the wave direction, they can extract energy from the waves. (Xie & Zuo, 2013).

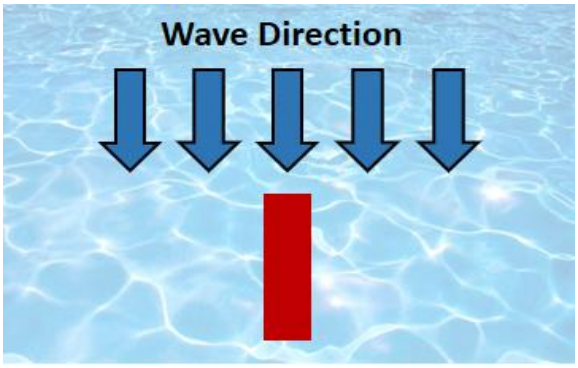

Fig. 1.15: The Attenuator

i. Terminator

These systems are perpendicular to the wave propagation direction. The sea wave hits the device and transfers its energy (Fig. 1.16).

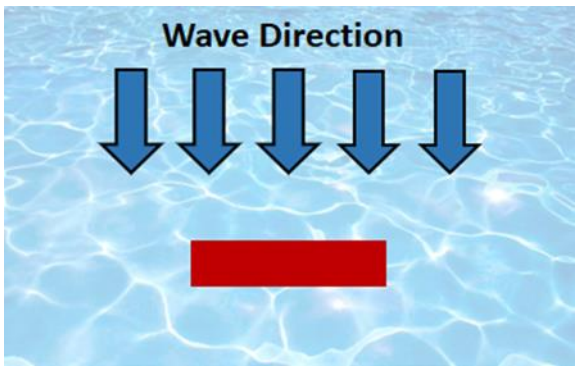

Fig. 1.16: The Terminator

1.6.4 Classification according to the principle of operation

There are eight categories within this classification:

a. Wave-activated bodies

Attenuators are devices designed to align with the direction of the incident wave (Fig. 1.17). The energy is extracted as the waves flow along the gadget's length. Usually, these devices have long multi-segment structures. Each segment is a floating pontoon that's connected by a joint. The movement of the attenuators is used to propel a hydraulic piston, which then turns a connected generator. They must be positioned precisely in the incident wave's direction to function correctly. Usually, an attenuator's front mooring mechanism is attached to the device.(Guedes Soares et al., 2012).

Fig. 1.17: Schematic diagram of Attenuators

b. Bulge wave

A typical example of a point-based energy generator is the one shown in the Pelamis sea snake system (Fig. 1.18). This device has dual semi-submerged cylinders connected by a pair of hinges (Qiao et al., 2020).

Fig. 1.18: Schematic diagram of Bulge Wave

c. Submerged pressure differential

A submerged point absorber uses the difference between the pressure between the trough and the crest of the wave above it. This allows the compression of the air inside its cylindrical chamber. When the crest of the wave passes over the top surface of the device, the pressure within the chamber increases, which then moves the top cylinder down. As the water pressure inside the device drops, the upper cylinder rises. This type of device can be used for various applications, such as reducing the visual impact of the device (Fig. 1.19). However, it's important to note that maintaining the device can be a bit challenging. (Casagranda, 2015).

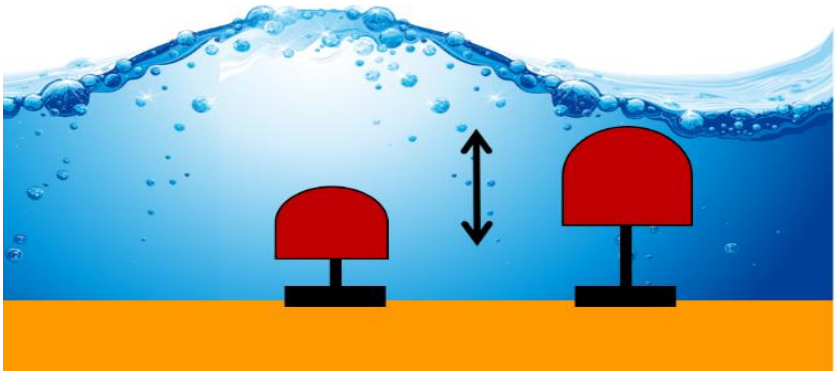

Fig. 1.19: Schematic diagram of submerged absorber

d. Oscillating wave surge

A surge converter is made up of a terminator that moves back and forth in response to the velocity of the incident wave (Fig. 1.20).

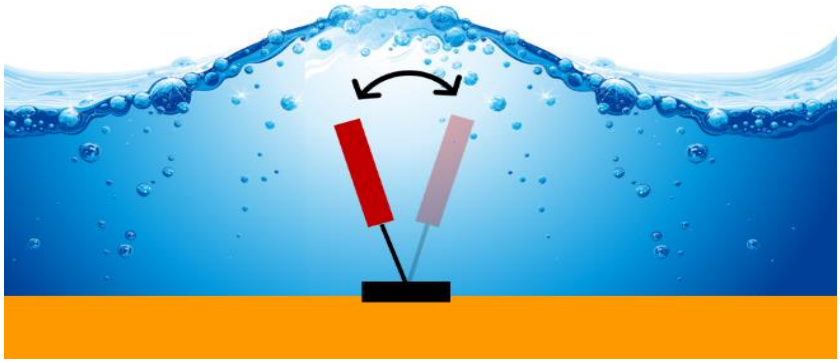

Fig. 1.20: Schematic diagram of Oscillating Wave Surge

e. Heaving buoy

A point absorber is a type of device that floats on the water's surface (Fig. 1.21). It moves due to the displacement of the incident wave caused by a passing motion. The device's relative heave motion is then used to extract power from the flowing incident. Although point absorber systems are commonly hydraulic, they can also be designed using a linear generator. These devices can be used at various sites and in most sea states. (Nachev, 2017).

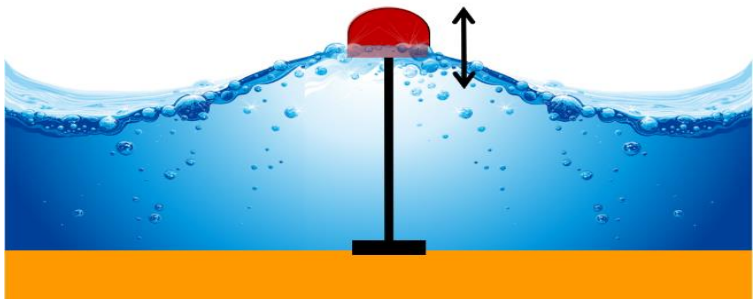

Fig. 1.21: Schematic diagram of Heaving Buoy

f. Cycloidal wave absorber

The devices of the Terminator concept have an axis that's parallel to the wave front (Fig. 1.22). They can physically intercept the waves. The energy conversion process is carried out using the relative rotation of the object in the water. This type of device is similar to a floater moving in pitch. (Drew, Plummer and Sahinkaya, 2009) .

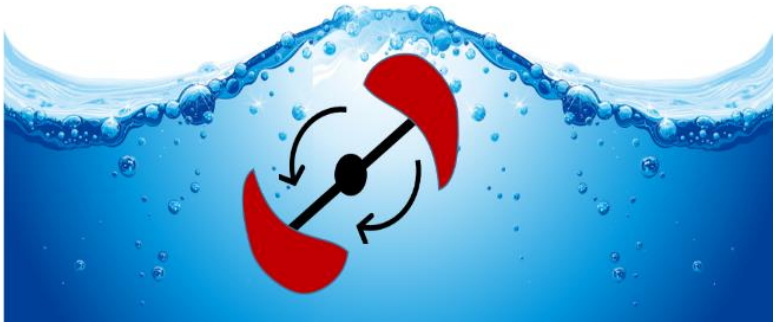

Fig. 1.22: Schematic diagram of Cycloidal Wave Absorber

g. Overtopping devices

An overtopping device collects incident wave seawater in a reservoir above sea level, then releases it back to the sea via turbines (Fig. 1.23). The Wave Dragon, depicted in Fig. 1.24, is an example of such a gadget. A pair of enormous curving reflectors collect waves in the middle receiving area. They flow up a ramp and over the top into an elevated reservoir, from which the water can return to the sea via several low-head turbines. (Guney, 2015).

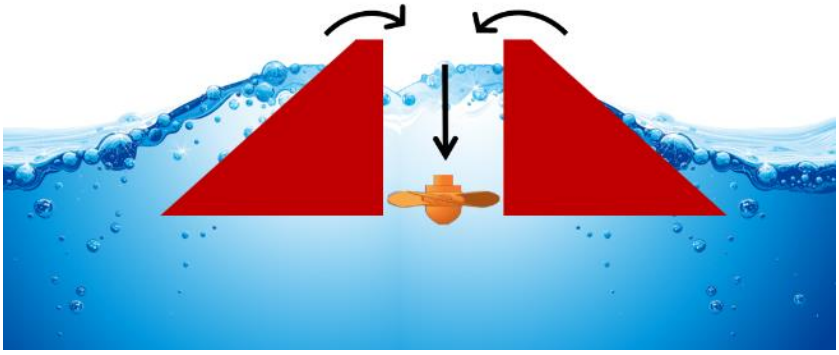

Fig. 1.23: Schematic diagram of an overtopping

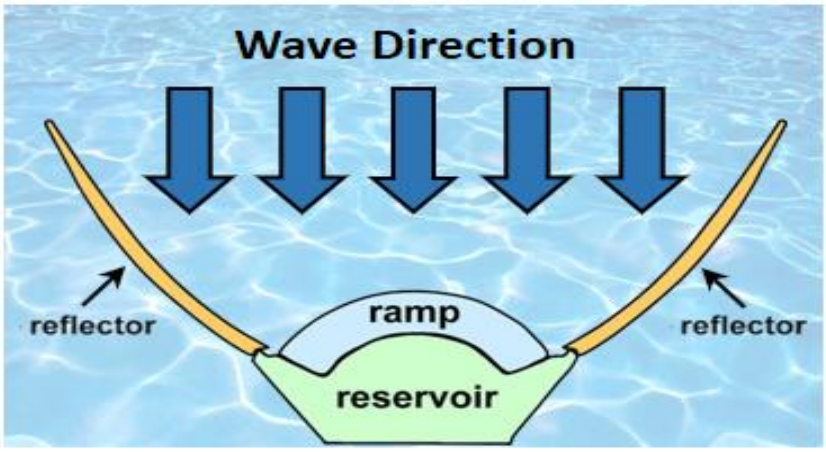

Fig. 1.24: The Wave Dragon

h. Oscillating water columns (OWCs)

The device known as an OWC is usually made up of a hollow fixed structure. As the water level rises, the incident waves force the trapped air inside the structure to move (Fig. 1.25). This action generates a flow through the turbine. Compared to open-sea devices, fixed OWCs are generally easier to construct. They were among the first full-scale projects in which electrical power could be produced.

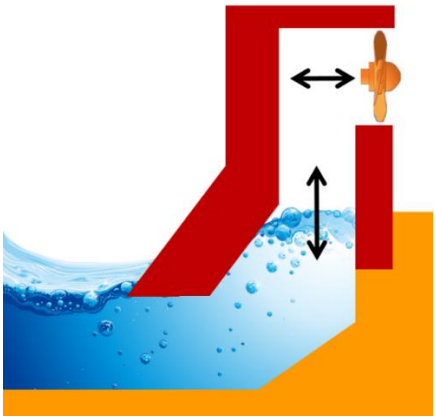

Fig. 1.25: Schematic diagram of OWCs

An optimization study is carried out continuously to improve various energy generation technologies. Among these technologies, the use of the OWC turbine, which was the focus of this optimization study, is included. An OWC is a WEC tool that utilizes the ocean's kinetic

energy to generate pneumatic power. In the WEC system, a turbine is used as the Power Take-Off (PTO) unit to generate energy from the pneumatic power. The OWC exhibits great potential and encouraging traits. Numerous pilot power plants have illustrated their technological and financial potential.

The fundamental operation of an OWC power plant is the conversion of wave energy into pneumatic energy using a concrete chamber that is partially submerged. The free surface in the chamber rises as the sea level outside the chamber rises due to the arrival of the waves, creating a flow from the cavity to the atmosphere (exhalation). When the wave subsides, the free surface inside the chamber falls, and the flow from the atmosphere enters the chamber (inhalation). So, a water column that oscillates and acts as a piston to create a bidirectional airflow is propelled by wave motion(Takao and Setoguchi, 2012). Fig. 1.26

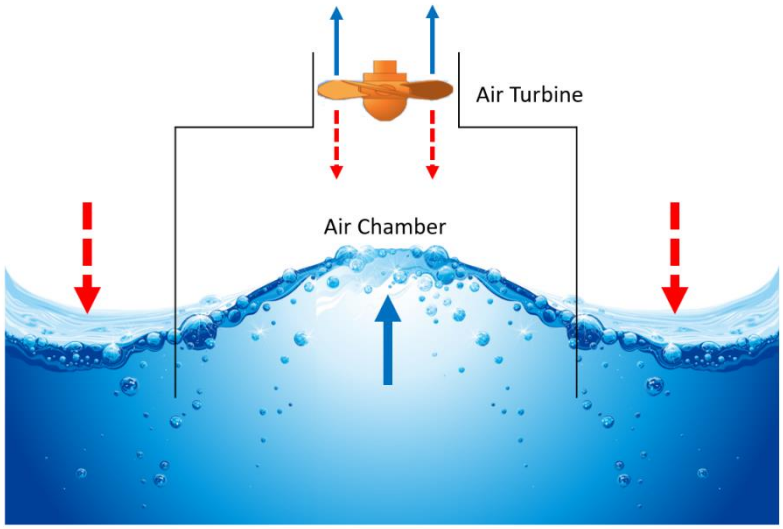

Fig. 1.26: Schematic diagram of OWCs

1.7 Computational fluid dynamics

The computational fluid dynamics (CFD) field is a rapidly growing field that provides a wide range of tools for analyzing and simulating fluid flow. This type of technology combines numerical analysis, computer visualization, and mathematical modeling to provide a complete understanding of the phenomena. It has been very important for various industries, such as energy, biomedical engineering, and environmental engineering, to have the ability to perform fluid flow simulations.

Due to technological advancements in the field, the number of people using CFD in their studies has increased significantly. The development of specialized software and high-speed computers has allowed researchers to perform complicated fluid flow simulations that were previously impossible. Researchers can now model and analyze fluid flows using numerical methods, which can now resolve the various Navier–Stokes equations.

As a result of that, can now perform accurate and comprehensive fluid flow simulations without the need for costly physical experiments. CFD is widely used in various fields, such as aerospace, automotive, electronics, nuclear, and industrial(Gunzburger and Nicolaides, 2003). In the field of aerospace, it is used to develop the design of spacecraft and aircraft components, such as propellers and wings (Fig. 1.27). It is also used in studies on the aerodynamic properties of aircraft during in-flight, takeoff, and landing.

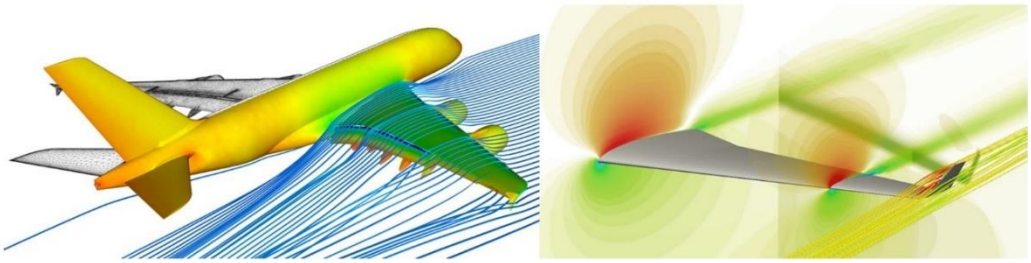

Fig. 1.27: Aircraft application. (Crahmaliuc, 2017)

Leading companies, such as Boeing, utilize the capabilities of aerospace design simulation software to tackle the challenges of enhancing fuel efficiency, meeting customer demands for passenger safety and comfort, reliability, reducing environmental impact, faster time to market, and designing for affordability (Fig. 1.28). Aerospace CFD tools encompass the entire spectrum of aerospace and defense product development, spanning applications that

encompass aerodynamics, aero structures, propulsion systems, environmental control systems, on-board hydraulic, pneumatic, and electronic systems, control and display software, space systems, as well as safety-critical systems design aspects like embedded software simulation, including bird strike simulation, lightning strike simulation, and aircraft icing simulation.(Johnson, Tinoco and Yu, 2005)

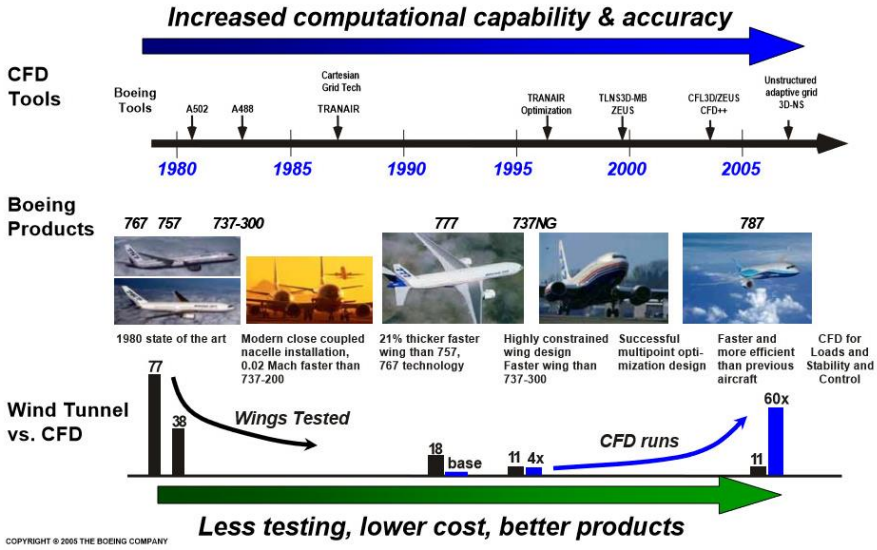

Fig. 1.28: Boeing Wing Development

In the automotive sector, it is used to improve the performance of vehicle bodies and cooling systems (Fig. 1.29). Also, it can be used to design efficient heat exchangers or predict the performance of a wind turbine.

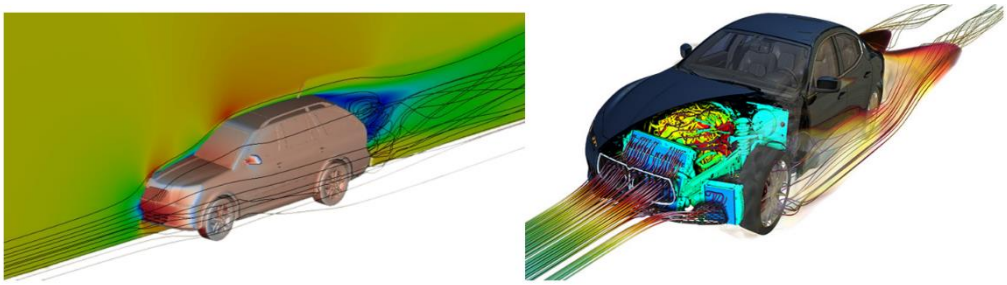

Fig. 1.29: Automotive application. (CFD Direct, 2016)

Automobile manufacturers are currently re-engineering virtually every part of their vehicles with the goals of achieving lightweight, improved energy efficiency, and smarter controls, all while maintaining safety and reliability. Additionally, they are working to address concerns

about rising fuel costs and environmental impacts by re-engineering all aspects of vehicle design, including aerodynamics, engines, transmissions, vehicle bodies, passenger comfort, and electrical and electronic systems.

In chemical processing, CFD is commonly used to develop the designs of various equipment, such as reactors and mixers. In environmental engineering, it is also used to analyze the flow conditions of pollutants in different bodies of water (Fig. 1.30).

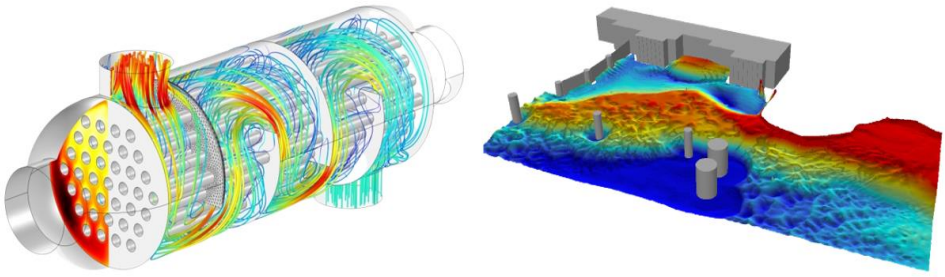

Fig. 1.30: Chemical and environmental application. (MR-CFD, 2023)

As well, Companies in various industry segments, including basic chemicals, synthetic materials, agricultural chemicals, paints, coatings, adhesives, and cleaning preparations, use CFD. The use of engineering simulation for the chemical and petrochemical industries has led to significant improvements in areas such as engineered materials, specialty chemicals, product and process performance and quality, plant product safety, business and technical viability, energy reduction, environmental protection, and cost minimization.

Also, CFD is used in the electronics industry, and the scope of its applications has become more widespread. It is used in various applications such as thermal management, component design, and electronic packaging (Fig. 1.31). The current generation of smart products comprises intricate electronic systems that must function without any errors in the real world. There is a need for rigorous analysis to meet the demands of device miniaturization, support for multiple wireless technologies, faster data rates, and longer battery life. Engineers designing wearable electronics and mobile computing products must optimize the product's form factor, performance, and battery life, while simultaneously delivering an exceptional user experience. To overcome the challenges of miniaturization, integration of functionality

across hardware, software, and mechanical subsystems, and lower power budgets. The advantages of this technology include reducing the time and cost of development, improving performance, and increasing reliability. (Jiyuan et al., 2018)

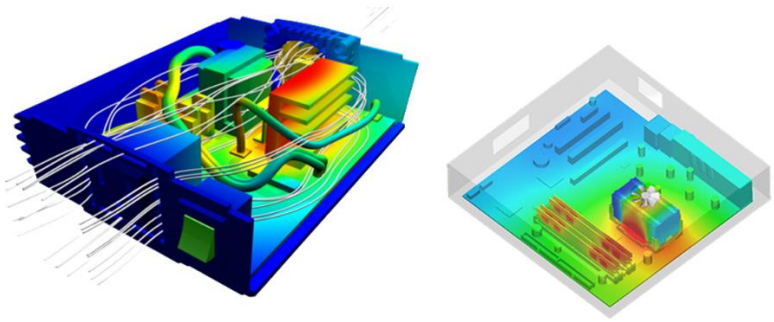

Fig. 1.31: Electronics application. (CFD Training, n.d.)

Metal-forming manufacturing has undergone a manufacturing revolution with the introduction of CFD. This technology enables engineers to optimize process parameters, improve product quality, and reduce defects. Its applications in metal forming are numerous, including die design optimization, simulation of heat transfer during forming, analysis of lubricant flow, and simulation of the entire forming process from start to finish (Fig. 1.32).

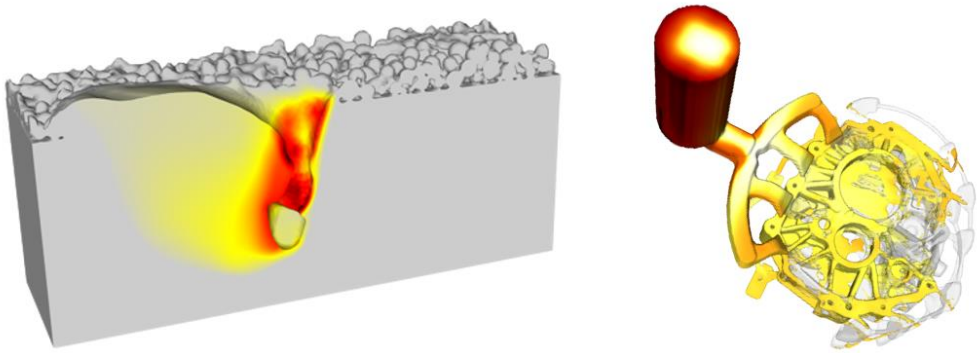

Fig. 1.32: Metal-forming manufacturing application. (Metal-AM, 2021)

CFD is a valuable tool for the nuclear industry, providing insights into the behavior of fluids, heat transfer, and mass transfer inside nuclear reactors and other nuclear facilities (Fig. 1.33). CFD simulations can help to optimize the design of nuclear reactors, improve their safety, analysis of coolant flow inside nuclear reactors, investigate the behavior of nuclear fuels inside the reactor core, optimize the performance of nuclear fuel assemblies, and ensure the safe storage and transport of nuclear waste.

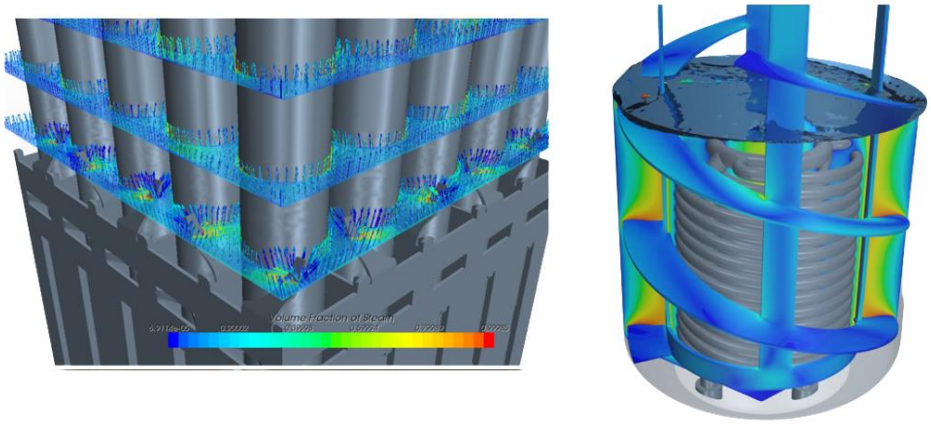

Fig. 1.33: Nuclear application. (Lo, 2014)

While CFD is widely known for its use in Formula One racing, it has also been adopted by other sports such as cycling (

Fig. 1.34), swimming, and sailing. In cycling, even the smallest modifications in bike design, training methods, nutrition, and helmet position can lead to significant performance gains. CFD plays a vital role in helping cycling teams to analyze the effects of these changes, including their impact on rider position and clothing choices. By employing 3D body scanning technology, coaches can use CFD analysis to optimize the order of cyclists in team events, maximizing the drafting effect for enhanced performance.

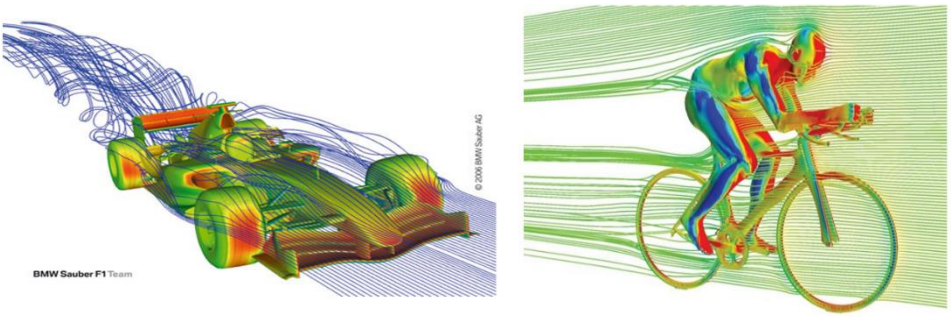

Fig. 1.34: Sports application. (Clarke, 2015)

Transient and steady-state CFD simulations are the two main categories. The steady-state simulations assume that the flow rate does not change over time. In pipelines, for instance, steady-state simulations can be useful when the flow rate is constant. On the other hand, in transient analyses, the fluid's behavior is considered in terms of time. This type is useful for problems with variable flow rates in turbines, valves, and pumps. Additionally, in Transient

flow simulation, the important unsteady behavior of the fluid, such as vortices and turbulence, can be captured.

Partial differential equations are used in computer software to perform CFD simulations, which are designed to visualize the effects of fluids on a system. These equations are commonly used to describe the fundamental concepts of fluid dynamics such as mass, energy, and momentum. The software divides a fluid domain into several small volumes, and it uses the boundary and initial conditions at each cell to perform the simulations (Fig. 1.35). The results of these simulations are then analyzed and displayed in a graphical display. The results of the CFD simulations provide valuable information about the various properties of fluids, such as their velocity, pressure, and temperature(Lakshminarayana, 1996).

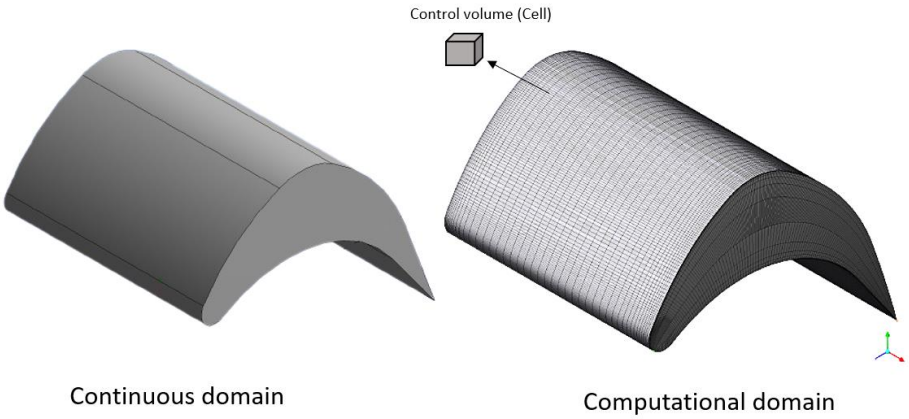

Fig. 1.35: Continuous and Computational domain.

1.7.1 The CFD Process

a. Define the Flow Problem

In order to conduct an analysis, several steps must be followed. First, the objective of the analysis must be clearly defined, including what is to be analyzed and what results are expected. Once the objective is defined, a suitable technique can be selected to achieve it. Next, it is important to determine the extent and properties of the object that will be measured for analysis, including its geometry. Operating and non-operating conditions must also be defined, along with the internal and external flow geometry. Finally, boundary conditions must be established, which may include the properties of the fluid,

the nature of its flow (laminar or turbulent), and the interchange of energy with its surroundings. (Ferziger & Perić, 2002; Sharma, 2022).

b. Geometry Design

i. Object Geometry

The object's geometry is the next aspect to consider, involving the creation of a graphical model that encompasses both its internal and external features. An example of internal geometry could be the interior of a pipe through which fluid flows, while external geometry could include the surface of an aircraft that is exposed to the wind during flight.

ii. Flow Geometry

Flow geometry is another aspect that needs to be modeled. This can refer to internal and/or external flow, such as water flowing through a pipe or wind passing over an aircraft. For example, if a pipe is filled with water and allowed to freeze, the volume of the resulting solid ice can be used to define the flow of water through the pipe by removing the pipe walls. This volume represents the area where the fluid flows and is the flow geometry/domain that will be created and meshed for analysis of the fluid's movement through the pipe.

The object geometry and flow domain are modeled in such a manner as to provide input for the grid generation. Thus, the modeling often takes into account the structure and topology of the grid generation.

c. Define Boundary Conditions

To ensure a finite flow domain, physical conditions must be established on the boundaries of the domain. These boundary conditions dictate the inputs of the simulation model. For instance, conditions such as velocity and volumetric flow rate determine how a fluid enters or exits the model, while conditions such as film coefficient and heat flux specify the exchange of energy between the model and its surroundings. Boundary conditions serve to link the simulation model with its environment, and without them, the simulation cannot be accurately defined and in most cases, cannot be executed. Typically, boundary conditions can be categorized as either steady-state or transient, with the former being

constant throughout the simulation and the latter varying with time, often to simulate cyclical or event-based phenomena. The simulation typically begins with an initial solution and uses an iterative method to reach a final solution for the flow field.

d. Grid Development / Meshing

The object and flow geometry is divided into smaller components called elements, with a node situated at each corner of every element. The mesh/grid is composed of these elements and nodes, and the process of creating it is referred to as meshing. Grid generation entails defining the structure and topology and then constructing a grid based on that topology.

e. Simulation Strategy

Performing simulations requires strategic decision-making, which includes choosing between space-marching and time-marching techniques. Time marching specifically involves solving time-dependent problems by calculating the solution at discrete time intervals. The process begins with the known initial state at time zero, where all variable values are determined. It then progresses by taking small time steps and approximating the solution at each interval. Additionally, decisions must be made regarding the selection of suitable turbulence or chemistry models and algorithms for the simulation.

f. Definition of Parameters

In CFD, a typical requirement is an input data file that contains the necessary parameter values for the selected simulation strategy, along with a grid file that provides information about the grid and boundary conditions. To perform a series of experiments, multiple analyses can be submitted for batch runs, with the ability to specify a range of values and adjust boundary conditions across a spectrum. The software automatically generates a sequence of analyses, executes them, and submits them for processing.

g. Running the Simulation

At this stage, the model is ready for simulation, which is carried out using a solver software program. The solver automatically generates a set of analyses, executes them, and submits them for processing.

h. Monitoring Results

During the simulation process, close monitoring of the solution occurs to determine if a "converged" solution has been achieved. The computed solutions are compared to analytical, computational, or experimental studies to assess the accuracy of the results. The sensitivity of the computed results is also analyzed to gain insights into potential discrepancies in precision and computational performance. Ultimately, the optimal design is selected based on these evaluations.

In the following sections, these steps will be utilized to conduct the optimization process for axial turbines. As the progress continues, each step will be outlined and thoroughly explained.

The accuracy of the results of these simulations depends on various factors, such as their complexity and the quality of the mesh. One of the most important factors that can affect the computational efficiency of a simulation is the meshing process. The number of cells should be carefully selected to ensure that the mesh is high-quality. This can be done by choosing a mesh with a finer consistency in a high-gradient area and with a lower concentration in a low-gradient area. Another key factor that can affect the accuracy of the results is the fluid properties and boundary conditions.

Despite the advantages of computational fluid dynamics, it still has some limitations. One of these is the prohibitive cost of software and hardware. Also, this technology can be very time-consuming, especially for large or complex systems.(Anderson and Wendt, 1995; Versteeg and Malalasekera, 2007)

1.8 CFD and turbomachinery

The use of CFD methods has become an integral part of the design and optimization process of turbomachinery components. They can be used to solve complicated fluid dynamics problems involving the movement of fluids, chemical reactions, and heat transfer. By computational methods and mathematical algorithms, engineers can perform simulations of complicated fluid flow and heat transfer in systems.

The design of turbomachinery equipment like turbines includes accounting for several factors, such as the operating conditions and blade geometry. Using CFD in turbomachinery design

helps to study the behavior of the flow through the analysis of the interaction between the fluid and the blade. In addition to analyzing the flow domain, CFD can also be used to study the effects of various operational factors such as ambient conditions and temperature. This process can allow us to identify the optimal operating conditions for the turbine. On the other hand, the various phenomena that can affect its performance, such as flow separation, stall, and surge, can be studied.

CFD to perform a detailed analysis uses a process (Fig. 1.36) known as iterative computational analysis to model the flow domain and perform various calculations related to its governing equations, such as the Navier-Stokes equations, by dividing the flow domain into smaller computational cells and solving the equations.

The governing equations of fluid flow represent mathematical statements of the conservation laws of physics, namely, the laws of mass, momentum, and energy conservation. These equations are crucial for understanding and modeling fluid flow in various natural and engineered systems. The mass conservation equation states that the rate of increase of mass of a fluid element is equal to the rate of flow of mass into the controlled volume. The momentum equation in three dimensions is based on Newton's second law, which relates the rate of change of momentum of a fluid particle to the forces acting on it. These forces can be classified into two categories: surface forces, such as pressure and viscous forces, and body forces, such as gravity and electromagnetic forces. The Navier-Stokes equations for a Newtonian fluid introduce a model for the viscous stress components, which are crucial for calculating fluid flow in three dimensions. The stresses can be expressed as functions of the local deformation rate, which includes linear elongating deformation and shearing linear deformation components, as well as volumetric deformation. The Navier-Stokes equations are named after the two 19th-century scientists who independently derived them and provide a fundamental basis for analyzing and understanding fluid flow in a wide range of physical and engineering applications. (Moukalled et al., 2016)

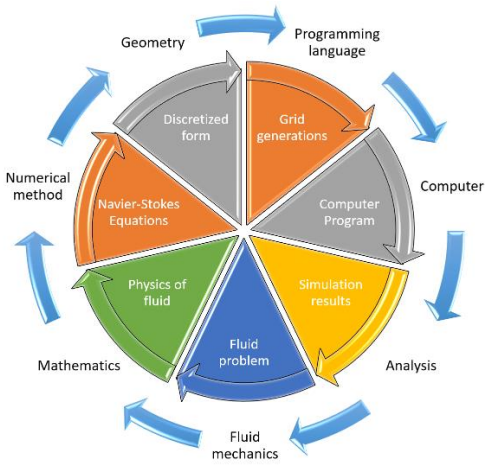

Fig. 1.36: Process of Computational Fluid Dynamics.

Through this process, engineers can gain a deeper understanding of flow physics and identify potential solutions to implement improvements to produce high output power and efficiency. In addition, these tools can also help to improve the design of the turbine by analyzing the effect of changes in the design parameters.(White, 2009).

Despite the advantages of CFD in turbomachinery, it still has several challenges. One of these is the accuracy of the models. They need to be able to capture the flow physics of the system, such as the interaction between the blade and the boundary layer. This process involves understanding the flow behavior and using advanced modeling techniques, such as detached and large Eddy simulations. Also, computational resources are required, especially for complex designs.

Another challenge that comes with the use of computational modeling is validation. This process involves comparing the simulation results with the data collected from the tests. Doing so can be very costly and time-consuming. In addition to this, the use of CFD requires the expertise to handle various computational aspects and fluid mechanics.(Anderson and Wendt, 1995)

Otherwise, the use of this technology is expected to keep growing in the design and optimization process of turbomachinery due to their ability to perform actual simulations of the operating conditions of the equipment. experimental methods, such as the use of wind

tunnel tests, are time-consuming and expensive. By using simulations, a component's performance under various operating circumstances can be evaluated quickly and easily.

1.9 Purpose

Improvement of any process is always necessary from an engineering perspective. Optimal and well-planned trials that take into account as many variations as possible are required to achieve this .This procedure must be reliable and concentrate on results rather than potential experimental blunders.

Numerous studies have concentrated on finding the most delicate variables impacting the operation of the turbines and optimizing the turbine designs for OWC. These methods are quick and accurate, and they forecast the best designs by figuring out how parameters and responses interact.

One method of finding the best design solution is through Design Exploration (DE). It is an effective strategy for investigating, comprehending, and maximizing engineering difficulties. Enough data is obtained on the existing design to provide answers to hypothetical scenarios that quantify the impact of design factors on product performance. By doing this, decisions are based on accurate information even if the design restrictions alter unexpectedly. DE could be viewed as an advancement above the conventional design optimization procedure.

Applying a DE technique has several benefits, one of which is that it is less expensive than an optimization algorithm because it takes fewer samples. The technique does have one disadvantage, though: the output is a response surface that may be an approximation or an interpolation, and it can be difficult to determine how well the adjustment was made and how well extrapolation will work in the future.

It is essential to apply computational simulation in addition to the DE. To manage a hundred or more experiments, each with a unique geometry, in order to examine their various behaviors is just impossible. The use of numerical simulation looks to be the best option because creating such a procedure would be extremely difficult and expensive if done through prototyping.

In conclusion, numerical simulation and the DE enable us to conduct the best analysis of the example presented in this document. The simulation is necessary to replicate the behavior of cases more affordably, resembling a lab environment, while the design of experiments is utilized to effectively and efficiently explore the sample space.

1.10 Aim of the study

In order to meet the increasing energy requirements of the future, the research project focuses on the development of a numerical model that can handle the flow conditions in an OWC plant, which includes an axial twin turbine. This method would allow for the analysis and optimize flow conditions. The automated design optimization process was divided into three stages (Fig. 1.37).

First, a CFD model will be created using the ANSYS CFX software to analyze the flow of a turbine during its operation in reverse and direct modes and validated with data from the bibliography. This will be used to extract the performance data of the turbine.

Second, build DS suited for the operation of the inflow axial impulse turbine. include creating a comprehensive representation of the various design parameters and constraints of a turbine. throwing this step iteratively adjusts the design parameters until the optimal solution is found.

Finally, discusses the characteristics of the optimum axial impulse turbine in detail and compares it with the existing axial impulse turbine.

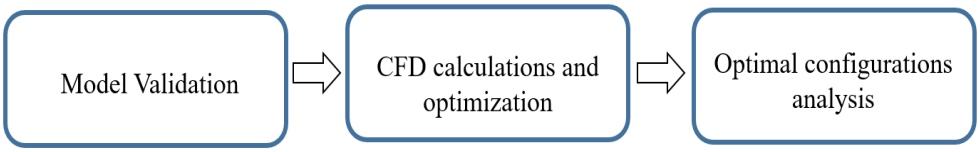

Fig. 1.37: A schematic of working stages.

1.11 Conclusions

In the field of turbomachinery, different types of turbines are widely used, with the selection depending on efficiency requirements, application, and operating conditions. The most commonly used turbine types include impulse, reaction, and Kaplan turbines. The advent of computational fluid dynamics (CFD) has significantly enhanced engineers' understanding of turbine performance and flow characteristics. This knowledge allows for improved design and reduction of energy losses.

CFD is a commonly used tool in the turbine design process to enhance efficiency and reliability. It helps in the identification of potential issues such as vortex shedding, pressure drop, and flow separation that can impact turbine performance. The combination of CFD analysis and various turbine types has led to the development of more reliable and efficient turbines. As technology continues to advance, these tools are expected to play a vital role in the design of future turbines.

The objective of this study is to develop a numerical model for the analysis and optimization of flow conditions in an Oscillating Water Column (OWC) plant featuring an axial twin turbine. The process includes creating a CFD model, constructing a Design Space (DS), and comparing the optimized turbine with existing designs. The aim is to enhance the turbine's efficiency and meet the growing energy demands of the future. The numerical simulations were carried out using ANSYS CFX software.

Chapter 2

LITERATURE SURVEY

2.1 Introduction

This chapter explores the development and implementation of a working wave converter plant, which are innovative technology designed to convert wave energy into electrical power. It will talk about the various already implemented project. Also, focus on OWC. The history and development of it will be explored over the years, as well as the promising technology it has become. Moreover, the existing literature on optimization using CFD will be surveyed, aiming to explore the advancements, methodologies, and applications that researchers and engineers have developed in this field. This survey serves as a foundation for understanding the current state-of-the-art techniques and their potential for further advancements in optimizing turbine geometry.

2.2 The development of wave converter plants

The potential of wave energy to provide renewable energy has gained significant attention in recent years. Ocean waves' energy can be a promising technology for commercial operations. This article looks into the current status of wave energy converters' commercial operations, as well as the challenges and future prospects.

The commercialization of wave energy converters is still in its early phases. There are currently only a few operational projects in the world. According to the IEA, the global installed wave energy capacity in 2020 was only 11.8 megawatts. Europe accounts for most of the world's installed wave energy capacity.

In Scotland, the Pelamis was developed as a wave energy converter that harnesses the movement of ocean waves. This device is composed of a series of linked sections that are designed to flex in response to wave activity. It operates by utilizing hydraulic pumps to convert the kinetic energy from the waves into electrical energy. The interconnected tubes of the device are engineered to respond to the motion of the waves and convert this energy into electricity. Pelamis was one of the pioneering commercial wave energy converters, with the initial deployment of the device taking place in Portugal. At present, the installed capacity of Pelamis in Portugal is estimated to be around 2.25 megawatts. Despite the favorable findings, the development of the Pelamis is still in its early stages, and its use is not yet widespread.(Kanellos, 2009).

Fig. 2.1: Pelamis wave energy converter.

The WaveRoller is a technology developed by a Finland-based company, which aims to harness the energy from ocean waves and convert it into electrical power. This bottom-mounted device features a panel that is anchored to the seafloor and moves with the waves' motion. At present, the WaveRoller has been deployed in both Portugal and Finland, with a total installed power capacity of 350 kilowatts. To generate electricity, the WaveRoller device utilizes a hydraulic system that includes various components, such as valves, cylinders, and hydraulic cylinders. The hydraulic pump is connected to the panel, which moves with the waves to generate power. The WaveRoller has been tested in various ocean conditions, including low-wave conditions, to validate its capacity to produce electricity.

The WaveRoller has demonstrated its robustness in harsh ocean conditions, such as strong waves and storms, where it continued to operate effectively. Despite being in its developmental stage, the WaveRoller holds great potential as a renewable energy source.(Gordon, 2019).

Fig. 2.2: Wave Roller off Peniche, Portugal.

The Oyster is a device that uses the power of ocean waves to convert its energy into usable electricity. It's made of an energy-harvesting flap that's connected to the seafloor. As the waves pass through it, the flap's movement causes a cyclic movement of a hydraulic pump, which then produces electricity. The Oyster energy converter has been extensively tested in various ocean conditions, and it has excelled in terms of its durability and efficiency. Aquamarine Power completed the development and testing of two full-scale ocean wave power plants at the Billia Croo facility in Orkney. The company's first plant, known as Oyster 1, has a capacity of approximately 315 kW, while the second plant, known as Oyster 2, has a capacity of 800 kW.(Curto, Franzitta and Guercio, 2021).

Fig. 2.3: The offshore Oyster devices.

The Wavestar energy converter created by the company is specifically designed to harness the power of ocean waves and convert it into electricity is located in Hanstholm, Denmark. With a power output of 600 kW. This innovative technology employs a set of hydraulic floats that are linked to a generator. Each of these floats has the ability to move independently of the others, which enables the system to adjust to fluctuating wave patterns.(Marquis, Kramer and Frigaard, 2010).

Fig. 2.4: WaveStar wave energy converter.

The EcoWave energy converter developed by the company harnesses the power of ocean waves using a unique water column system. The system is comprised of a submerged chamber that remains open at the bottom, with a turbine situated inside it. The rise and fall of water levels in the chamber cause oscillations in the air that drive the turbine, which in turn powers a generator. This technology, capable of generating 100 kW of power. After Spain and Gibraltar, Eco Wave Power is also undertaking the construction of wave power plants in Portugal and California. *(Eco Wave Power, 2019)*

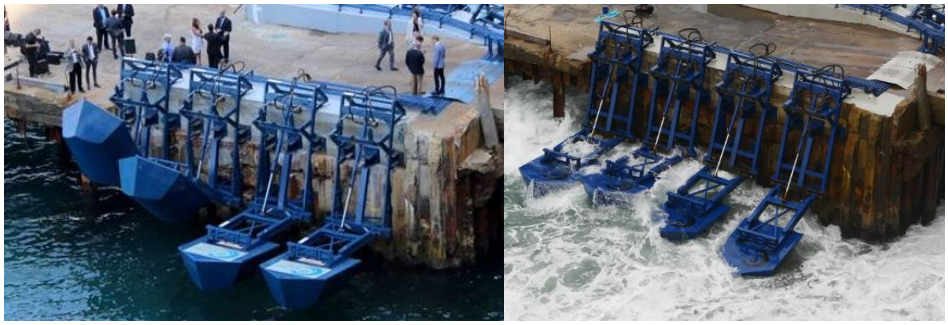

Fig. 2.5: Wave Energy Power Station in Gibratal.

In 2019, a PTO system based on the seahorse was installed at Brazil's Pecem surf farm, which is one of the world's first commercial-scale wave farms. The project, which is located off Cear's coast, is dedicated to demonstrating the viability of wave energy. The Seahorse PTO system, which is a component of the project, can generate up to 1 MW of power from ocean waves. Through extensive testing, the system has been able to perform well in challenging ocean conditions. (Zuini & Cepellos, 2015)

Fig. 2.6: Seahorse power take-off system

In Australia, the CETO wave energy technology was developed by Carnegie Wave Energy, a company that specializes in developing and commercializing wave energy systems. The CETO system is a fully submerged buoy that utilizes a hydraulic pump to capture the kinetic energy from ocean waves and convert it into electricity. With a total installed power capacity of 1 MW, the CETO system operates in arrays, with multiple buoys connected to a single onshore facility for the conversion of the generated electricity.

The buoy's hydraulic pump is powered by the up-and-down motion of the buoy, which occurs as waves pass by. The hydraulic pressure generated by the pump is then used to drive a turbine that produces electricity. The CETO system has undergone extensive testing in

various ocean conditions, and the company has demonstrated its ability to produce reliable, cost-effective, and environmentally sustainable electricity from wave energy. (CETO Technology, 2019).

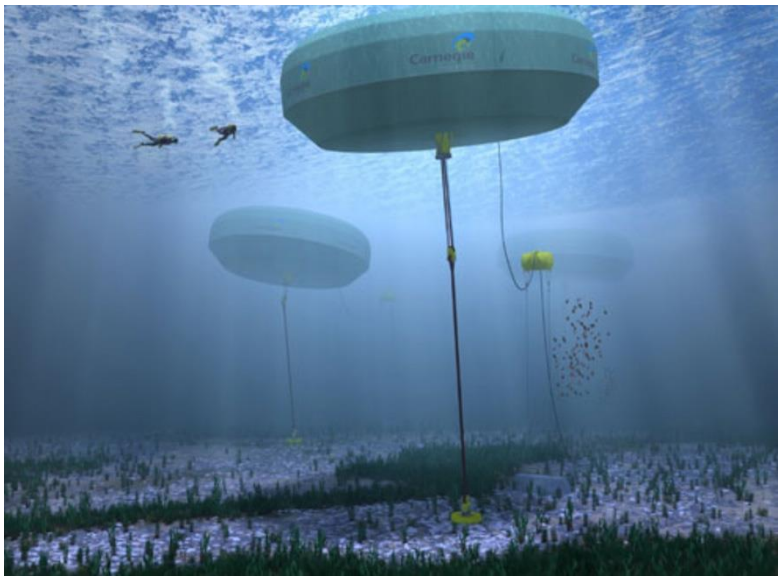

Fig. 2.7:The CETO wave energy device.

A Danish company known as Wave Dragon was able to successfully deploy a floating offshore wind turbine. This device converts the energy of ocean waves into usable electricity. It consists of a floating platform that's connected to the seabed. Two arms extend out from the platform's sides, and these are designed to push the waves into a central region of the reservoir. The reservoir contains a number of turbines that are driven by the water flow generated by the waves, and which are connected to a generator that produces electricity .In March 2003 a 20 kW prototype (scale 1:4.5) was installed. The Wave Dragon has undergone extensive testing in various ocean conditions and has demonstrated good performance in terms of energy conversion efficiency and survivability in harsh ocean conditions and it can work seamlessly on different types of waves. The device has also been shown to be scalable, with larger versions capable of producing up to 11 MW. (Tedd and Peter Kofoed, 2009).

Fig. 2.8: Wave Dragon.

An American company called AquaBuOY developed a device that utilizes a buoy to move along the waves. It's connected to a generator powered by a hydraulic pump. The company's device, which is called AquaBuOY, uses the movement of ocean waves to generate electricity. It's made up of a buoy that's connected to the ocean floor. Its mechanical system converts the buoy's movement into electricity. The system's hydraulic pump is driven by the waves passing movement, and it pumps seawater to a turbine, which then produces electricity. The AquaBuOY device can be connected to an underwater cable, which then transfers the generated power to the shore. Through extensive testing, the company has been able to demonstrate its ability to perform well in challenging ocean conditions. (Thealiennextdoor, 2015).

Fig. 2.9: AquaBuOY.

A wave energy converter known as Wavebob utilizes the movement of waves to produce electrical power. It's composed of a structure that's submerged, and it's connected to an ocean floor mooring system. The power take-off mechanism of the device converts the buoy' movement into electricity. The Wavebob system utilizes a gearbox and a hydraulic cylinder to drive a generator that converts the buoy's up-and-down movement into power. The average electrical output of an individual unit is around 500 Kilowatts. It has been tested in various ocean conditions, and it has performed well in terms of its efficiency and durability. (Weber *et al.*, 2009).

Fig. 2.10: Wavebob.

2.3 Overview of OWC WECs

Ocean Wave Energy Converters (OWC) and Wave Energy Converters (WEC) are technologies designed to harness the power of ocean waves and convert it into electricity. In this paragraph, an overview of OWC and WECs will be provided, including their key features, advantages, and challenges.

An OWC is designed to utilize the kinetic energy of ocean waves. It's constructed of a submerged chamber that's open to the waves. As waves come in, they suck in the air from the inside and send it through a turbine, which then produces electricity. Once the waves go away, the air returns to the chamber through a valve.

The different types of OWC WECs are shoreline, nearshore, and offshore. Shoreline devices are placed on the coastline and use the natural slope of the beach to create the required difference in water height between the inside and outside of the chamber. Nearshore devices are placed in shallow water and require the construction of a breakwater to create the necessary difference in water height. Offshore devices are placed in deeper water and require a floating platform to support the device.

The working principle of an OWC WEC is based on the oscillation of air inside the chamber as waves enter and exit. As waves enter the chamber, they compress the air inside, causing it to flow through the turbine and generate electricity. When the waves recede, the air flows back into the chamber through a one-way valve, ready for the next wave to enter.

The simple design of an OWC is one of the main advantages it offers. They require few moving parts and can be easily maintained, reducing the cost of operation and maintenance. In addition, OWC WECs are relatively quiet compared to other WECs, making them ideal to marine life.

Despite their various advantages, OWCs are still not ideal for every situation. One of the main limitations that they have is their dependence on the waves' frequency and size. This means that they can only function effectively when there are waves. In addition, changes in sea level and tides can affect the height of the water that the chamber can take.

2.4 History and development of OWC

The use of an OWC, also referred to as a whistling buoy, was the earliest recorded application of this navigation aid. During the 19th century, it was seen as a replacement for the traditional bell buoys. J. M. Courtney of New York invented a whistling buoy, and in 1885 (Fig. 2.11), it was reported that there were 34 such devices along the US coast. (Delmonte *et al.*, 2014).

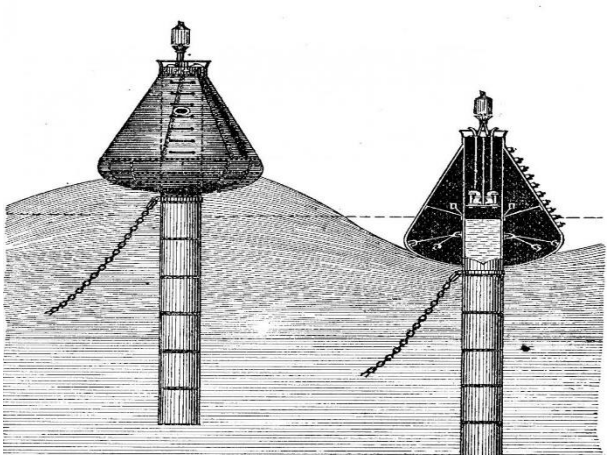

Fig. 2.11: Courtney's whistling buoy

After around half a century, the next significant invention of wave power was the first operational marine power generator (OWC) in 1947 by Masuda in Japan. This device, powered by an impulse turbine, was placed in Osaka Bay. It generated electricity for powering navigation lights.

To ensure constant lighting, rechargeable batteries that charge from the turbine and generator in prosperous times have been used. This led to the creation of a commercial range of buoys available today from the Ryokuseisha company in Japan. Despite the relatively small output of each unit (70–500 W), this type of application is still widely used.

From 1976 to 1979, a team of experts from the International Energy Agency conducted tests on the operation and maintenance of offshore wind turbines (OWCs) aboard a floating barge. The vessel, known as the Kaimei (Fig. 2.12), was docked off the coast of Yura in Yamagata Prefecture. Japan was the lead national partner for the project(Masuda and McCormick, 1986). Other international partners included the US, Ireland, and the UK.

The eight OWC chambers were mounted on the barge. They were tested against various types of turbines, such as self-rectifying Wells and conventional ones. A variety of PTO units were also tested.

Fig. 2.12: The Kaimei

During the 1980s and 1990s, various shoreline OWCs were constructed and tested in various countries, such as India, China, and Japan. One of the largest OWCs built in Japan was the port of Sakata (Fig. 2.13)(Suzuki, Arakawa and Takahashi, 2004) . The five-chambered OWC was constructed as part of a harbor wall. It was equipped with a tandem Wells turbine. It has been operational since 1989 and has a rating of 60 kilowatts.

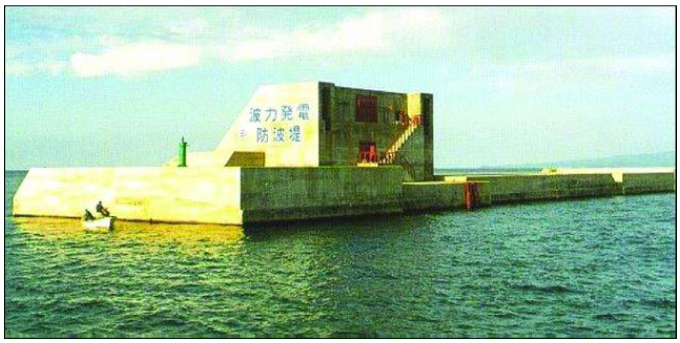

Fig. 2.13: OWC plant at Sakata harbor

Queen's University in the UK constructed the plant (Fig. 2.14). The plant was decommissioned and returned to nature after it was decommissioned in 2000. The turbine from this plant was restored and displayed at a museum in Munich.

Fig. 2.14: Queen's University plant on Islay

As a follow-up to the project known as the Islay prototype, Queen's also designed the LIMPET plant, which was constructed near the original site. Compared to the prototype, the LIMPET plant was designed to face southwesterly toward the Atlantic gales. It has been in operation since 2000. The original turbine system was replaced, and the plant is now used as a testing ground for the various types of turbines used in the commercial projects of a company known as Voith Hydro Wavegen (Fig. 2.15). The plant has logged over 60 000 hours of operation. (Delmonte et al., 2014)

Fig. 2.15: Voith Hydro Wavegen LIMPET OWC

Over time the concepts that have been introduced evolved into the concept of floating offshore wind plants. These are not designed to be placed on the shoreline but are in shallow water, which is less than 20 meters deep. Although these plants have the advantage of larger waves with high energy, they are still incredibly challenging to operate in. For example, in 1995, the first OSPREY prototype was destroyed during a storm.

Several floating prototype units have been produced one of them the Australian Oceanlinx which produced the MK1 full-scale prototype unit in 2005 to generate 500kW, MK2 3rd scale

prototype in 2007 Represented a 1.5MW-rated generating plant, and MK3PC 3rd scale prototype Represented a 2.5MW rated capacity unit (Fig. 2.16).(Oceanlinx, 2011)

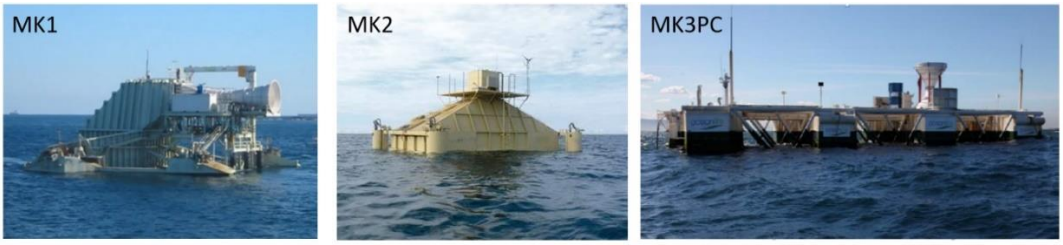

Fig. 2.16: Oceanlinx prototypes

However, the floating OWCs technology still has time to overcome the challenges before it can be considered a viable option for large-scale power generation.

The design and construction of an OWC are some of the most critical issues that affect its economics. In order to maximize the efficiency of the system, the design and construction of an OWC are often integrated into a breakwater. This method was successfully used in Japan for the first time in 1990. Aside from reducing the project's cost, this method also provides the facility with easier access to maintenance and construction. Until recently, single OWCs or large-scale OWCs were the main focus of OWC technology development. However, the development of hybrid waves and wind energy structures has been more prominent over the past years.

The multi-chambered OWC, known as the multi-oscillating water column, is commonly referred to as an arrangement of systems that can be used together. These include the generators, structure, and airflow. However, due to the varying power output of the system, it is not feasible to fully utilize its potential. Modern M-OWC concepts are generally focused on addressing the issue of power output variability.

In 2008, the construction of an OWC with a breakwater at the port of Mutriku in northern Spain (Fig. 2.17) was completed. The facility featured 16 collector chambers and 16 Wells turbines with a combined output of 18 kilowatts. (Torre-Enciso *et al.*, 2009)

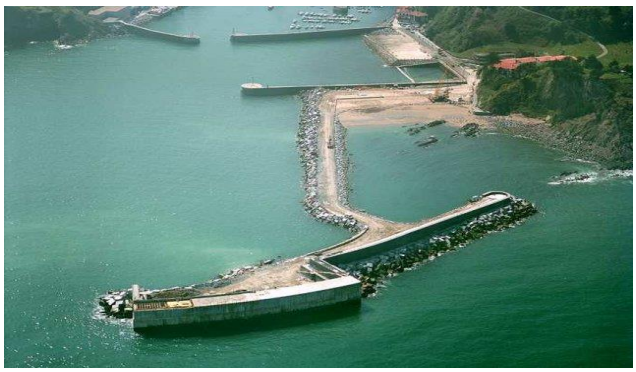

Fig. 2.17: Mutriku harbor, Basque Country, Spain

Boccotti proposed a different type of OWC for a breakwater. It has a long wave crest and a narrow fore-aft aperture. The U-shaped shape of the OWC cross-section allows it to have a more comprehensive water column without placing the opening too far below the water's surface. Another advantage of this concept is that it increases the total column length without going below the sea surface.

This type of OWC is used in the construction of breakwaters in Italy. In 2015, a full-scale OWC was completed in the harbor of Civitavecchia (Fig. 2.18). It has a total installed power of 2.6 MW. One hundred thirty-six independent OWC chambers generate power. Each chamber has a set of turbo generators that can generate up to 18 kW.(Arena, 2014)

Fig. 2.18: Harbor of Civitavecchia, near Rome, Italy

Multiple types of water chambers have been researched for their ability to support OWCs, some of which use separate air turbines or share a single air turbine. This necessitates the use of high-pressure air ducts and low-pressure air valves to be rectified.

Within the group of multiple OWCs, three plant types have been identified, as outlined by (Doyle and Aggidis, 2019):

- An OWC array featuring multiple chambers, each equipped with its own turbine and generator, all mounted in a single frame to form a unified device (Fig. 2.19).

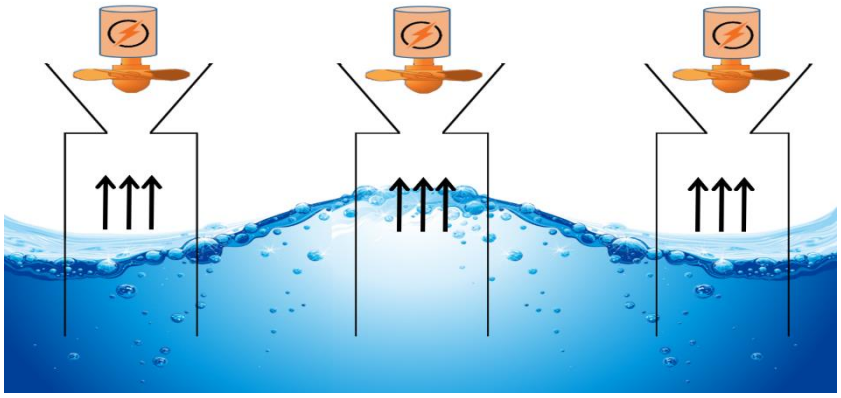

Fig. 2.19: Schematic diagram of OWC array concept

- Segmented OWC, the turbines from several OWCs are mechanically connected while remaining segregated and connected to a single generator (Fig. 2.20).

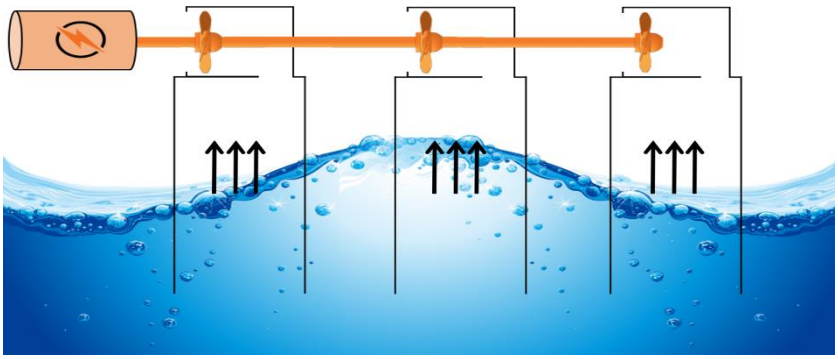

Fig. 2.20: Schematic diagram of segmented M-OWC concept

- In modular OWC, multiple chambers provide airflow that is combined. As a result, the integration of the various OWC systems takes place before the PTO stage to produce a constant unidirectional airflow (Fig. 2.21).

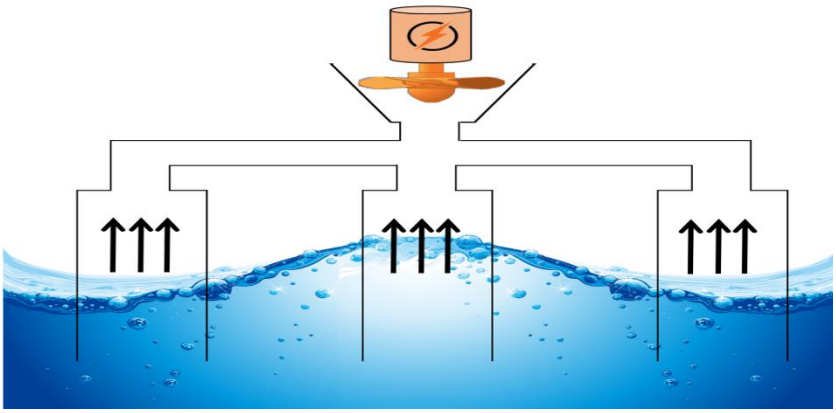

Fig. 2.21: Schematic diagram of modular M-OWC concept

Early on, a unidirectional turbine was used in combination with a valve correction system. However, self-correcting air turbines (turbines that allow the flow in both directions), such as the Wells turbine and other recently proposed ones, were used to replace this method (Okuhara *et al.*, 2012)

A lab model of a new topology with two unidirectional -impulse turbines has been developed at the Indian Institute of Technology in Madras (Jayashankar *et al.*, 2009)

Fig. 2.22 depicts the twin unidirectional topology's fundamental configuration. Two unidirectional impulse turbines, T_A and T_B, connected to electrical generators, are used in the power take-off mechanism. In the context of a direct flow, it was hypothesized that air would enter the OWC through the turbine T_B during inhalation and exit the OWC through T_A during exhalation. However, during inhalation, some air leaks through the T_A in the reverse flow direction whereas while exhaling leaves through the T_B. Thus, the efficiency of the system relies on two key factors: 1) the turbine efficiency in direct flow, and 2) the blocking capacity of the turbine when working in reverse flow.

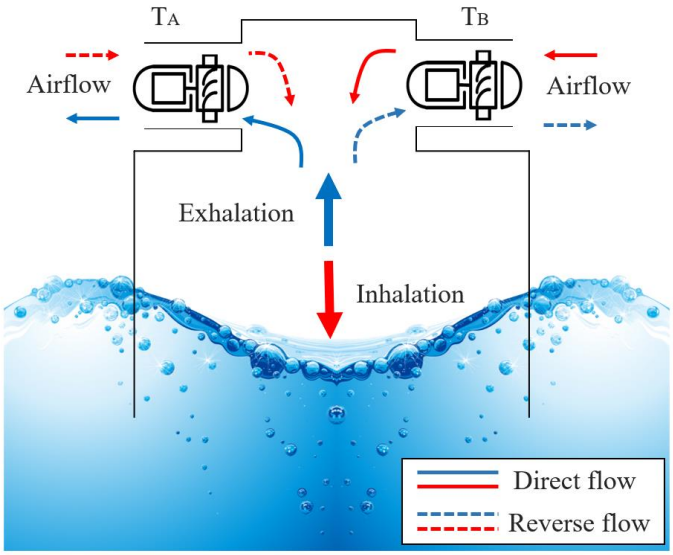

Fig. 2.22: Principle of unidirectional turbine topology.

2.5 Optimization of wells and impulse turbine

Optimizing wells and impulse turbines has been an important research topic in hydropower engineering for many years. The research presented in this thesis is focused on the design optimization of axial impulse turbines using CFD. Over the years, researchers have explored various approaches to optimize these components, including experimental studies, numerical simulations, and analytical models. This section will provide an overview of the previous work done in this field, highlighting the major findings and contributions.

Mohamed et al. modified the turbine design and increased the efficiency of a reaction turbine by applying systematic refinements to the airfoil blade shape. (Mohamed *et al.*, 2011)

A wide operational range was reported to yield an 11.3% increase in power production with the modified airfoil design. Additionally, using optimization techniques on a non-symmetric airfoil shape, the performance prediction of self-pitch-controlled blades was investigated. (Mohamed and Shaaban, 2013). Both Wells turbines.(Raghunathan, 1995) and impulse turbines (Gomes *et al.*, 2012)

underwent modifications to the blade camber line and thickness. In the latter study, the previously optimized 2D blade sections were extruded along the width direction to create a 3D geometry of the axial impulse turbine. The comparison revealed that the ideal design

yielded a 5% gain in efficiency. In addition, using multi-fidelity analysis techniques,(Badhurshah and Samad, 2015; Ezhilsabareesh, Rhee and Samad, 2018) were able to determine the ideal number of rotor blades and guide vanes. After evaluating how design choices affected pressure drop and shaft power, an efficiency increases of roughly 11% was realized. Based on surrogate modeling approaches, optimization of the wells turbine's blade sweep angle 50 was also carried out. The optimized sweep angle increased the rotor torque by almost 28%. (Halder, Rhee and Samad, 2017) . The efficiency of the centripetal radial turbine was increased through design optimization techniques. By enabling modifications of several geometrical factors in each sector, parametric geometries of the rotor blades, downstream guiding vanes, and the duct were produced. In order to optimize the design of the downstream portion, the damping coefficient and pressure losses were looked into. It was determined that using a diffuser with a 7-degree diffusion angle results in kinetic energy recovery at the turbine outlet and raises the turbine's overall efficiency by more than 10%. The inflow turbine, also known as the improved centripetal radial turbine, achieved a peak efficiency of 80%, a notable advance in this turbine category. (Ansarifard *et al.*, 2019)

2.6 Conclusions

The development of the OWC technology and the wave converter plant's implementation have shown significant progress in the renewable energy industry, which is good news for the environment. The technology has the potential to efficiently utilize ocean waves and minimize the impact on marine life.

The successful operation of a wave converter plant has shown the potential of the OWC technology to be utilized in real-world applications. The advancements technological that have occurred in the field of ocean wave energy conversion have shown that it is a promising tool for meeting the increasing energy demands of the world while reducing greenhouse gases. However, more research is needed to make the technology more cost-effective.

CFD software has revolutionized turbine optimization. These advanced software packages, with their capabilities and user-friendly interfaces, have transformed the turbine design process. As a result, numerous optimization studies focusing on turbines have emerged. With CFD software, comprehensive flow analysis can be performed, design parameters can be

optimized, and energy losses can be reduced. By simulating fluid dynamics, pressure distribution, and velocity profiles, areas for improvement can be identified, resulting in enhanced turbine performance.

Chapter 3

COMPUTER MODELING AND OPTIMIZATION

3.1 Introduction

In this chapter, the details of the simulated model utilized in the study are explored, which serves as the foundation of the investigation. This simulation plays a vital role in understanding the system under examination, requiring precise capture of its geometry, boundary conditions, and fluid properties to ensure the reliability of our results. By creating a digital laboratory, the simulated model enables us to perform experiments and validate hypotheses, the detailed exploration of our approach in this chapter built a solid groundwork for the subsequent analysis and interpretation of the simulation results.

A model of a unidirectional axial turbine that operates with airflow in both direct and reverse directions will be created. The turbine will work in both directions during the process of inhalation and exhalation, as explained in the previous chapter (refer to Fig. 2.22).

3.2 Turbine Characteristics

The torque coefficient C_T, input power coefficient C_A, turbine efficiency η, and flow coefficient $\emptyset$ were used to define the OWC turbine performance in a steady state (Takao et al., 2002). as follows:

$$\eta = \frac{T_{0,\,Total}\,\omega}{\Delta P\; Q_{\,Total}} \tag{3.1}$$

$$\eta_{rot} = \frac{T_{0,\,Total}\;\omega}{\Delta P_{rot}\;\; Q_{\,Total}} \tag{3.2}$$

$$C_A = \frac{\Delta P\;\; Q_{\,Total}}{\left(\frac{1}{2}\rho\left(V_a^2+U_r^2\right)ZblV_a\right)} \tag{3.3}$$

$$C_T = \frac{T_{0,\,Total}}{\left(\frac{1}{2}\rho\left(V_a^2+U_r^2\right)Zblr_R\right)} \tag{3.4}$$

$$\emptyset = \frac{Va}{Ur} \tag{3.5}$$

Where r_R and ρ are the turbine's mean radius and air density, respectively. The blade speed is denoted by U_r, while the mean radial velocity at r_R is denoted by V_a. Q_{Total} is the volumetric flow rate, ΔP is the total pressure drop across the settling chamber and the atmosphere, which can be determined by subtracting the total pressure at the outlet of the domain from the total pressure at the inlet, and ΔP_{rot} is the total pressure drop across the rotor, which can be calculated by subtracting the total pressure after crossing the rotor blade from the total pressure before the inlet to the rotor blade. The output torque is *To*, while the angular velocity is ω. *z, l,* and *b* refer to the number of blades, blade chord length, and Blade height respectively.

In order to evaluate the performance of the system, flow angles were plotted in both direct flow mode and reverse flow mode via variable flow coefficients. These angles are measured relative to certain axes shown in the Fig. 3.1 . These angles will be analysed in a later section.

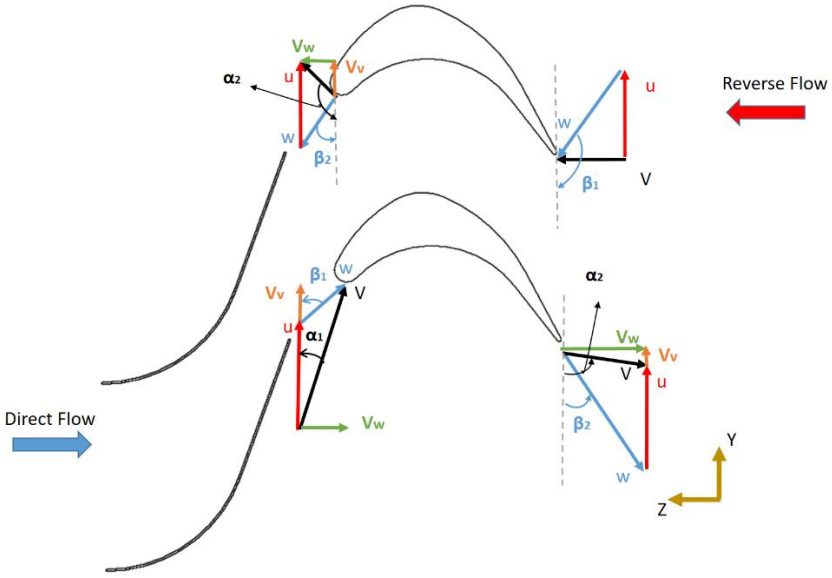

Fig. 3.1: Reference of flow angles.

The optimization process was carried out using a steady computational model. This method was used to save time and computational resources.

Due to the nature of the ocean wave, the pressure of the OWC device has been assumed to have a sinusoidal consistency.(Ashraful Alam et al., 2016; Pereiras et al., 2014)

$$\Delta P = \Delta Pmax * Sin\left(\frac{2\pi t}{T}\right) \tag{3.6}$$

Where ΔP, ΔP_{max}, t, and T represent, the total pressure drops inside the entire system, its amplitude, time, and the period of the OWC motion respectively.

The assumption is that a turbine's performance is quasi-steady to allow testing of the system in a non-steady manner. This is often used in the operations of OWC turbines. The performance of turbines is computed by considering the data collected during steady conditions. This allows it to calculate the pressure and flow rate accurately.

$$\eta_{N.S} = \frac{\frac{1}{T}\int_0^T \omega \ T_o Total \, dt}{\frac{1}{T}\int_0^T \Delta P \ Q \, Total \, dt} \tag{3.7}$$

To analyze the performance of the system, the unsteady efficiency ($\eta_{N.S}$) was plotted against the unsteady flow coefficients ($\boldsymbol{\Phi}$), which are defined as:

$$\Phi = \frac{(Qmax/Ar)}{Ur} \tag{3.8}$$

Where A_r, is the flow passage area. The reverse flow is then taken into account to calculate the amplitude of the maximum flow coefficient.

The performance of a single turbine is evaluated by analyzing the data collected under steady conditions. The calculation of the flow rate for each turbine is performed in both the direct and reverse directions (Fig. 3.2), and the equation (3.9) is used to determine the blocking efficiency as well.

$$\eta_{block} = \frac{QDirect}{QTotal} \tag{3.9}$$

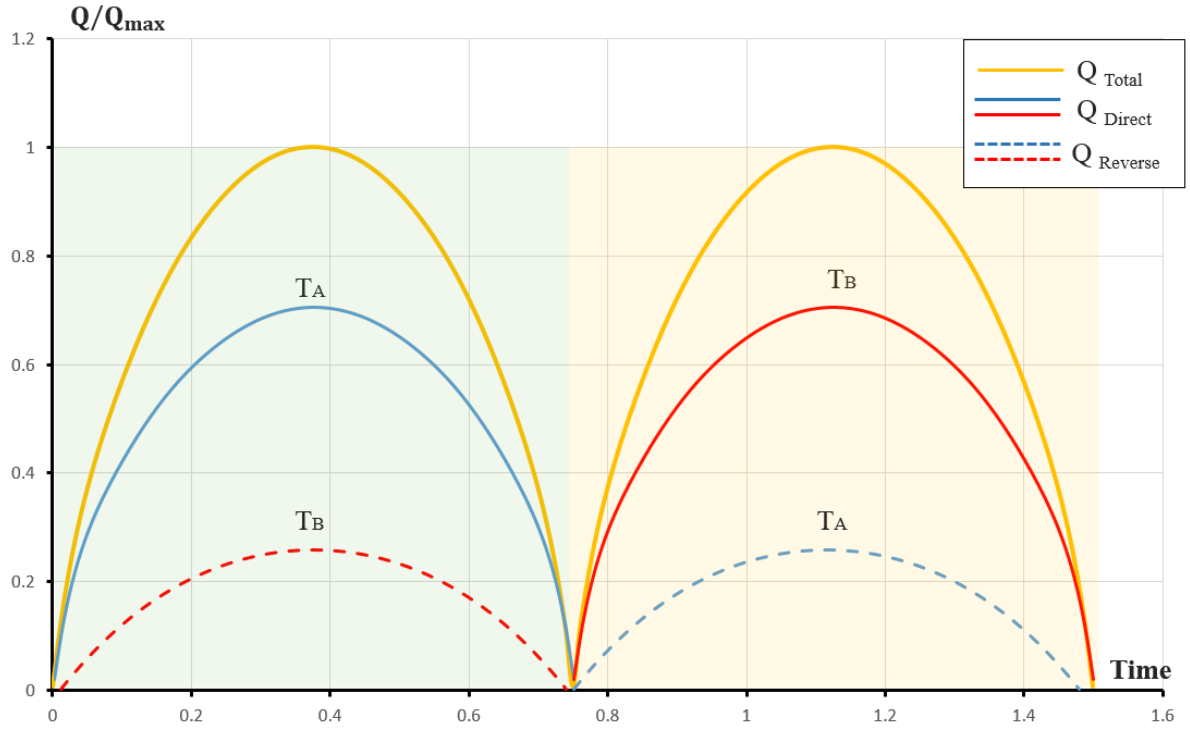

Fig. 3.2: Flow rate distribution under sinusoidal total flow rate.

3.3 Optimization Methodology

The current optimization study is to find the best new guiding vane and rotor profile to improve turbine performance and efficiency. An automated optimization process will be employed, utilizing the Ansys Design Exploration module, which utilizes a Design of Experiments (DOE) and Response Surface approximation to assess the relationship between the design parameters and the objective function. (ANSYS, 2014; Ezhilsabareesh et al., 2018)

3.3.1 Design of Experiments (DOE)

DOE is a technique utilized in optimization theory to select and execute experiments efficiently. It involves carrying out several carefully planned tests, which are designed to alter the input variables according to predefined rules. The main objective of this process is to find out what factors caused the changes in output response. DOE involves the process of planning, analyzing, and conducting controlled experiments to determine the effects of different factors on a response variable. Unlike traditional methods that can be time-consuming, DOE enables simultaneously investigating multiple factors in a thorough and efficient manner. (Lorenzen, 1993)

There exists a wide variety of algorithms and methods, each with its own unique features and applications, However, despite their individuality, these approaches share common characteristics. They all try to identify optimal sampling points that efficiently explore the space of random input parameters or seek to extract essential information using a minimal number of points The goal of these algorithms and methods is to enhance the efficiency of gathering and analyzing required information.

In order to implement the automated optimization process, it is necessary to fill the design space with design points, which will enable the creation of a response surface model. Among the various sampling techniques available, one approach for filling the design space is through the use of the Central Composite Design (CCD) method (Exploration, ANSYS Design, 2014).

a. Central composite design (CCD)

Central Composite Designs, also referred to as Box-Wilson Designs, are a specific type of experimental design used in response surface (RS). These designs are particularly useful for

constructing second-order polynomial models for response variables. Central Composite Designs are characterized by their five-level fractional factorial structure, which allows for efficient exploration of the design space and the study of both linear and quadratic effects.

In CCD, there are three different types of design points: factorial points, axial points, and center points (Fig. 3.3). Factorial points capture the main effects of factors and interactions, those points are vertices of the n-dimensional cube which are coming from the full or fractional factorial design where the factor levels are coded to –1, + 1. while axial points allow for the assessment of curvature and potential nonlinearity in the response surface, points are located on the axes of the coordinate system symmetrically with respect to the central point at a distance $|b| > 1$ from the design center. Center points are included to estimate the error variability and to provide replication for the experiments.

Many works (Ansarifard et al., 2019; Halder & Kumar, 2020) can be found using this technique successfully. Points are selected and distributed to make sure that every point is placed as far apart from one another as possible within the designated design space (Halder & Kumar, 2020)

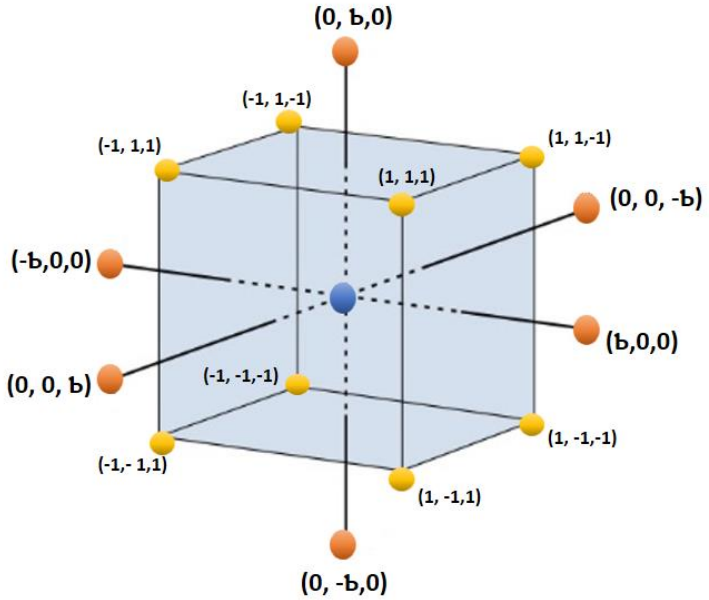

Fig. 3.3: Sampling space configurations for 3D CCD designs. factorial points (yellow) axial points (red) points and center points (blue)

3.3.2 Response surface (RS)

Response Surfaces (RS) are functions that describe the relationship between input parameters and output parameters. The primary objective of using RS is to approximate the response variable across the design space based on the results obtained from a Design of Experiments (DOE). The RS is an analytical function that serves as an approximation of the true underlying system behavior, allowing for the estimation of optimal input parameter settings that lead to desired responses. thus the optimization process is quick and does not require additional experiments or simulations to be performed. (Jones & Montgomery, 2019)

The concept of response surfaces was initially introduced in 1951 (Box & Wilson, 1951), where the proposal involved using a first-degree polynomial model to approximate a response variable. Since then, numerous techniques have been developed, each possessing distinct characteristics that yield different responses. In the ANSYS software, users have a range of response choices, including Genetic Aggregation, Standard Response Surface - Full 2nd-Order, Kriging, Non-Parametric Regression, and Neural Networks. These options provide diverse approaches to modeling and analyzing response variables, allowing for flexibility and customization in data analysis and optimization processes.

A Response Surface was created based on the estimation point from the CCD method as mentioned above, it offers the continuous change of the relationship between the objective function and the input design parameters. To enhance the accuracy of generated design points and ensure alignment with the requirements, there are different algorithms have been used. Among these methods is Genetic Aggregation, which offers the potential for auto-refinement.

a. Genetic Aggregation

The genetic aggregation model is one of the response surface methodologies that utilize an iterative genetic algorithm to solve optimization problems. Its core aim is to identify the optimal response levels for each output variable or parameter under consideration. By strategically selecting the most favorable response modes and integrating them, this model generates a set of response surfaces. These surfaces collectively yield the highest attainable response across various settings for each parameter or output variable.

The genetic algorithm employed in this approach iteratively explores and refines the values of input parameters or variables, ultimately maximizing the desired output parameter. Through this iterative process, the genetic aggregation model progressively converges toward the optimal solution, offering valuable insights into the relationships between variables and their impact on the overall response.

3.3.3 Optimization

After thoroughly exploring the design and understanding the relationships between input and output parameters, the next step is to embark on the optimization process. The tool DesignXplorer will be utilized in this process, incorporating a range of algorithms to identify the most optimal candidates, considering multiple objectives and performance trade-offs. The Response Surface Optimization (RSO) is one of the DesignXplorer types, the RSO utilizes a DOE-based approach and draws information from the RS. The computational time for this optimization is minimal, the time is spent in the DOE step.

The multi-objective genetic algorithm (MOGA) was employed as the optimizer to discover the most efficient design. The MOGA approach defined feasible solutions based on the optimization issue bounds, and the ideal answer was explored by assessing the maximum permissible Pareto front. MOGA is superior at calculating global optimal.(Ansarifard et al., 2020; Halder et al., 2017). Below is a schematic diagram of the process described above Fig. 3.4.

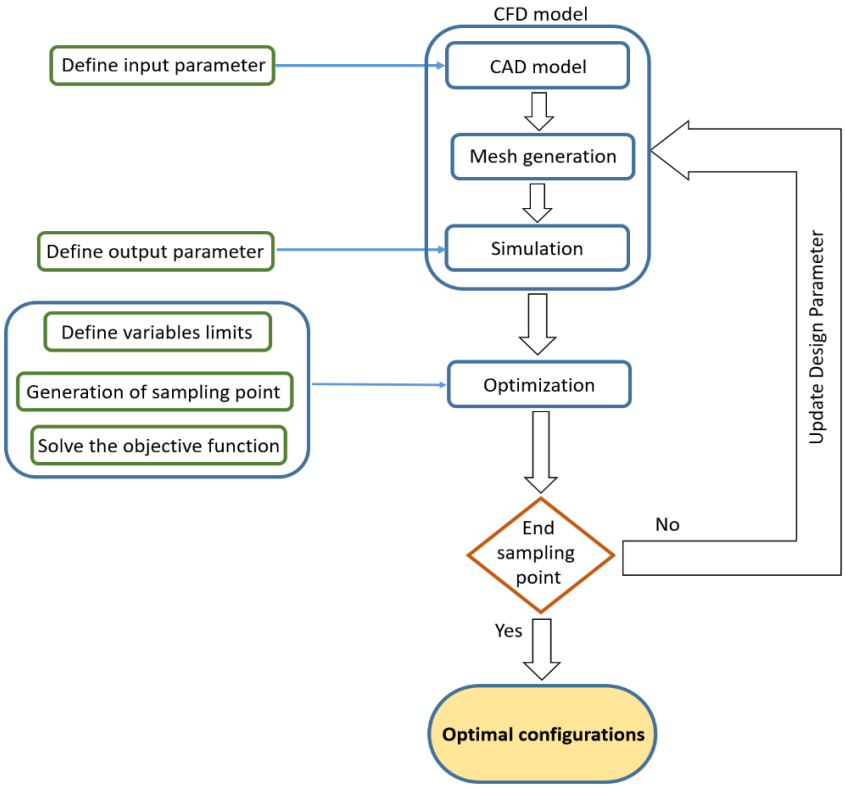

Fig. 3.4: Optimization procedure

3.3.4 Design variables and objective function

As mentioned, the current study is an automated optimization process of impulse turbines. wherein the primary focus is on maximizing efficiency, which serves as the objective function. This led to the Geometry-Design Modeler program being used to construct a base guide vane and blade profile with twelve design variables. By adjusting a wide range of parameters, this parametric guide vane and blade form might provide sufficient flexibility to generate a substantial design space. However, the quantity of input parameters was closely correlated with the computing time and cost of simulations. Therefore, it is necessary to decrease the number of study parameters in order to lower the computing cost. (Badhurshah & Samad, 2015).

The design of the rotor blades and how they were adjusted in relation to the guiding vanes were the main topics of the optimization study. Five parameters were found to be more effective than the other parameters available to regulate the blade's 2D profile through an

initial literature search. (Ansarifard, 2019; Ansarifard et al., 2019). These parameters were the radius of the guide vane (R_g), the angle of the guide vane (α_1), the rotor tip radius (R_t), the radius of the pressure side on the rotor (R_r), and the trailing edge relative angle of the rotor (β_2). These variables are shown in the parametric guide vane and blade profile in Fig. 3.5.

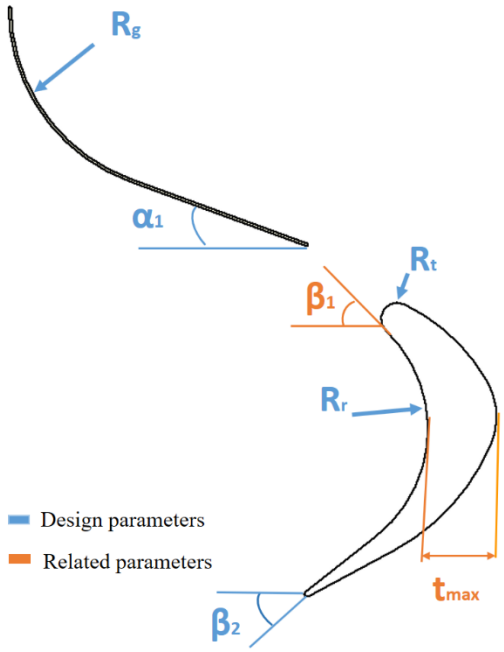

Fig. 3.5: Parameters used as the design variables (blue) and related parameters (red).

By changing the previous parameter also effected on the values of some other related parameters, such as inlet relative edge angle of the rotor (β_1) and maximum thickness of the rotor ($t_{max.}$)

Table 1 specifies the reference design's lower and upper ranges for the input parameters and their values (the initial outflow turbine geometry).

Table 1: Design variables with upper and lower limits

Design variables	Lower bound	Upper bound	Initial geometry
α_1 (Degree)	15	45	20
R_g (mm)	32.5	35	33.5
R_t (mm)	2	3.3	3
R_r (mm)	22.372	29	24.858
90-β_2 (Degree)	32	65	60

3.4 Numerical Model

3.4.1 Model Overview

The primary model of this study is an OWC (Oscillatory Water Column) Plant, including an axial twin air turbine. The model was solid modeled (Fig. 3.6) using the Geometry Design Modeler program in the ANSYS software package with the exact dimensions as the experimental setup in Refs. (Takao et al., 2011).

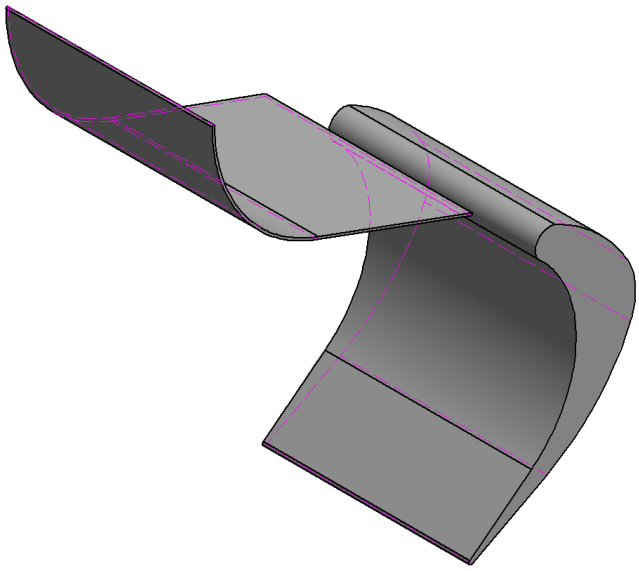

Fig. 3.6: 3D outside view of the model

The entire shape of the examined rotor is depicted in a 3D view in Fig. 3.6. The precise dimensions and arrangement are discussed in depth and illustrated in the following sections, along with the size and shape of each component.

3.4.2 Model Dimensions

The detailed dimensions of the studied rotor are shown in Fig. 3.7.

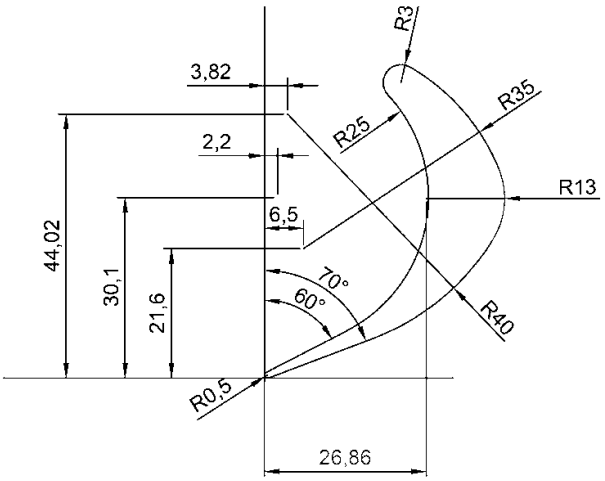

Fig. 3.7: Rotor profile (dimensions in mm)

The simulated turbine consists of 30 rotors with the following profile: the chord length of the rotor blade: 54mm; height: 44mm; tip diameter: 298mm; tip clearance: 1mm; solidity at mean radius: 2.02; the radius of leading-edge: 1.5mm; the radius of trailing edge: 0.5mm; hub to tip ratio: 0.7.

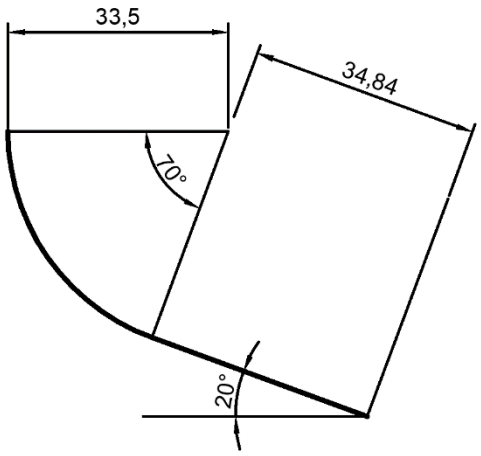

Fig. 3.8: Guide vane profile (dimensions in mm)

The guide vane profile used in this study consists of a straight line and a circular arc, as shown in Fig. 3.8. The chord length of guide vanes: is 70 mm; thickness: is 0.5 mm; solidity at mean radius: is 1.74. The setting angles of guide vanes are Θ = 20º to investigate the effect of guide vane setting angles on the performance (Fig. 3.8).

The rotor and guide vane were set in the configuration as shown in Fig. 3.9.

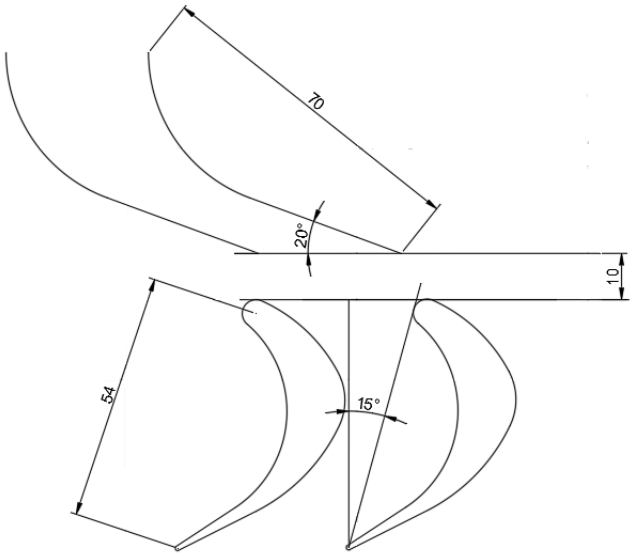

Fig. 3.9: Turbine configuration

The guide vane (G.V) and rotor blade domains comprise the entire simulated domain. A separate flow path is created for each domain, utilizing the Design Modular module. The length of the guide vane domain is 300mm, and the rotor domain is 400mm, as shown in Fig. 3.10.

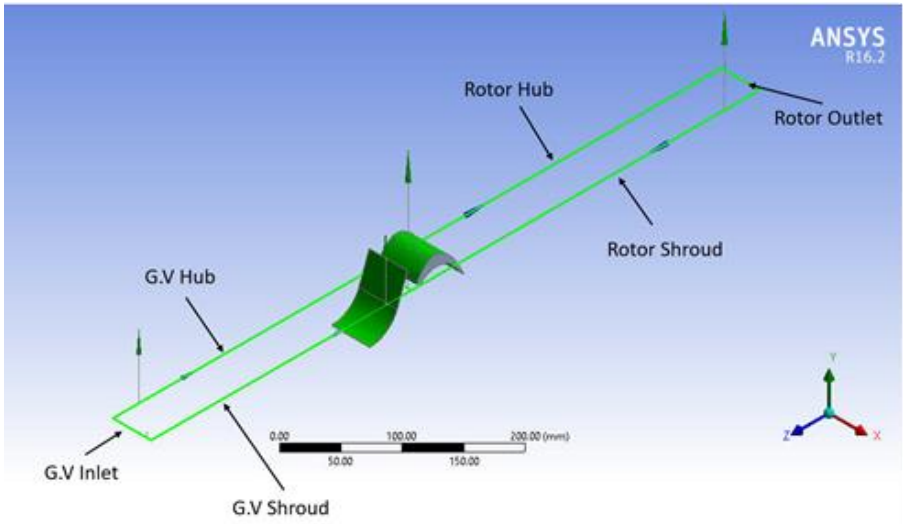

Fig. 3.10: Flow Path(snapshot from Design Modular software window)

3.4.3 Mesh Generation

After sketching the model in Geometry Design Modeler and creating the flow patterns, as indicated previously. TurboGrid software is employed to construct the model's mesh, comprised of Hexahedral cells of Quadrilateral type. Fig. 3.11 depicts a snapshot from the TurboGrid software and the mesh after generation.

Using an Intel Xeon Processor E5-2680 V3, 2.50 GHz with 48 GB RAM and 48 MB cash memory, the mesh was generated, and the boundary types were assigned and defined. The mesh details explained in the following sections with details

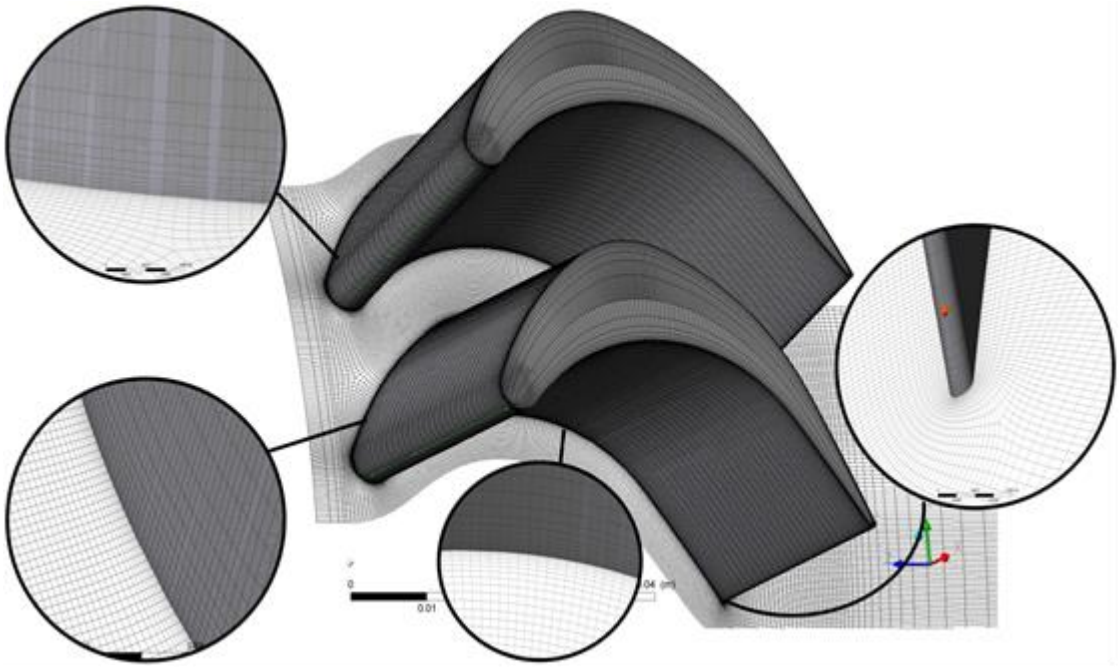

Fig. 3.11: Model volume mesh (snapshot from Tutbogrid software window)

a. Element Types

Table 2: Element Types details

Type	No. Elements
Hexahedral	5,855,150
Quadrilateral	643,666

b. Element Parts

Table 3: Element Parts Total

	No. Elements
Rotor	906,838
G.V	358,281
Total	1,265,119

Due to simulation boundary conditions, the rotor domain is separated into three parts: the rotor inlet (r-in), rotor blade(r), and rotor outlet (r-out).

Table 4: Element Parts details

	No. Elements		No. Elements
GV	1,320,960	r-SHROUD	85,220
GV-BLADE	35,200	r-in	172,260
GV-HUB	41,280	r-in -HUB	2,970
GV-INLET	5,760	r-in -SHROUD	2,970
GV-SHROUD	41,280	r-out	622,050
r	3,739,880	r-out -HUB	10,725
r-BLADE	134,500	r-out -OUTLET	18,850
r-HUB	60,160	r-out -SHROUD	10,725

the size of all mesh densities generated by setting the boundary layer refinement control to be the first element offset method and the near wall element size is the specified target value Y^+ to Reynolds number with the accepted range.

3.4.4 Solver Assumptions

The model was set up using the turbo-mode tool in ANSYS-CFX. The turbine domain is made up of one rotating section and two stationary sections. A stationary domain was utilized

at the inlet guide vanes (GVs). The location of the second stationary domain was chosen to lie between the rotor's output and the domain outlet Fig. 3.12.

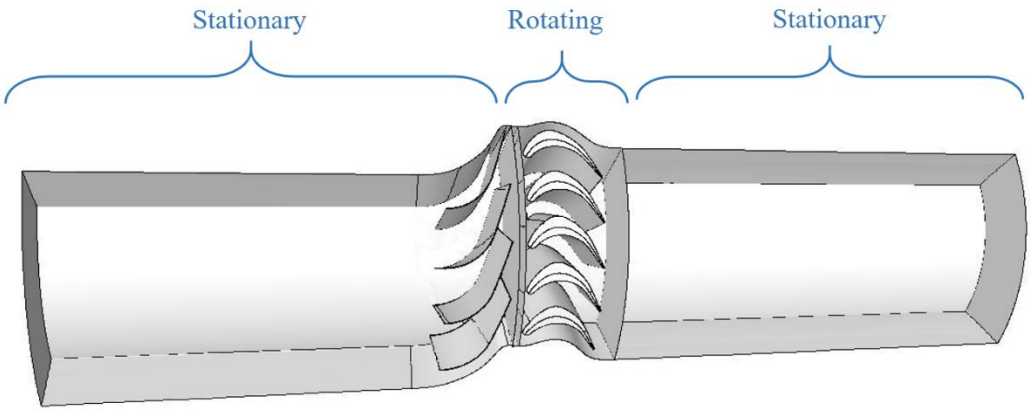

Fig. 3.12: Rotating section and stationary sections

3.4.5 Boundary Conditions

The periodic interface technique was used to simulate the rotating motion between the guide vane and rotor (Fig. 3.13) since the simulation model is a spinning turbine that rotates at rotation speed between 500-700 rpm to maintain the Reynolds number in acceptable value. A frozen rotor interface exists between the stationary and rotor domains (Liu et al., 2016). A periodic angular segment of the turbine, consisting of five rotor blades and four GVs, was chosen as the computational domain to reduce computation time and CPU (Pereiras et al., 2014). At the inlet, the normal speed was set. In order to simulate a range of flow coefficients Ø from 0.25 to 1.5, simulations were run over a range of normal speed at the inlet between 1.66 m/s and 9.97 m/s at a constant rotating speed (Table 5**)**. A pressure outlet was specified as the outlet border. Periodic boundaries were considered, and shared planes between either side of the two domains were regarded as interfaces.

Table 5: Inlet velocity range

Ø	0.25	0.5	0.75	1	1.25	1.5
Vin (m/s)	1.66	3.32	4.99	6.65	8.31	9.97

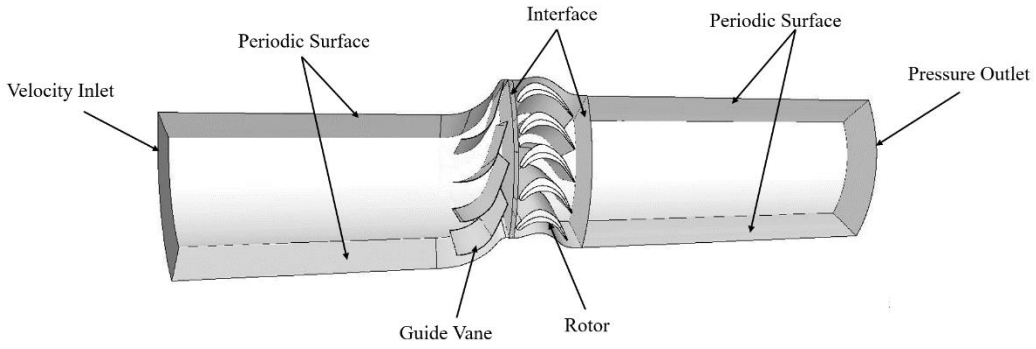

Fig. 3.13: Boundary conditions

In order to select the most suitable turbulence model a battery of simulations was carried out. The most used models for turbomachines are included within the Two-equation family, both k-epsilon and k-omega. The results obtained in this work reveal that there is only a slight difference between them as it is shown in the Fig. 3.14 . Many works ((Ansarifard et al., 2019; Halder et al., 2017; Pereiras et al., 2014) can be found using successfully both models. the k-omega model can provide more precise predictions of near-wall flows. for that, it was decided to employ a K-omega group.

The SST k-omega model stands out as a turbulence model that offers increased accuracy and versatility compared to the Standard k-omega model. However, it is worth noting that the SST k-omega model is computationally more demanding. The selection of the most suitable model depends on the unique characteristics of the simulated flow. it is observed that the Standard k-omega and SST models exhibit similar performance as shown in Fig. 3.14. Therefore, for the present study, the standard k-omega turbulence model was chosen. The simulations were conducted using the flow coefficient that yields maximum turbine efficiency (Ø=0.50) and mesh density with 1.2 million cells.

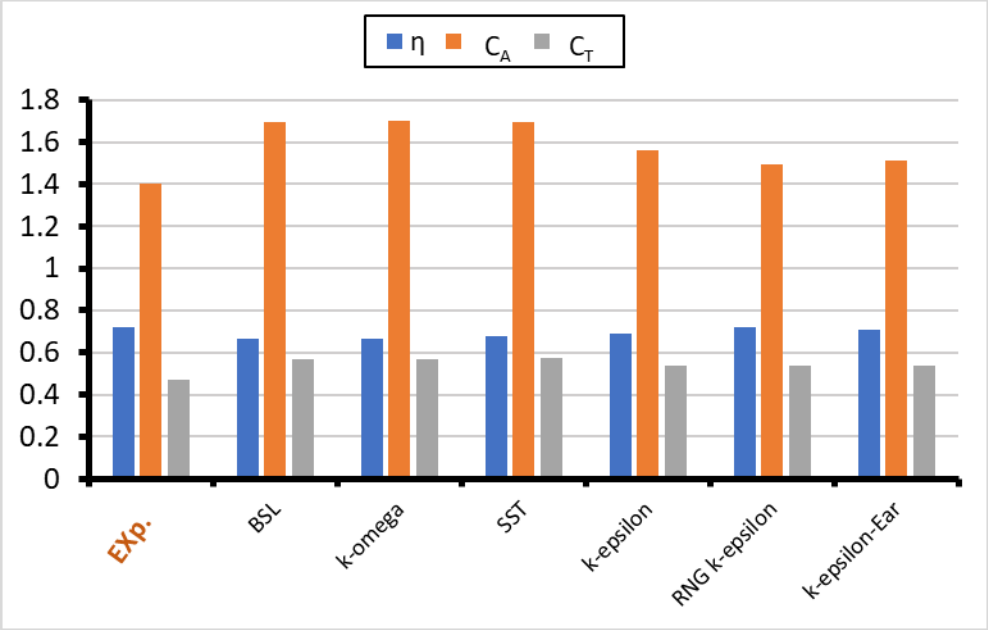

Fig. 3.14: comparison of turbulence models experimental tests (Takao et al., 2011). (Ø=0.50) (1.2 M cells)

All simulations used a convergence criterion of an RMS residual target of 10^{-6} and solved the flow as steady incompressible Reynolds-averaged Navier-Stokes (RANS) equations and unidirectional. For spatial discretization, the High-resolution advection scheme with second-order precision was utilized.

3.4.6 Mesh Sensitivity Analysis

To determine the number of grid elements needed for the current work. The mesh sensitivity analysis was carried out. The analysis of the results obtained for the terms of input coefficients C_A, torque coefficient C_T and the efficiency η, model is conducted using different mesh resolutions.

Four different mesh densities with 1.2, 2.1, 4.1 and 5.1 million cells were used for the numerical model domain discretization. As shown in Fig. 3.15, the deviation percentages for each cell number were evaluated compared to the maximum cell number (5.1 million). The results obtained from the case with 1.2 million cells provided the error of 0.93%, 0.46%, and 1.39% for C_T, C_A, and η respectively. Furthermore, these results were highly similar to those obtained by 5 million cells.

As a result, the case with a lower number of cells (1.2 million) was utilized in the simulations to minimize time and CPU consumption.

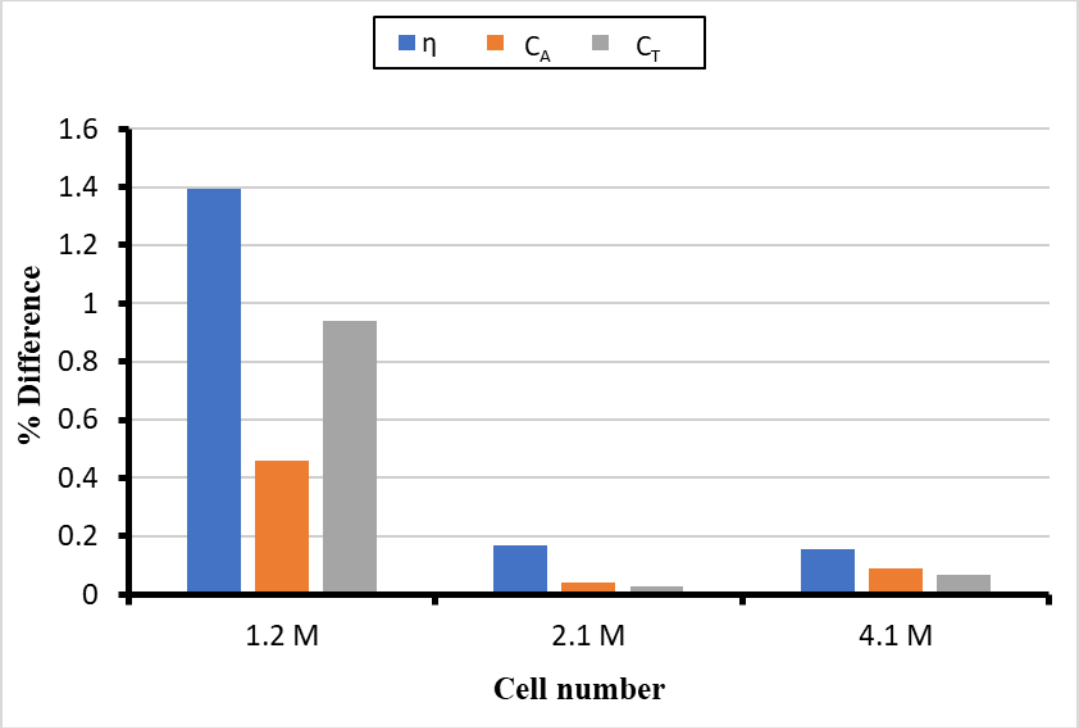

Fig. 3.15: Mesh independence studies, comparing the deviation from Case 5.1 M (maximum cell number) (Ø=0.50).

3.4.7 Model Validation

The numerical model was validated against wind tunnel measurements for unidirectional impulse turbines obtained by (Takao et al., 2011). Geometrical details of this turbine were provided in section **3.4.2**.

The torque coefficient, input coefficient, and efficiency predicted by CFD were compared to published experimental values in both flow directions. According to these results and seeing Fig. 3.18, at approximately Ø = 0.5, peak efficiency is observed. As the value of Ø increases, the efficiency shows a significant and rapid improvement until reaching this maximum point. Subsequently, there is a gradual decline in efficiency, albeit at a much gentler rate, leading to values of approximately $\eta \approx 0.4$ for higher flow rates. The CFD model underestimates the efficiency by 7%, but the trend is very well predicted and the difference is small enough to

consider that the model is validated. Furthermore, in both the torque coefficient and input coefficient, the CFD-predicted results follow a similar trend to the experimented data in both directions of the flow in torque coefficient, and input coefficient. The maximum difference between the experimental and numerical values is approximately ± 7.17% for the torque coefficient Fig. 3.17 and around ± 9.9% for the input coefficient Fig. 3.18.

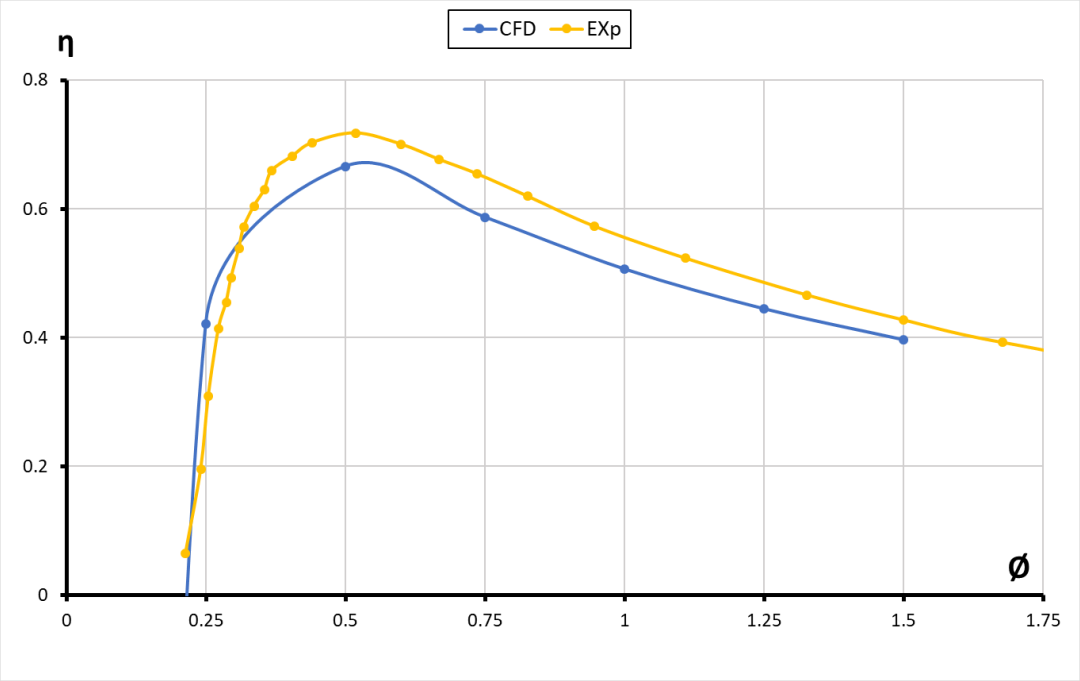

Fig. 3.16:Validation with experimental results from (Takao et al., 2011) the efficiency

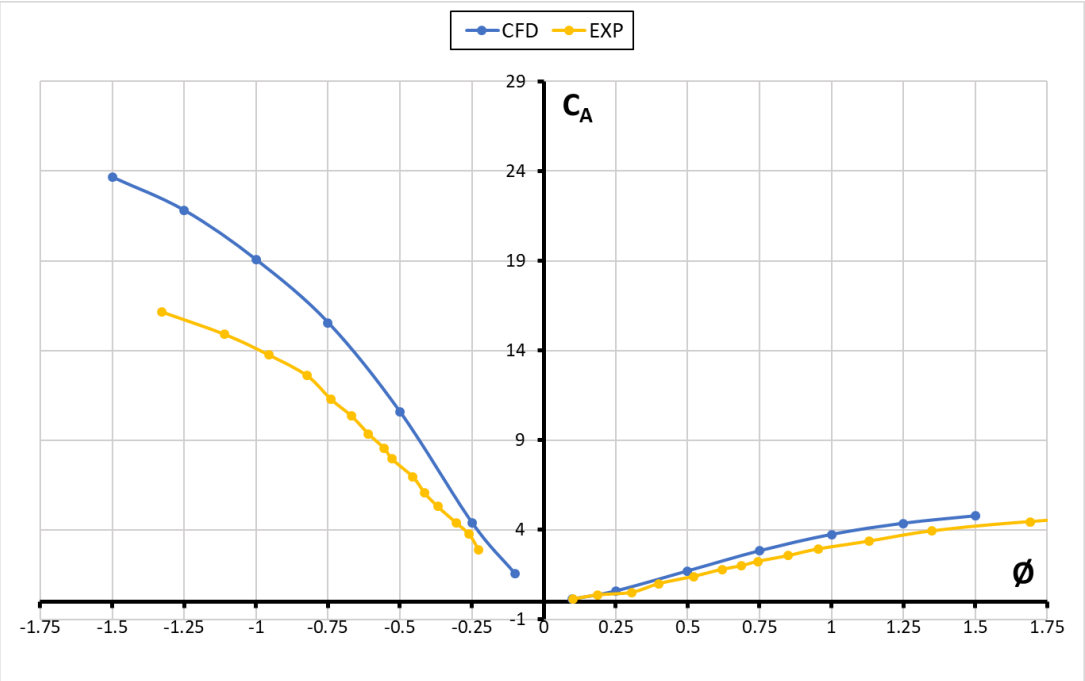

Fig. 3.17:Validation with experimental results from (Takao et al., 2011)) the input coefficient

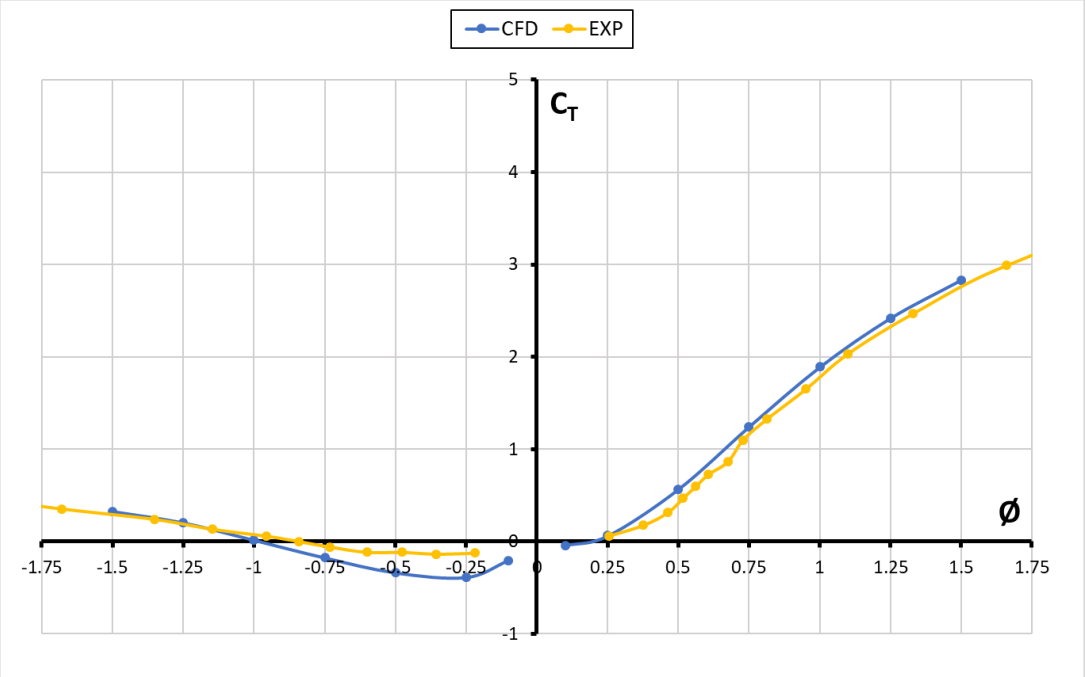

Fig. 3.18:Validation with experimental results from (Takao et al., 2011) torque coefficient

3.5 conclusion

The model was created using the ANSYS software package, with the Geometry Design Modeler employed for solid modeling. TurboGrid was used to construct the model's mesh, and CFX was utilized for simulating the model. To simulate the rotating motion between the guide vane and the rotor in the spinning turbine, the periodic interface technique was implemented. By selecting a computational domain with five rotor blades and four guide vanes, the computation time was reduced. The simulations encompassed a range of flow coefficients from 0.25 to 1.5, varying the normal speed at the inlet while maintaining a constant rotating speed. The inclusion of periodic boundaries and a pressure outlet ensured an accurate representation of the turbine's performance.

In this study, a numerical model was developed using the standard k-omega turbulence model and a mesh density of 1.2 million cells. To ensure the accuracy of the model, it was validated against published wind tunnel data. The results indicated a close agreement between the CFD model and experimental data, although the efficiency was slightly underestimated by 7%. However, the model accurately predicted the trends in torque and input coefficients, with maximum differences of approximately ±7.17% and ±9.9% respectively. In conclusion, the simulated model and CFD tools utilized in the study have enabled us to explore fluid dynamics with precision and accuracy. The details provided in this chapter pave the way for further analysis, discussion, and the eventual interpretation of the simulation results, contributing to the objective of the study.

Chapter 4

RESULTS AND DISCUSSIONS

4.1 Introduction

The DOE has been performed to determine the optimal configuration. Following the completion of the DOE, the genetic aggregation technique was used to construct response surfaces without refinement. Then, to decide the quality of DOE predictions, were simulated and incorporated alongside the initial DOE points.

Subsequently, the response surfaces of the most influential variables were manually refined to use them for analysis of the underlying problem. Ultimately, the Response Surface Optimization procedure was carried out using the MOGA method to identify candidates that optimize efficiency.

4.2 Results

Table 6 showcases the performance of design points with varying values of R_g, α_1, R_t, R_r, and β_2 for flow coefficient 0.50 . These design parameters, which are explained in the previous chapter (refer to Fig. 3.5), were selected within a specified range as indicated in the Table 1.

Table 6: The five geometrical parameters and the obtained efficiency

Name	α_1 (degree)	R_g (mm)	β_2 (degree)	R_r (mm)	R_t (mm)	η
1	32.5	34	59.5	24.858	2.6	0.564
2	20	34	59.5	24.858	2.6	0.660
3	45	34	59.5	24.858	2.6	0.447
4	32.5	33	59.5	24.858	2.6	0.564
5	32.5	35	59.5	24.858	2.6	0.564
6	32.5	34	54	24.858	2.6	0.576
7	32.5	34	65	24.858	2.6	0.555
8	32.5	34	59.5	22.372	2.6	0.542
9	32.5	34	59.5	27.3438	2.6	0.583
10	32.5	34	59.5	24.858	2	0.565
11	32.5	34	59.5	24.858	3.2	0.606
12	28.958	33.717	57.942	24.154	2.770	0.593
13	36.041	33.717	57.942	24.154	2.430	0.529
14	28.958	34.283	57.942	24.154	2.430	0.594
15	36.042	34.283	57.942	24.154	2.770	0.529
16	28.958	33.717	61.058	24.154	2.430	0.588
17	36.042	33.717	61.058	24.154	2.770	0.511
18	28.958	34.283	61.058	24.154	2.770	0.580
19	36.042	34.283	61.058	24.154	2.430	0.519
20	28.958	33.717	57.942	25.562	2.430	0.603
21	36.042	33.717	57.942	25.562	2.770	0.541
22	28.958	34.283	57.942	25.562	2.770	0.604
23	28.958	33.717	61.058	25.562	2.770	0.597
24	36.042	33.717	61.058	25.562	2.430	0.534
25	28.958	34.283	61.058	25.562	2.430	0.599
26	36.042	34.283	61.058	25.562	2.770	0.534
27	32.5	34	59.5	24.858	2.6	0.564
Ref.	20	33.5	60	24.858	3	0.664

The accuracy of the algorithm in predicting the relationship between the input and output parameters was continuously monitored. To further enhance accuracy, a manual integration

step was carried out to incorporate the best candidate obtained from the optimization process into the response surface. The optimization process was then iterated, repeating this step until a significant accuracy (with an error = 0.14%) was achieved between the predicted results and the CFD results. In the Table 7, η_{RS} denotes the efficiency predicted by the response surface, η_{CFD} shows the efficiency obtained from CFD simulations and %Err determines the percentage of error between the η_{RS} and η_{CFD} results.

After 24 iterations, the best-optimized candidate was identified, resulting in the highest increase in efficiency between the initial and optimized geometry, amounting to 5.04%. The operation requires a total of 216 hours to complete, with each individual run taking 9 hours.

Table 7: Comparison of the CFD-verified and predicted results

Name	η_{RS}	η_{CFD}	%Err	% increase
Initial	-	0.664	-	-
Optimized	0.698	0.699	-0.14	5.04

The optimized design characteristics are shown in Table 8. Also, Fig. 4.1 displays both rotor geometries the initial and optimized.

Table 8: Design characteristics of the optimized turbine

Design variables	Initial geometry	Optimized geometry
α_1 (Degree)	20	19.07
R_g (mm)	33.50	32.83
R_t (mm)	3	3.15
Rr (mm)	24.85	28.47
t_{max} (mm)	11.85	15.47
β_1 (Degree)	47.96	58.66
90-β_2 (Degree)	60	53.76

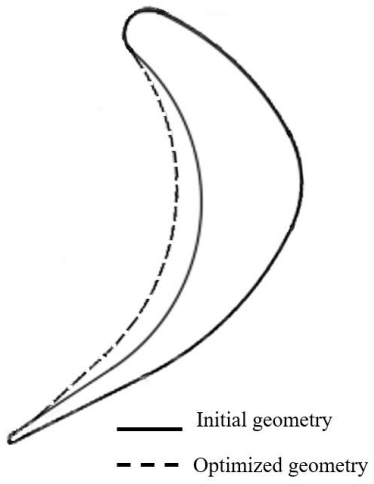

Fig. 4.1: Initial and optimized rotor geometry.

It is seen that the most prominently altered parameters are the rotor's pressure side radius (R_r) and the trailing edge relative angle of the rotor (β_2). Fig. 4.1 demonstrates how modifications in these two parameters distinctly affect the blade's geometry, resulting in a thicker profile and reduced deflection.

4.3 Sensitivity analysis of input parameters

Fig. 4.2 displays the sensitivity of the output parameters to the rate of change for each input parameter. The trends of efficiency at the optimal design point have been used to construct the local sensitivity statistics, which demonstrate the rate at which each input parameter affects the output parameters. Examines the influence of each input parameter on the output parameters separately (ANSYS, 2014). A parameter is indicated with a positive sign if its increase results in the optimization journey's objective function being satisfied. In other words, the positive and negative bars in the Figure, respectively, illustrate the parameter's increase and reduction in relation to its starting values. Fig. 4.2 makes it clear that, of the list of design parameters examined in this step, The parameter of highest sensitivity regarding efficiency is the guide vane angle (α_1), The guide vane angle plays a critical role in shaping the fluid flow that enters the rotor blades. By manipulating the guide vane angle, the turbine can precisely manage the flow direction, velocity, and energy conversion process., followed by the radius of pressure side on the rotor (R_r), and the rotor tip radius (R_t).

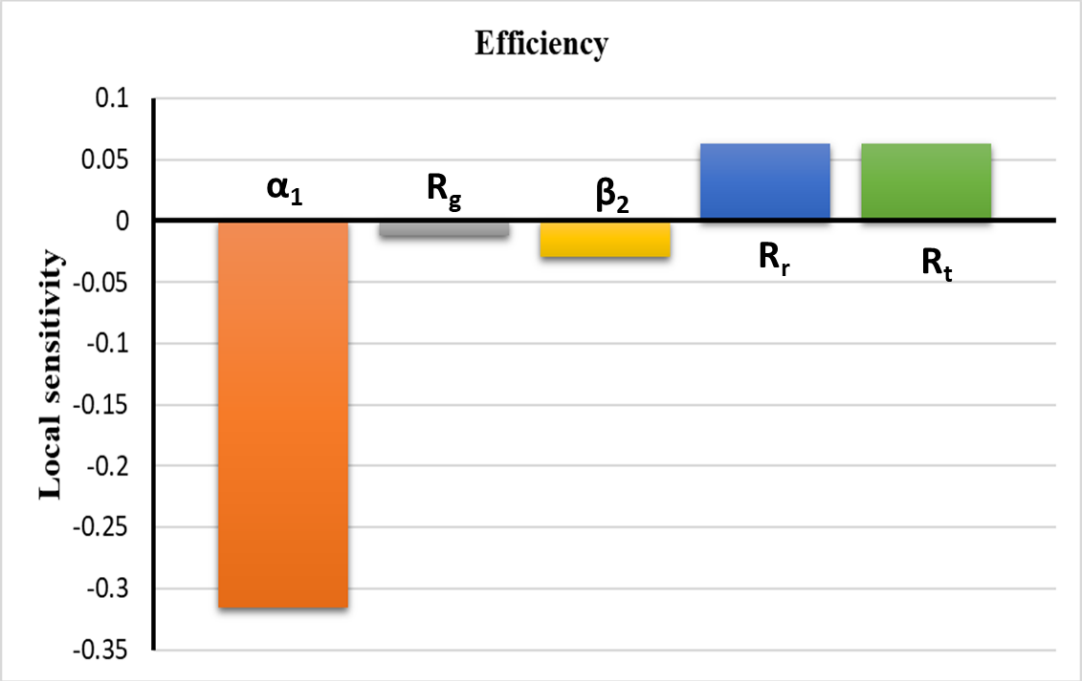

Fig. 4.2: Local sensitivity of input parameters on efficiency.

4.4 Efficiency surface plot

The 3D response of efficiency based on the two most sensitive parameters (α_1 angle and R_r radius) is shown in Fig. 4.3 It is important to note that modifications to the input parameter combination can lead to the optimal design point. The optimal efficiency was determined according to the variation limits specified by these two input parameters, as this figure demonstrates.

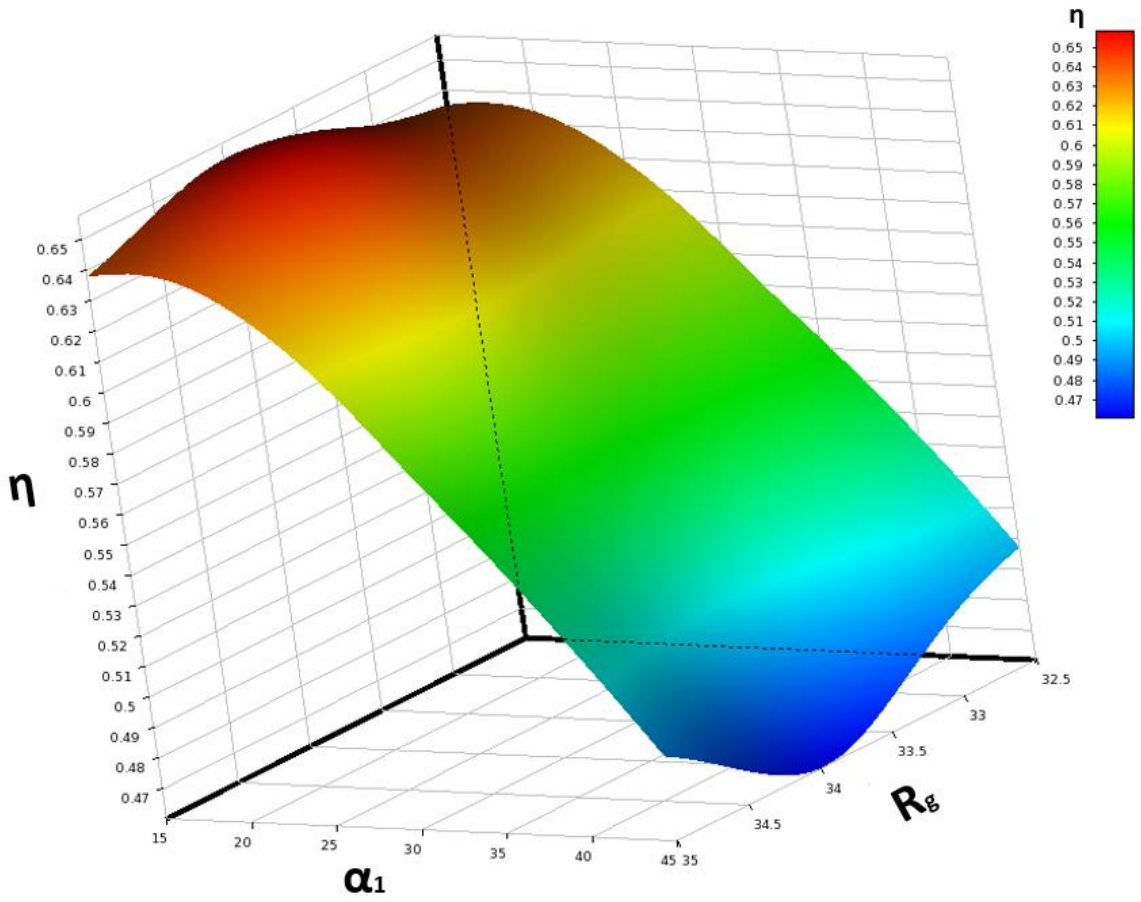

Fig. 4.3: Turbine efficiency response versus the most sensitive input parameters.

4.5 Comparison of turbine characteristics between the initial and optimized geometry

The performance of the optimized axial impulse turbine geometry was compared to the initial geometry found in Table 1. This comparison was conducted following the completion of six runs, with each run requiring a duration of nine hours.

According to Fig. 4.6, the optimized geometry, which was created by determining the optimum configuration of the input parameters used in this study, the optimized geometry, at low flow coefficients, exhibited a 28% improvement in efficiency relative to the initial design.

This observation is supported by a slight increase in the torque coefficient (C_T). Interestingly, this increase in generated torque contradicts the theoretical expectation, considering that the

optimized blade geometry leads to reduced flow deflection (smaller β_2). However, the optimized blade design features increased thickness, which results in amplified flow velocities within the rotor channels. Consequently, this causes higher velocities at the outlet, ultimately contributing to the slight rise in generated torque.

The optimized geometry shows a noteworthy increase in the C_A during the reverse mode (Fig. 4.5), even though it was not explicitly targeted in the optimization objective function. This observation is particularly intriguing as it highlights the potential for improved performance in a Twin Turbine System, as will be demonstrated later. Additionally, when examining the C_T in reverse mode (Fig. 4.6), it becomes evident that the optimized geometry is likely to generate a stronger braking effect during reverse operation.

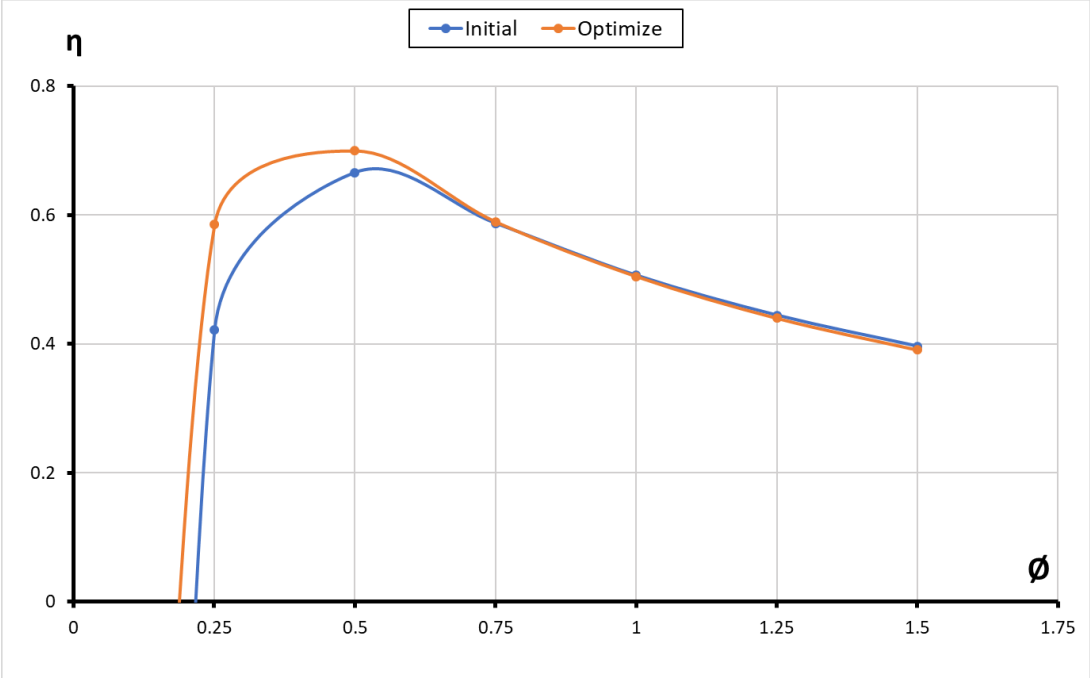

Fig. 4.4: Comparison of the efficiency of the optimized design with the initial turbine geometry.

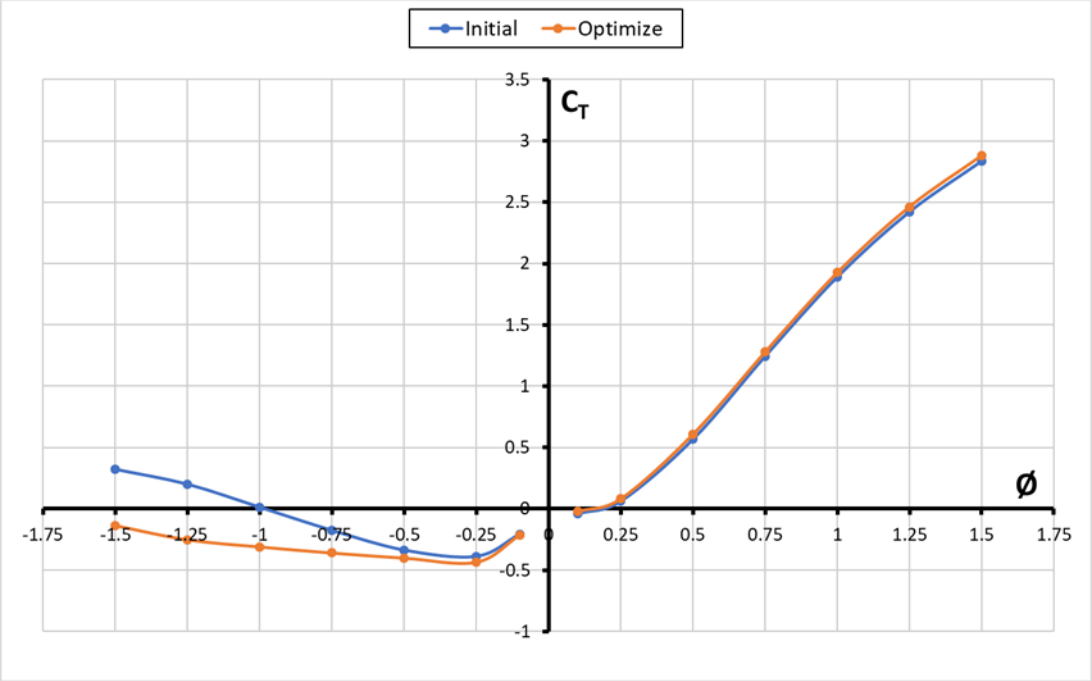

Fig. 4.5: Comparison of the torque coefficient of the optimized design with the initial turbine geometry.

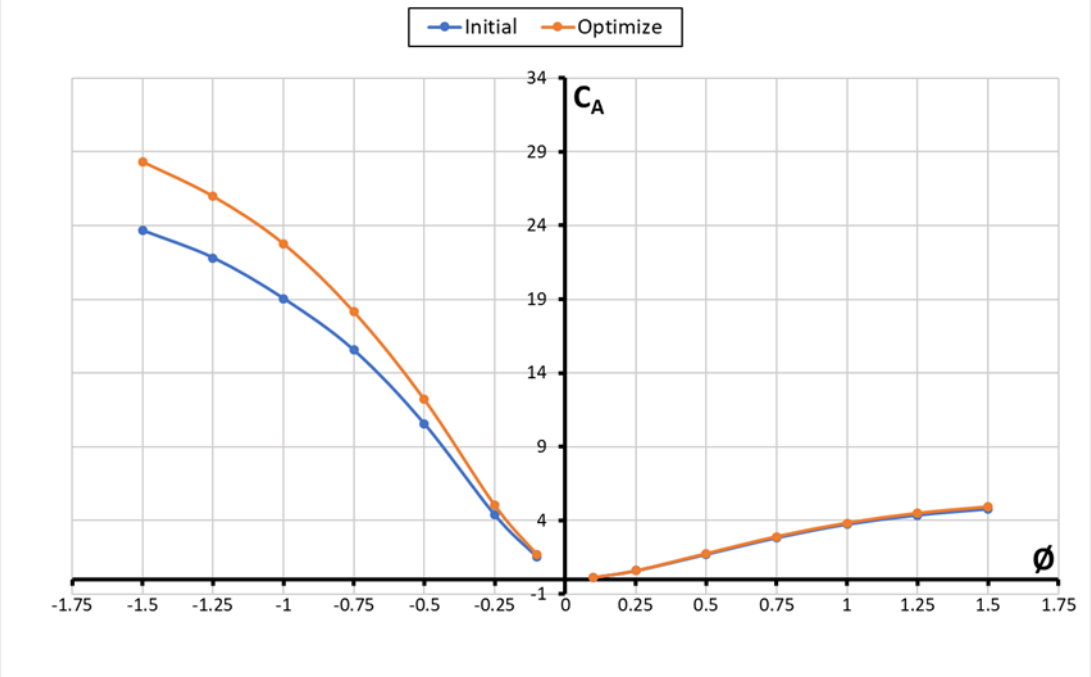

Fig. 4.6: Comparison of input coefficient of the optimized design with the initial turbine geometry.

4.6 Loss distribution – Rotor efficiency

In order to know exactly where the improvement comes from a flow analysis was conducted. Loss distribution and its sources have been analyses for both initial and optimized geometry.

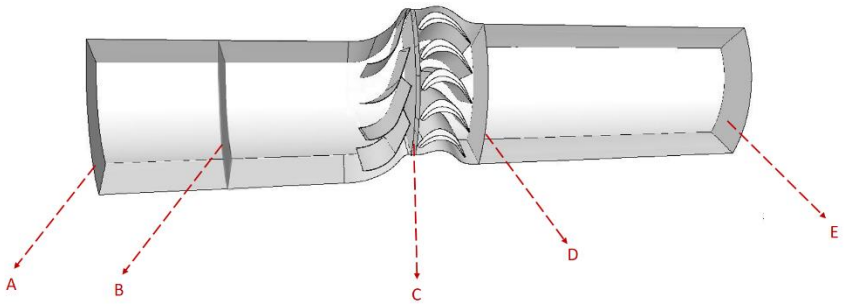

Fig. 4.7: The flow analysis domains.

As shown in Fig. 4.7 the total domain (A-E) is divided into four parts inlet(A-B), G.V(B-C), rotor(C-D), and outlet(D-E). The total pressure drop was measured and analyzed separately for each domain as follows considering the subscription is referred to as the section letter for direct flow (A, B, C, D&E) and **i+1** the section following the one before. The reverse flow on the contrary, takes **i-1** for the next domain.

$$\%Energy\ loss_{domain} = \frac{P_i - P_{i+\frac{1}{i}-1}}{\Delta P_{A-E}} \tag{4.1}$$

Except the rotor domain, which is calculated calculate as follows:

$$\%Energy\ loss_{rotor} = \frac{(P_C - P_D)\left(\frac{T_o\ \omega}{Q}\right)}{\Delta P_{A-E}} \tag{4.2}$$

The findings show that the rotor blade shape has a substantial impact on the turbine's performance, including torque and input power. When Fig. 4.6 and Fig. 4.8 are compared, it is evident that the optimized geometry at lower flow coefficients greatly reduced the energy losses in the rotor domain by about 66.2% & 22.3% at Ø=0.25,0.50 respectively.

Comparing Fig. 4.8 and Fig. 4.9 clear difference is seen between both geometries at low flow coefficients. The loss at the rotor is much smaller in the optimized geometry, which is why the efficiency at low flow coefficients seen in Fig. 4.6-a is better in optimized geometry.

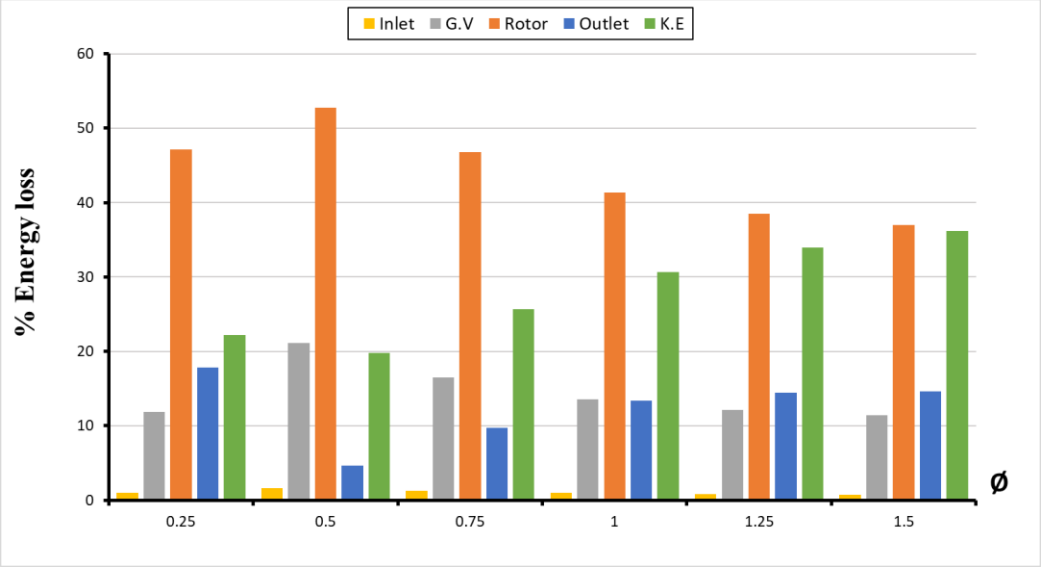

Fig. 4.8: Loss distribution for initial geometry in direct flow.

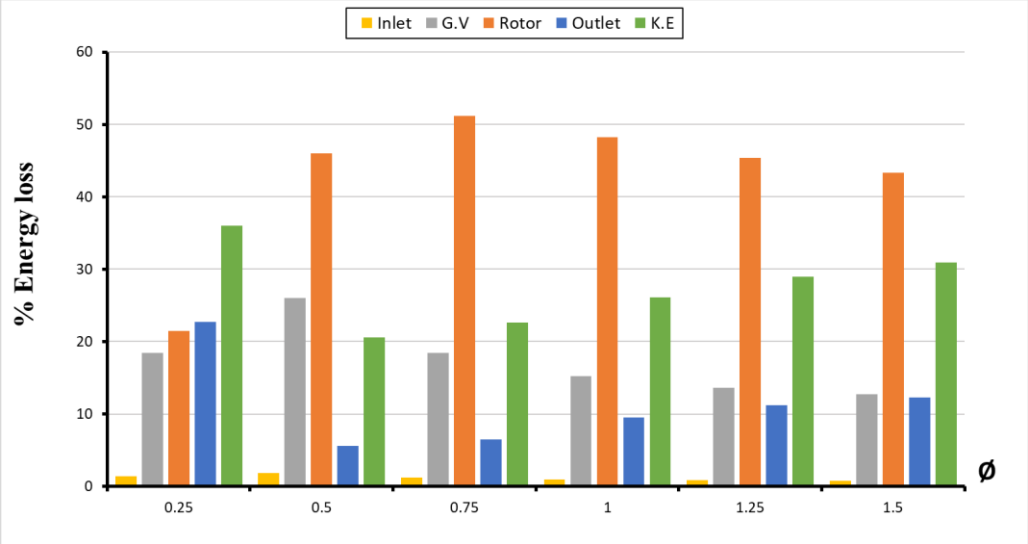

Fig. 4.9: Loss distribution for optimized geometry in direct flow.

This is clearly appreciated in the rotor efficiency, which is a crucial factor in the performance of any turbine. It is defined as the ratio of the actual power output of a turbine to the theoretical power that can be extracted from the fluid flow through the rotor blades(Denton, 1993). Fig. 4.10 shows a comparison between the initial and optimized curves for rotor efficiency where it is shown that the maximum efficiency reached by the optimized geometry exceeds 10% of the previous one. Although, at large flow coefficients the initial geometry has a slightly better performance. From that picture is clear that the best efficiency point has been

displaced towards lower flow coefficients. This is produced, as it will be shown afterward, due to the reduction of incidence losses at the rotor leading edge of the new blade.

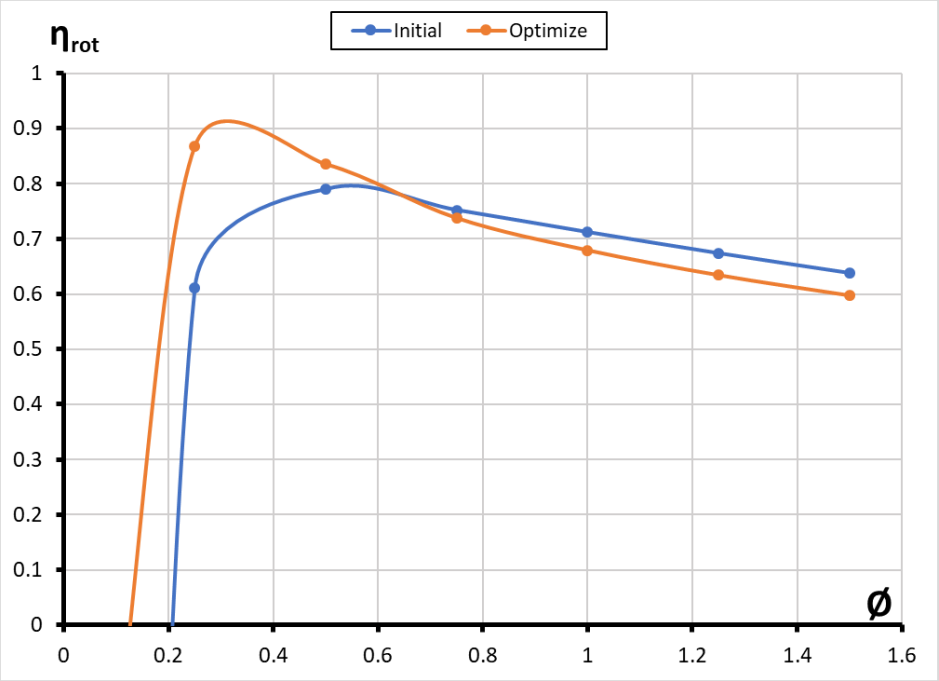

Fig. 4.10: Comparison between the initial and optimized curves for rotor efficiency in direct flow.

An analysis of the velocity streamlines around a rotor shows how changes in the rotor tip radius (R_t), the radius of the pressure side on the rotor (R_r), and the trailing relative edge angle of the rotor (β_2) can affect the efficiency of the rotor at low-speed flow. Fig. 4.11 shows the effect of these changes on the flow around the rotor for Ø=0.25 in the direct flow direction. Have clearly reduced the vortex created at the blade leading edge, improving remarkably the performance of the rotor at low flow coefficients.

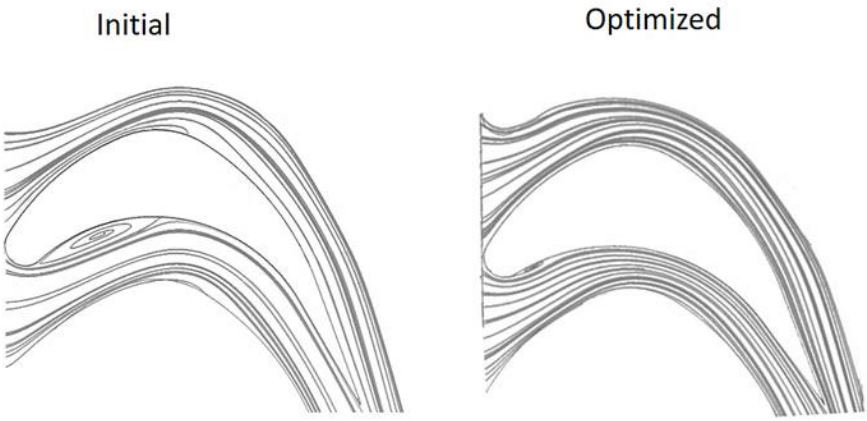

Fig. 4.11: Velocity streamline for direct flow in the hub at Ø=0.25

The angles of flow are then analyzed to reveal the flow patterns. The flow angles can be perceived in the inlet and outlet of a rotor, respectively. In Fig. 3.1 , references used in this analysis are depicted. The analysis begins with the direct flow, where the (α_1) at the rotor inlet is scrutinized to determine the extent to which the flow is guided by the guide vane. The analysis reveals that the flow is effectively guided, given that the flow angle closely approximates the geometry solid angle (α*=20°).

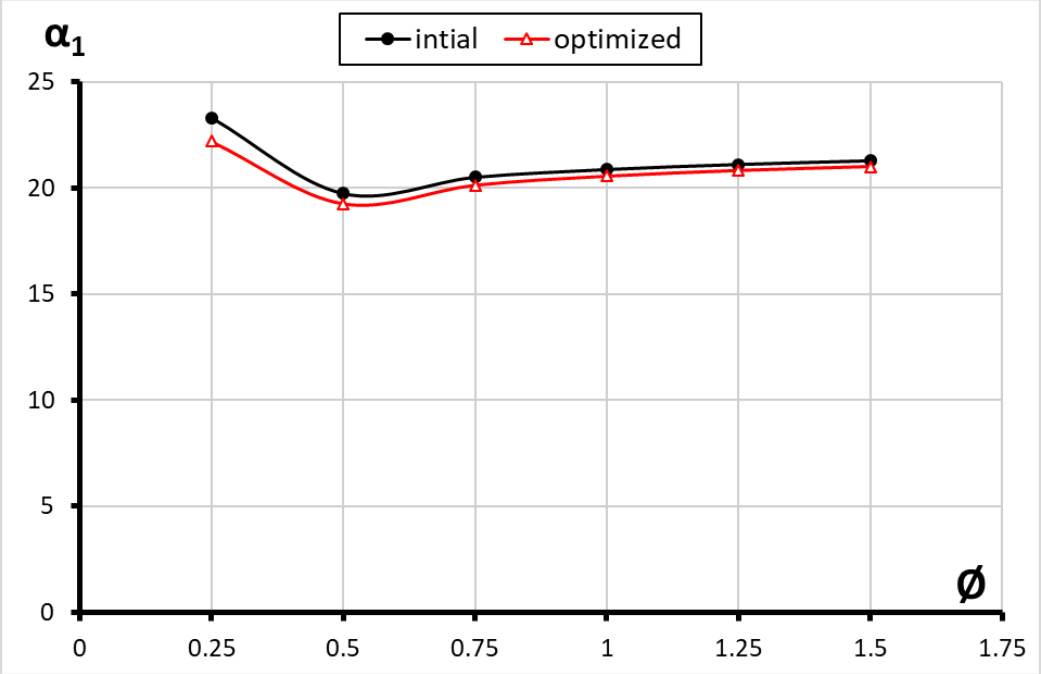

Fig. 4.12: Absolute flow angle at the leading edge of the rotor in direct flow.

However, an assessment of the relative flow angle with the inlet relative edge flow angle of the rotor (β_1) reveals that low flow coefficients (Ø=0.25) lead to a significant incidence of losses at the rotor inlet. As shown in Fig. 4.8 and Fig. 4.13, this is due to the notable difference between the two angles β_1 = 149° and β* = 47.96° , with β* representing the inlet relative edge angle of the solid rotor . Consequently, this discrepancy leads to a considerable decline in the overall efficiency of the system.

In addition to that, the behavior of β_1 is similar for both geometries due to the nearly identical value of α_1. Nonetheless, the crucial factor lies in the difference between β_1 and β*, which is significantly greater in the original geometry. The disparity affects the rotor's overall performance across the entire range of flow coefficients.

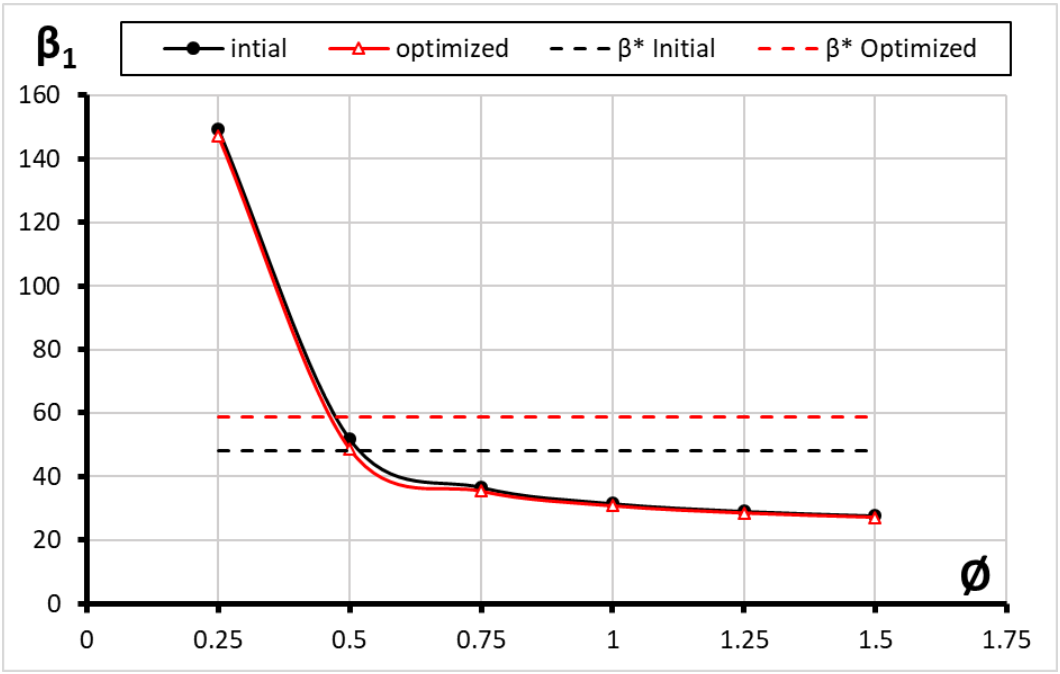

Fig. 4.13: Relative flow angle at the leading edge of the rotor in direct flow.

Upon comparing the flow angle at the rotor outlet to the trailing relative edge angle (β_2), it is observed that the difference does not exceed 2% (Fig. 4.14). This finding indicates that the guidance provided by the rotor at the trailing edge is highly effective.

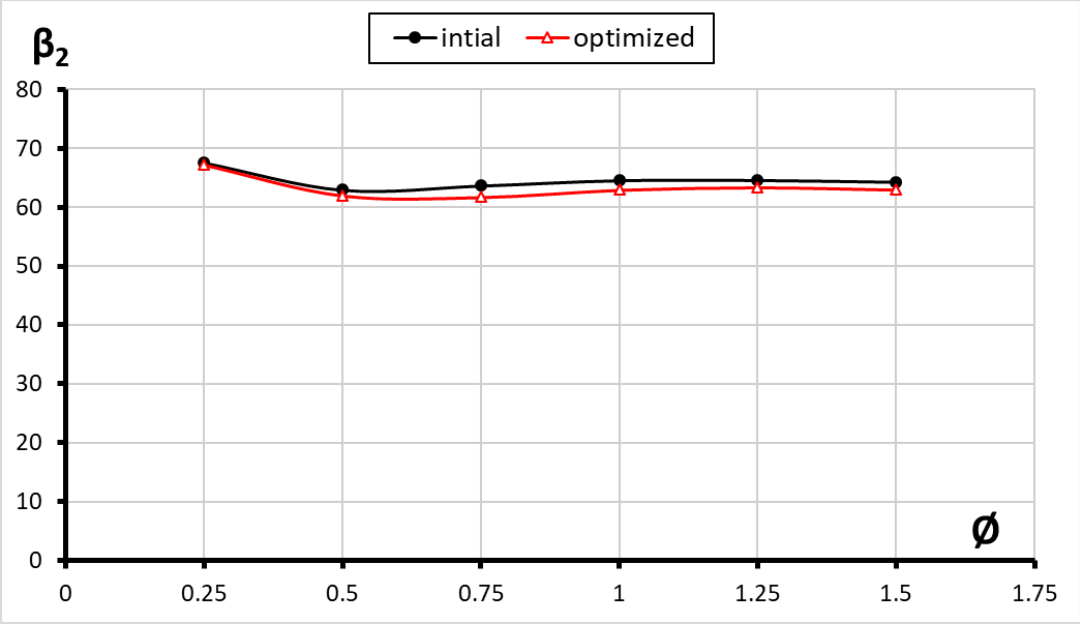

Fig. 4.14: Relative flow angle at the trailing edge of the rotor in direct flow.

However, as flow coefficients increase, the analysis of rotor losses in Fig. 4.8 and Fig. 4.9 highlights a substantial difference between the absolute flow angle (α_2) and the optimal 90° angle, as illustrated in Fig. 4.15.

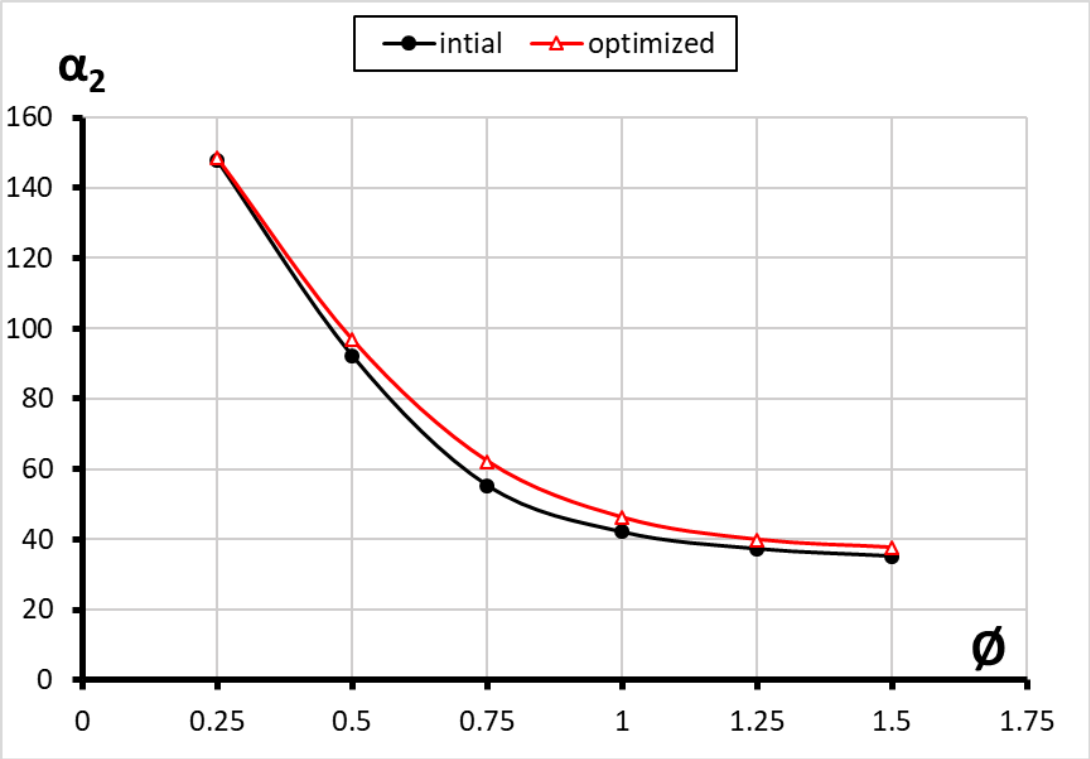

Fig. 4.15: Absolute flow angle at the tail edge of the rotor in direct flow.

In the reverse flow of turbine operation, the flow exits from the rotor and traverses the guide vanes. As is seen in Fig. 4.18 & Fig. 4.19 the loss distribution for both initial and opt geometry is quite similar. Nevertheless, there are slight differences caused by the changes in the geometry. It is shown that the loss is concentrated in the GV for the initial geometry, whereas the rotor takes more importance in the optimized geometry. Since the geometry upstream of the rotor in reverse mode is the same, this increment comes from what is happening within the rotor.

Firstly, due to the new β_1 in reverse mode (see Fig. 3.1) the incidence loss has increased because the difference between β_1& β^* in reverse mode (Fig. 4.17) is larger in the case of the optimized geometry, thus leading to a larger incidence loss. Besides, the thickness of the blades of the optimized geometry leads to an unexpected flow detachment with the rotor

channel, see Fig. 4.20. This is particularly important at lower flow coefficients where the loss at the rotor takes more importance in the loss distribution, see Fig. 4.19.

Comparing Fig. 4.18 and Fig. 4.19 it can be seen that the difference between initial and optimized geometry tends to be constant which suggests that as the flow coefficients increase, the flow detachment within the rotor gets less important. In contrast, the incidence loss takes full weight. This reasoning is also supported by Fig. 4.21, where it is shown that the behavior of the incidence loss at the GV inlet is almost the same for both geos. So as expected, the loss at the GV is almost similar for both geometries

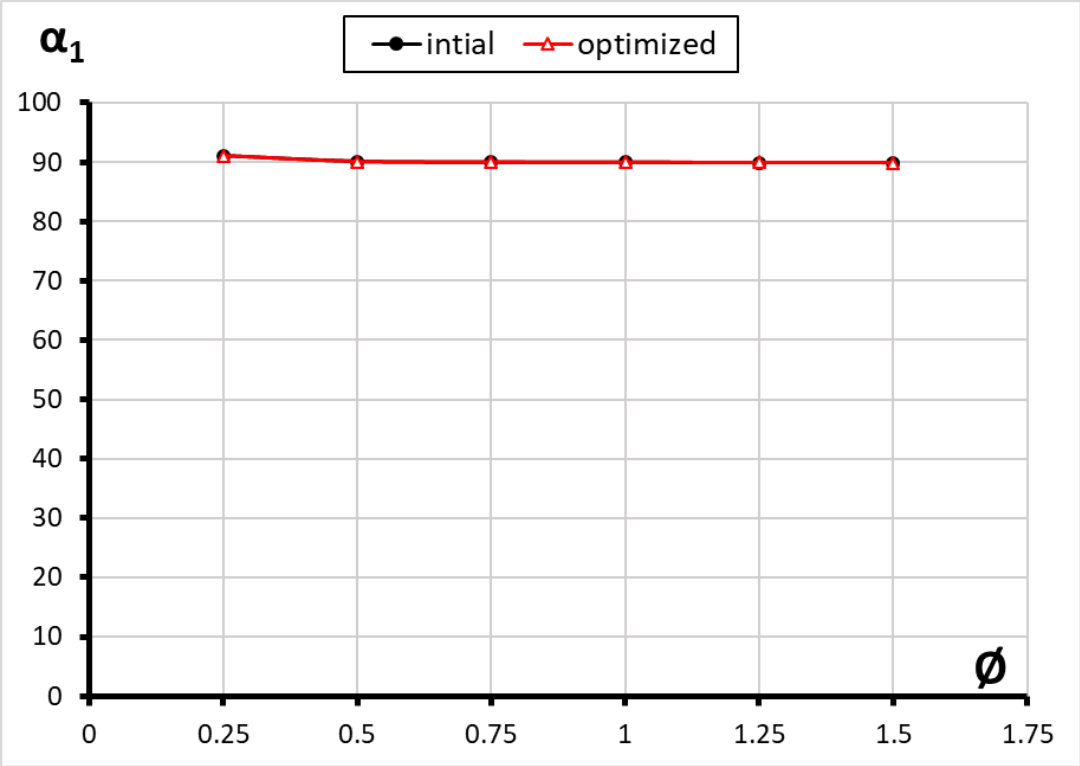

Fig. 4.16: Absolute flow angle at the leading edge of the rotor in reverse flow.

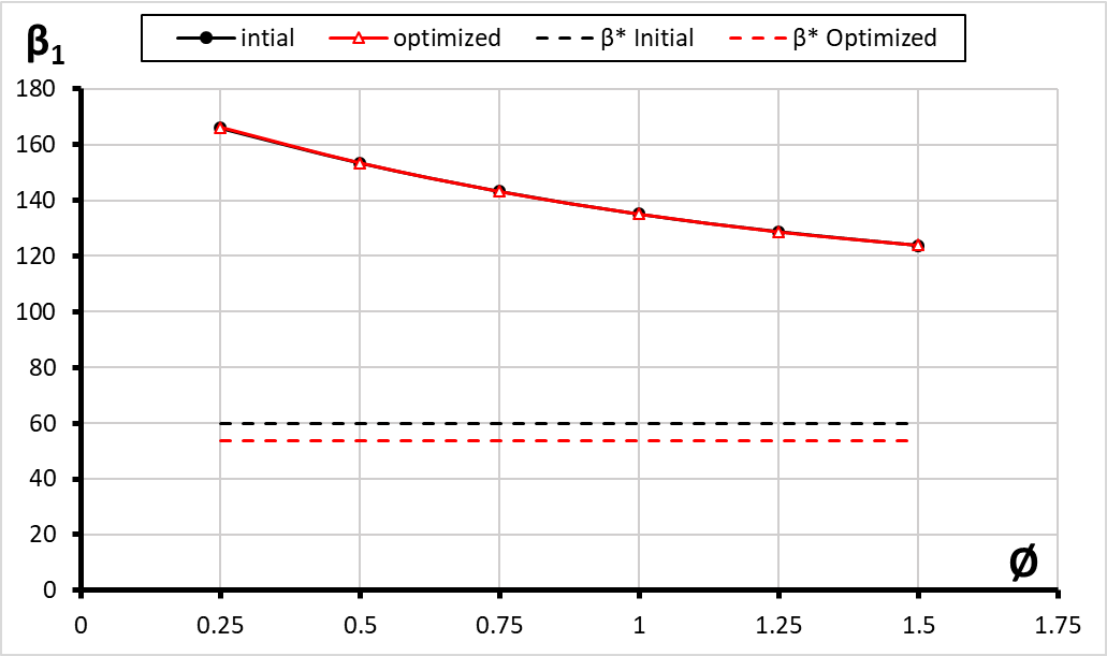

Fig. 4.17: Relative flow angle at the leading edge of the rotor in reverse flow.

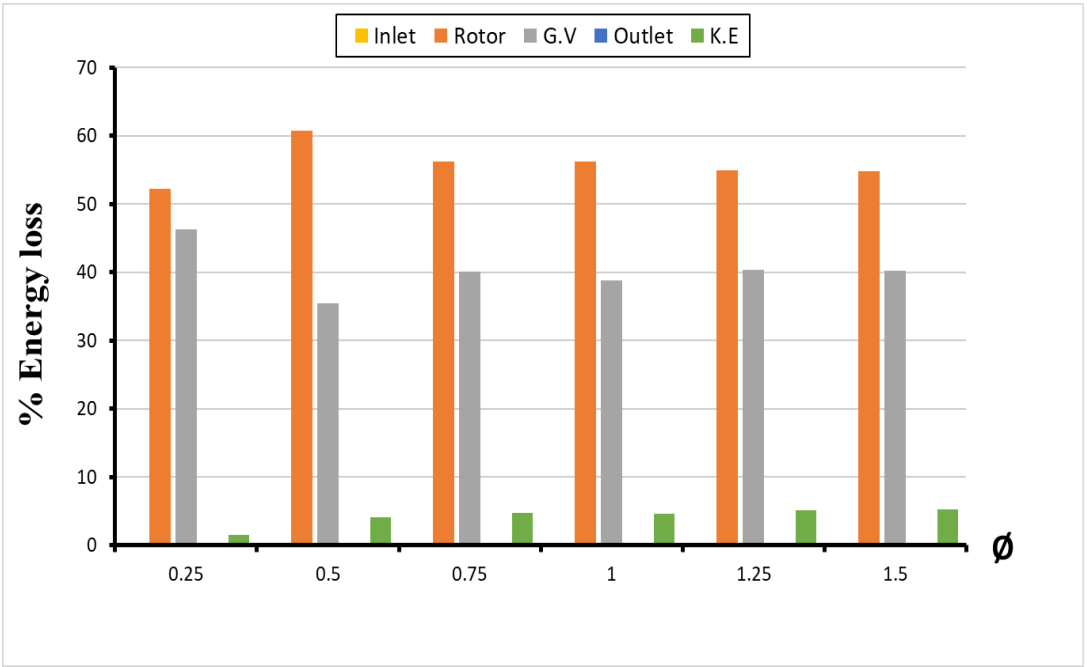

Fig. 4.18: Loss distribution for initial geometry in reverse flow.

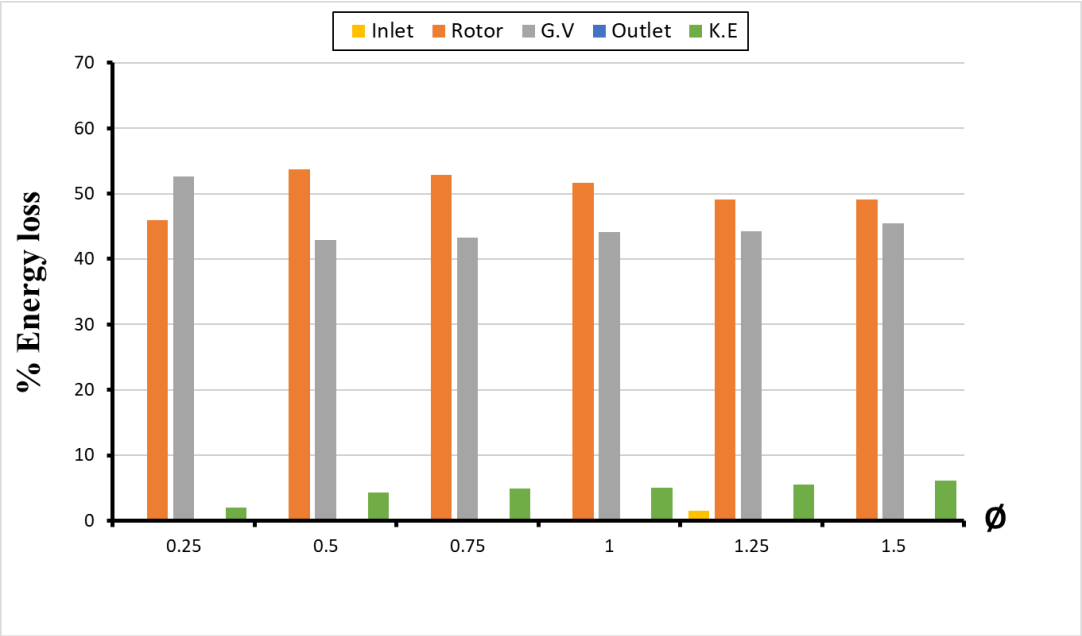

Fig. 4.19: Loss distribution for optimized geometry in reverse flow.

This disparity leads to the separation of velocity streamlines, as illustrated in Fig. 4.20. Additionally, inadequate alignment at the blade leading edge may result in excessive secondary losses within the channel between rotors, which causes the separation in the velocity streamlines in this zone Fig. 4.20

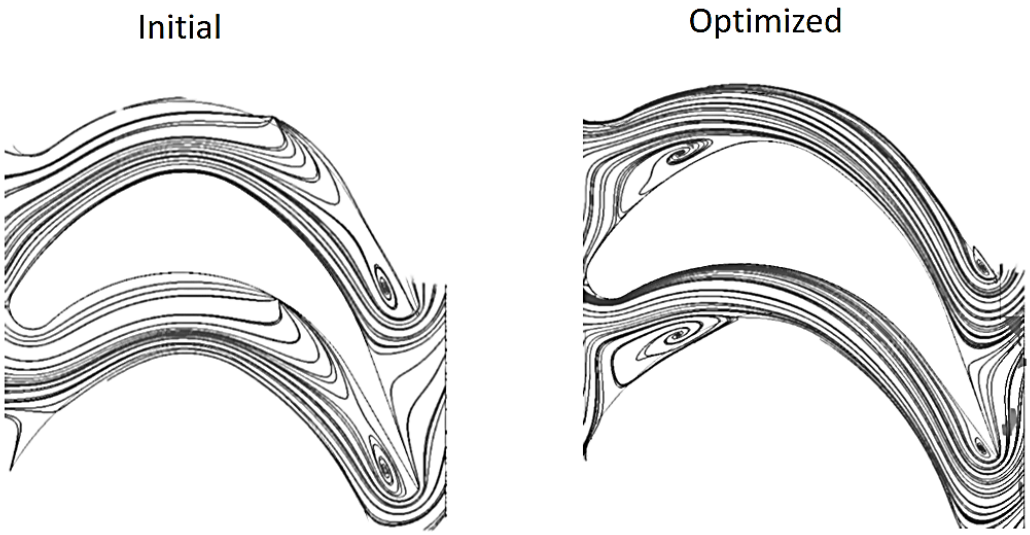

Fig. 4.20: Velocity streamline for reverse flow in the hub at Ø=0.25

The analysis of the absolute and relative flow angles at the rotor outlet shows the blade does not make good guidance at the trailing edge (Fig. 4.21 & Fig. 4.22), also creating large losses at the guide vane's leading edge, as depicted in Fig. 4.18 & Fig. 4.19 . However, this is not problematic since reducing the flow rate through the turbine in reverse flow is desirable. These losses impede the flow in this direction and redirect the air through the other turbine, which operates in direct flow and produces energy.

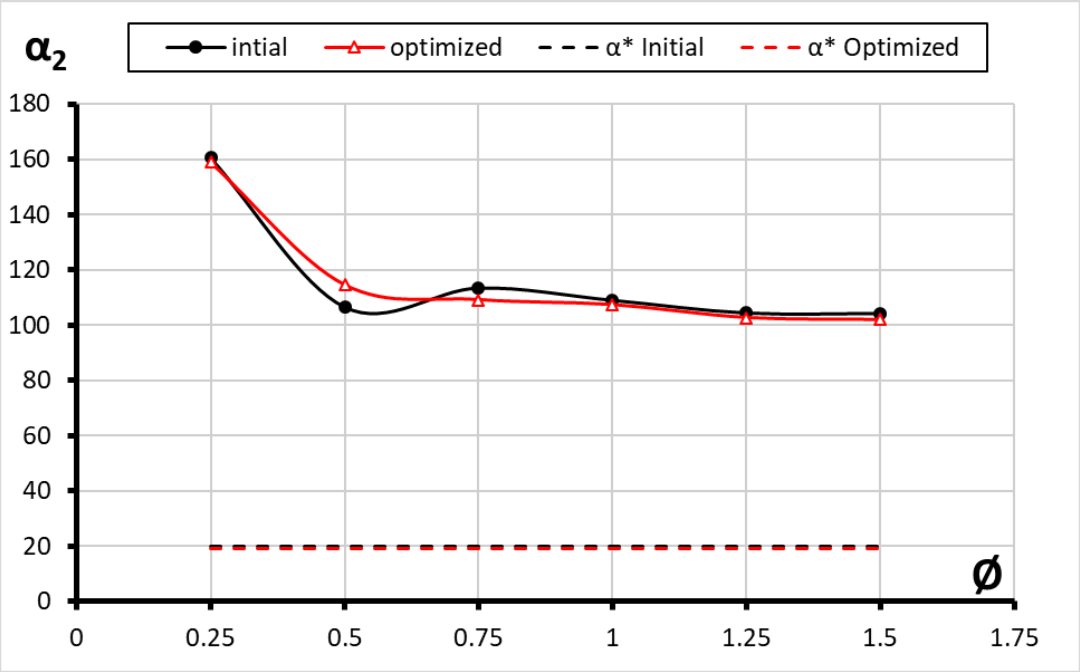

Fig. 4.21: Absolute flow angle at the tail edge of the rotor in reverse flow

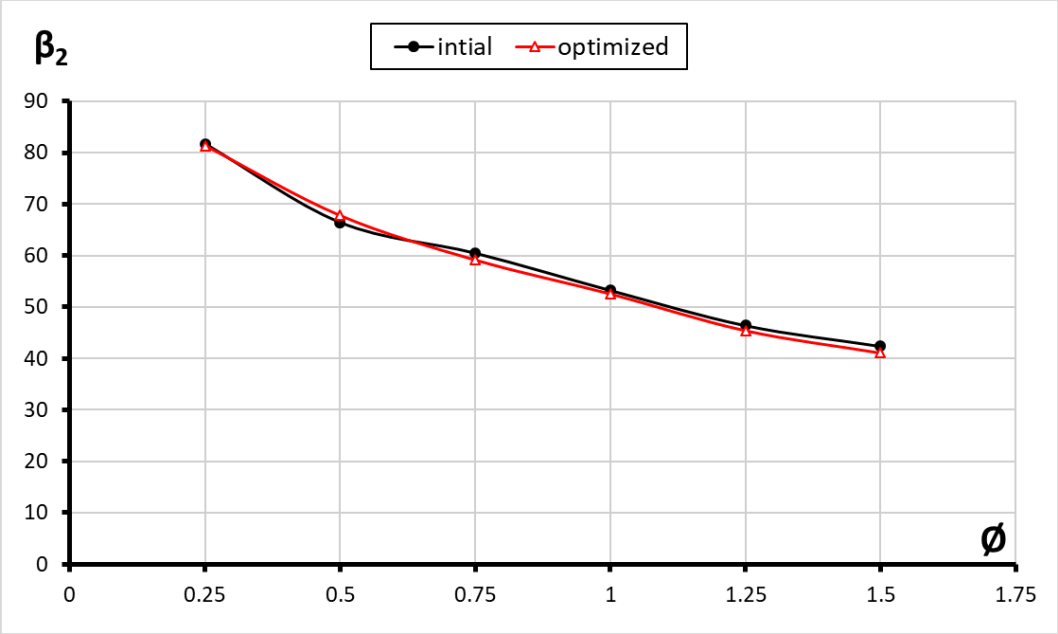

Fig. 4.22: Relative flow angle at the tail edge of the rotor in reverse flow

4.7 Analysis of Unsteady performance

The final comparison of the performance of the initial and optimized geometry is based on unsteady flow conditions, In Fig. 4.22, two efficiencies are shown. Firstly, the non-steady efficiency of a system composed of two turbines working together. And, secondly, and very important as well, how the performance of the system in terms of flow leakage through the turbine in reverse mode, blocking efficiency.

Looking at the non-steady efficiency seen that the optimized geometry. exceeds the initial geometry by 12% at the efficiency peak. This is a great success of this work. Besides, note that the location of the maximum efficiency has migrated towards lower values of the flow coefficient.

On the other hand, for amplitudes above one, the performance of both turbines is clearly similar. This is reasonable taking into account that, according to Fig. 4.6, the performance of both geometries is almost equal for the largest flow coefficient.

Upon analyzing the results of the blocking efficiency it is clear that the optimized geometry presents a better behavior. Thus, part of the success in terms of non-steady efficiency is due to

this slight improvement in the blocking efficiency, which is approximately 2% for the whole range of flow coefficients amplitudes.

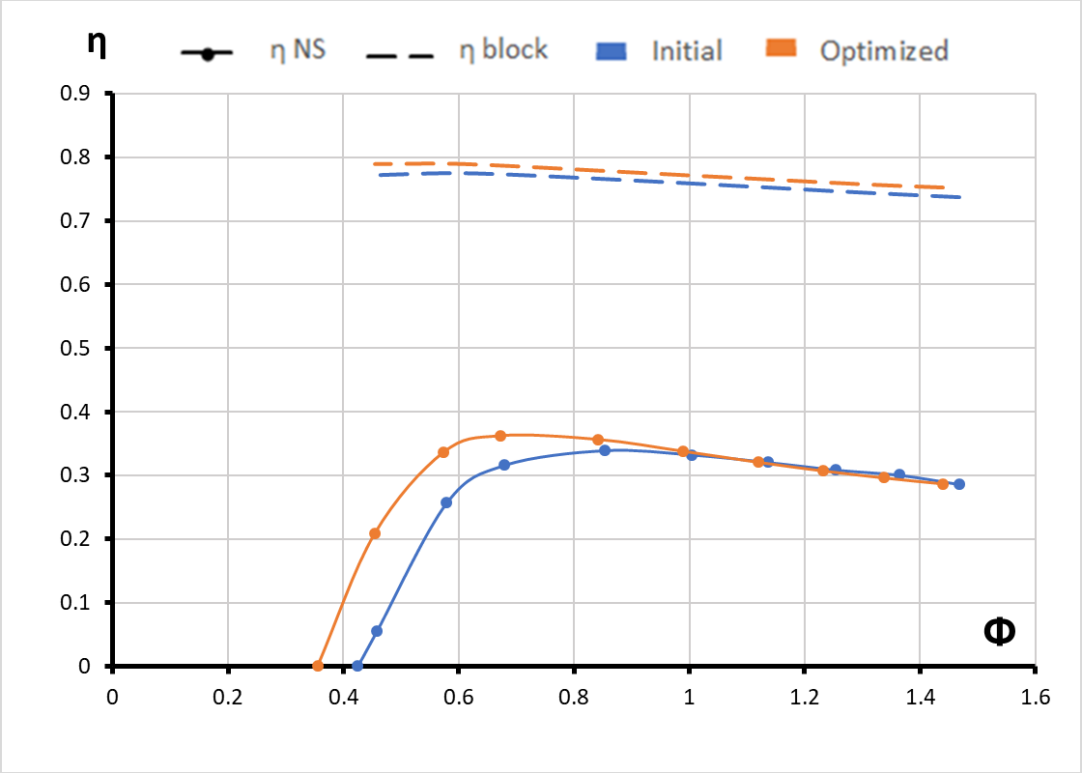

Fig. 4.23:Comparison of the Unsteady performance between the initial and optimized

Chapter 5

Conclusions

Computational fluid dynamics (CFD) has transformed turbine design by providing engineers with a deeper understanding of performance and flow characteristics, enabling them to improve efficiency and reduce energy losses. By employing CFD simulations, engineers can identify and address issues such as vortex, pressure drop, and flow separation, resulting in more reliable and efficient turbine designs. The combination of CFD techniques with different turbine types has led to advancements in reliability and efficiency, with CFD expected to continue playing a vital role in future turbine designs, driving further enhancements in performance and energy output.

In this thesis, the focus was on analyzing the airflow characteristics throughout the various sections of an axial turbine using numerical simulations, the specific objective was to customize the turbine design to optimize its performance for the typical operation of an oscillating water column. To facilitate the study, a 3D-CFD model of a unidirectional axial turbine was created and validated against data from the bibliography. Throughout the research, the main emphasis was on evaluating the turbine's efficiency as the key parameter for enhancement at each step of the study.

Automated design optimization techniques were employed to enhance the efficiency of the axial turbine. Parametric geometries of rotor blades and guide vanes were created by allowing variations of a list of geometrical parameters in each section. To analyze the impact of these parameters on the performance, a Design Exploration process was conducted. The Central

Composite Design (CCD) method was employed to populate the design space with design points. Furthermore, response surface optimization algorithms were utilized to assess the influence of these parameters on turbine performance. Notably, the Genetic Aggregation algorithm was employed to generate the response surfaces.

The efficiency of a single axial flow impulse turbine was significantly improved through the modification of key parameters, including the guide vane radius (R_g), rotor tip radius (R_t), pressure side radius on the rotor (R_r), trailing edge relative angle of the rotor (β_2), and guide vane angle (α_1), which is the parameter of the highest sensitivity regarding efficiency. By applying an automated analysis was conducted to optimize the turbine design within a wide design space encompassing 51 simulated models. This thorough exploration led to the identification of the optimal turbine geometry.

The optimum design made remarkably enhanced by showcasing a 28% increase in efficiency for low flow coefficients when compared to the original design. Moreover, the findings strongly indicate that the optimized geometry, especially at lower flow coefficients, led to a notable decrease in energy losses within the rotor domain. To be specific, at flow coefficients of Ø=0.25 and Ø=0.50, the optimized geometry exhibited energy loss reductions of approximately 66.2% and 22.3% respectively. The evaluation of unsteady performance further optimized the turbine, resulting in a peak non-steady efficiency that was 12% higher than that of the initial turbine. The blocking efficiency experienced a modest improvement of approximately 2% across the entire range of flow coefficient amplitudes.

The alteration in shape has yielded a notable advancement in the airflow patterns surrounding the rotor blade structure. This modification has successfully minimized the separation in the velocity streamline and reduce the vortex created at the blade leading edge, leading to a significant reduction in losses within the rotor zone. The optimized blade design features increased thickness, which results in amplified flow velocities within the rotor channels. Consequently, this causes higher velocities at the outlet, ultimately contributing to the slight rise in generated torque. Consequently, this has resulted in an increase in overall efficiency. It is important to highlight that these improvements were achieved while preserving the desired airflow dynamics in the entry and exit regions, as well as maintaining the turbine's efficiency at high flow coefficients.

The optimized geometry exhibits a significant enhancement in the (CA) during the reverse mode, highlighting the potential for improved performance in a Twin Turbine System. This enhancement specifically contributes to the improvement in blocking efficiency, further enhancing the system's overall performance.

By employing an automated optimization approach, the optimization time was significantly reduced as it eliminated the need for manual geometry design, mesh generation, and solving. Furthermore, this approach can be expanded to optimize various other blade parameters, employing a multi-objective approach to further enhance performance.

References

Anderson, J. D., & Wendt, J. (1995). *Computational fluid dynamics* (Vol. 206).

Ansarifard, N. (2019). *CFD analysis and optimisation of unidirectional radial turbine geometry for application with oscillating water column wave energy converters, PhD thesis, University of Tasmania.* https://doi.org/https://doi.org/10.25959/100.00032532

Ansarifard, N., Fleming, A., Henderson, A., Kianejad, S. S., & Chai, S. (2019). Design optimisation of a unidirectional centrifugal radial-air-turbine for application in OWC wave energy converters. *Energies*, *12*(14). https://doi.org/10.3390/en12142791

Ansarifard, N., Kianejad, S. S., Fleming, A., Henderson, A., & Chai, S. (2020). Design optimization of a purely radial turbine for operation in the inhalation mode of an oscillating water column. *Renewable Energy*, *152*, 540–556. https://doi.org/10.1016/j.renene.2020.01.084

ANSYS, Inc. (2014). *Design-exploration-users-guide*.

Arena, F. (2014). *Un impianto REWEC3 per la produzione di energia elettrica da moto ondoso: dall'invenzione del prof. Paolo Boccotti alla costruzione del primo prototipo Workshop: ENERGIA DAL MARE Le Nuove Tecnologie Per i Mari Italiani*. http://www.enea.it/it/enea_informa/ events/energia-dal-mare/Arena1.pdf

Ashraful Alam, M. M., Sato, H., Takao, M., Okuhara, S., & Setoguchi, T. (2016). A twin impulse turbine for wave energy conversion - The performance under unsteady airflow. *International Journal of Fluid Machinery and Systems*, *9*(4), 300–306. https://doi.org/10.5293/IJFMS.2016.9.4.300

Badhurshah, R., & Samad, A. (2015). Multiple surrogate based optimization of a bidirectional impulse turbine for wave energy conversion. *Renewable Energy*, *74*, 749–760. https://doi.org/10.1016/j.renene.2014.09.001

Box, G. E. P., & Wilson, K. B. (1951). On the Experimental Attainment of Optimum Conditions. *Journal of the Royal Statistical Society: Series B (Methodological)*, *13*(1), 1–38. https://doi.org/10.1111/j.2517-6161.1951.tb00067.x

Casagranda, G. (2015). *Wave-to-Wire Model of a Wave Energy Converter equipped with an All-Electric Power Take-Off* [Master Thesis]. Norwegian University of Science and Technology.

CETO Technology. (2019, July 20). https://www.carnegiece.com/ceto-technology/

CFD Direct. (2016). https://cfd.direct/cloud/cost/

CFD training. (n.d.). Retrieved June 1, 2023, from http://cfdtraining.epizy.com/?i=1

Clarke, G. (2015). *Insightreplay*. http://insightreplay.com/tech-sports-computational-fluid-dynamics/

Crahmaliuc, R. (2017). *Simscale*. https://www.simscale.com/blog/5-cfd-simulations-aircraft-design/

Curto, D., Franzitta, V., & Guercio, A. (2021). Sea wave energy. A review of the current technologies and perspectives. In *Energies* (Vol. 14, Issue 20). MDPI. https://doi.org/10.3390/en14206604

Delmonte, N., Barater, D., Giuliani, F., Cova, P., & Buticchi, G. (2014). Oscillating water column power conversion: A technology review. *2014 IEEE Energy Conversion Congress and Exposition, ECCE 2014*, 1852–1859. https://doi.org/10.1109/ECCE.2014.6953644

Denton, J. D. (1993). *THE AMERICAN SOCIETY OF MECHANICAL ENGINEERS I LOSS MECHANISMS IN TURBOMACHINES*. http://asmedigitalcollection.asme.org/GT/proceedings-pdf/GT1993/78897/V002T14A001/4457435/v002t14a001-93-gt-435.pdf

Doyle, S., & Aggidis, G. A. (2019). Development of multi-oscillating water columns as wave energy converters. In *Renewable and Sustainable Energy Reviews* (Vol. 107, pp. 75–86). Elsevier Ltd. https://doi.org/10.1016/j.rser.2019.02.021

Drew, B., Plummer, A. R., & Sahinkaya, M. N. (2009). A review of wave energy converter technology. In *Proceedings of the Institution of Mechanical Engineers, Part A: Journal of Power and Energy* (Vol. 223, Issue 8, pp. 887–902). https://doi.org/10.1243/09576509JPE782

Eco Wave Power. (2019). How It Works. https://www.ecowavepower.com/our-technology/how-it-works/

Energy Agency, I. (2021). *Statistics report Key World Energy Statistics 2021*.

Engineersedge. (2012a). https://www.engineersedge.com/pumps/axial_flow.htm

Engineersedge. (2012b). https://www.engineersedge.com/pumps/mixed_flow.htm

Ezhilsabareesh, K., Rhee, S. H., & Samad, A. (2018). Shape optimization of a bidirectional impulse turbine via surrogate models. *Engineering Applications of Computational Fluid Mechanics*, *12*(1), 1–12. https://doi.org/10.1080/19942060.2017.1330709

Falcão, A. F. O., & Henriques, J. C. C. (2016). Oscillating-water-column wave energy converters and air turbines: A review. In *Renewable Energy* (Vol. 85, pp. 1391–1424). Elsevier Ltd. https://doi.org/10.1016/j.renene.2015.07.086

Gomes, R. P. F., Henriques, J. C. C., Gato, L. M. C., & Falcão, A. F. O. (2012). Multi-point aerodynamic optimization of the rotor blade sections of an axial-flow impulse air turbine for wave energy conversion. *Energy*, *45*(1), 570–580. https://doi.org/10.1016/j.energy.2012.07.042

Gordon, P. (2019, May 10). *AW-Energy WaveRoller generates ocean energy near Portugal*. Https://Www.Smart-Energy.Com/Renewable-Energy/Aw-Energy-Waveroller-Generates-Ocean-Energy-near-Portugal/. https://www.smart-energy.com/renewable-energy/aw-energy-waveroller-generates-ocean-energy-near-portugal/

Guedes Soares, C., Bhattacharjee, J., Tello, M., & Pietra, L. (2012). Review and classification of wave energy converters. *Maritime Engineering and Technology - Proceedings of 1st International Conference on Maritime Technology and Engineering, MARTECH 2011*, 585–594. https://doi.org/10.1201/b12726-82

Guney, M. S. (2015). Wave energy conversion system. *Journal of Naval Science and Engineering*, *11*(2), 25–51.

Gunzburger, M. D., & Nicolaides, R. A. (Eds.). (2003). *Incompressible Computational Fluid Dynamics* (illustrated, reprint). Cambridge University Press.

Halder, P., Rhee, S. H., & Samad, A. (2017). Numerical optimization of wells turbine for wave energy extraction. *International Journal of Naval Architecture and Ocean Engineering*, *9*(1), 11–24. https://doi.org/10.1016/j.ijnaoe.2016.06.008

Iglesias, G., & Garcia Novo, P. (2013). *Renewable energy sources charged with energy from the sun and originating from the earth - Moon interaction - Wave energy inverters - Wave energy inverters*.

Ingram, G. (2009). *Basic Concepts in Turbomachinery*.

IRENA. (2023). *Renewable capacity highlights*. www.irena.org/publications.

Jayashankar, V., Anand, S., Geetha, T., Santhakumar, S., Jagadeesh Kumar, V., Ravindran, M., Setoguchi, T., Takao, M., Toyota, K., & Nagata, S. (2009). A twin unidirectional

impulse turbine topology for OWC based wave energy plants. *Renewable Energy*, *34*(3), 692–698. https://doi.org/10.1016/j.renene.2008.05.028

Johnson, F. T., Tinoco, E. N., & Yu, N. J. (2005). Thirty years of development and application of CFD at Boeing Commercial Airplanes, Seattle. In *Computers and Fluids* (Vol. 34, Issue 10, pp. 1115–1151). https://doi.org/10.1016/j.compfluid.2004.06.005

Jones, B., & Montgomery, D. (2019). *Design of Experiments: A Modern Approach* (1st ed.). Wiley.

Kanellos, M. (2009, September 29). *Pelamis Wave Power Jettisons Its CEO, Rough Waters Ahead?* https://web.archive.org/web/20091003125522/http://www.greentechmedia.com/green-light/post/pelamis-wave-power-jettisons-its-ceo-rough-waters-ahead

Lakshminarayana, B. (1996). *Fluid Dynamics and Heat Transfer of Turbomachinery*.

Lehmann, M., Karimpour, F., Goudey, C. A., Jacobson, P. T., & Alam, M. R. (2017). Ocean wave energy in the United States: Current status and future perspectives. In *Renewable and Sustainable Energy Reviews* (Vol. 74, pp. 1300–1313). Elsevier Ltd. https://doi.org/10.1016/j.rser.2016.11.101

Liu, Z., Cui, Y., Kim, K. W., & Shi, H. D. (2016). Numerical study on a modified impulse turbine for OWC wave energy conversion. *Ocean Engineering*, *111*, 533–542. https://doi.org/10.1016/j.oceaneng.2015.11.005

López, I., Andreu, J., Ceballos, S., Martínez De Alegría, I., & Kortabarria, I. (2013). Review of wave energy technologies and the necessary power-equipment. In *Renewable and Sustainable Energy Reviews* (Vol. 27, pp. 413–434). https://doi.org/10.1016/j.rser.2013.07.009

Lorenzen, T. (1993). *Design of Experiments*. CRC Press. https://doi.org/10.1201/9781482277524

Lo, S. (2014). *Imperial*. https://www.imperial.ac.uk/media/imperial-college/research-centres-and-groups/nuclear-engineering/14-CFD-1.pdf

Maehlum, M. A. (2013). *Wave Energy Pros and Cons*. https://www.solarreviews.com/blog/wave-energy-pros-and-cons

Marquis, L., Kramer, M., & Frigaard, P. (2010). First Power Production figures from the Wave Star Roshage Wave Energy Converter. *3rd International Conference on Ocean Energy, Bilbao*.

Masuda, Y., & McCormick, M. E. (1986). Experiences in pneumatic wave energy conversion in Japan. In *Coastal Engineering* (pp. 1–33). ASCE.

Metal-AM. (2021). https://www.metal-am.com/articles/cfd-simulation-for-metal-additive-manufacturing-applications-in-laser-and-sinter-based-processes/

Mohamed, M. H., Janiga, G., Pap, E., & Thévenin, D. (2011). Multi-objective optimization of the airfoil shape of Wells turbine used for wave energy conversion. *Energy*, *36*(1), 438–446. https://doi.org/10.1016/j.energy.2010.10.021

Mohamed, M. H., & Shaaban, S. (2013). Optimization of blade pitch angle of an axial turbine used for wave energy conversion. *Energy*, *56*, 229–239. https://doi.org/10.1016/j.energy.2013.04.035

MR-CFD. (2023). https://www.mr-cfd.com/industries/chemical-engineering/

Nachev, A. (2017). *Comparative analysis of winch-based wave energy converters* [Bachelor Thesis]. KTH Industrial engineering and management.

Oceanlinx. (2011). *Wave energy at its best*. https://www.slideshare.net/CleantechRepublic/ocean-linx

Okuhara, S., Takao, M., Takami, A., & Setoguchi, T. (2012). A Twin Unidirectional Impulse Turbine for Wave Energy Conversion. *Open Journal of Fluid Dynamics*, *02*(04), 343–347. https://doi.org/10.4236/ojfd.2012.24a043

Peng, W. W. (2008). *Fundamentals of Turbomachinery*. John Wiley & Sons, Inc., Hoboken.

Pereiras, B., Valdez, P., & Castro, F. (2014). Numerical analysis of a unidirectional axial turbine for twin turbine configuration. *Applied Ocean Research*, *47*, 1–8. https://doi.org/10.1016/j.apor.2014.03.003

Qiao, D., Haider, R., Yan, J., Ning, D., & Li, B. (2020). Review of wave energy converter and design of mooring system. In *Sustainability (Switzerland)* (Vol. 12, Issue 19). MDPI. https://doi.org/10.3390/su12198251

Raghunathan, S. (1995). THE WELLS AIR TURBINE FOR WAVE ENERGY CONVERSION. In *Aerospace Sci* (Vol. 31).

Rodrigues, L. (2008). Wave power conversion systems for electrical energy production. *Renewable Energy and Power Quality Journal*, *1*(6), 601–607. https://doi.org/10.24084/repqj06.380

Savree. (2019). https://savree.com/en/encyclopedia/steam-turbine

Suzuki, M., Arakawa, C., & Takahashi, S. (2004). Performance of Wave Power Generating System Installed In Breakwater At Sakata Port In Japan. *Fourteenth International Offshore and Polar Engineering Conference*.

Takao, M., & Setoguchi, T. (2012). Air turbines for wave energy conversion. In *International Journal of Rotating Machinery* (Vol. 2012). https://doi.org/10.1155/2012/717398

Takao, M., Setoguchi, T., Kaneko, K., Kim, T. H., & Maeda, H. (2002). Impulse Turbine for Wave Power Conversion with Air Flow Rectification System. In *International Journal of Offshore and Polar Engineering* (Vol. 12, Issue 2).

Takao, M., Takami, A., Okuhara, S., & Setoguchi, T. (2011). A twin unidirectional impulse turbine for wave energy conversion. *Journal of Thermal Science*, *20*(5), 394–397. https://doi.org/10.1007/s11630-011-0486-1

Tedd, J., & Peter Kofoed, J. (2009). Measurements of overtopping flow time series on the Wave Dragon, wave energy converter. *Renewable Energy*, *34*(3), 711–717. https://doi.org/https://doi.org/10.1016/j.renene.2008.04.036

Titah-Benbouzid, H., & Benbouzid, M. (2015). An Up-to-Date Technologies Review and Evaluation of Wave Energy Converters. *INTERNATIONAL REVIEW OF ELECTRICAL ENGINEERING-IREE*, *10*(1), 52–61. https://doi.org/10.15866/iree.v10i1.5159ï

Torre-Enciso, Y., Ortubia, I., López De Aguileta, L. I., & Marqués, J. (2009). Mutriku Wave Power Plant: from the thinking out to the reality. *8th European Wave and Tidal Energy Conference*, 319–329.

Venkanna, B. K. (2009). *Fundamentals of Turbomachinery*. Asoke K. Ghosh, PHI Learning Private Limited.

Versteeg, H. K., & Malalasekera, W. (2007). *An Introduction to Computational Fluid Dynamics Second Edition*. Pearson Education Limited. www.pearsoned.co.uk/versteeg

Weber, J., Mouwen, F., Parish, A., & Robertson, D. (2009). Wavebob-Research & Development Network and Tools in the Context of Systems Engineering. *Proceedings of the Eighth European Wave and Tidal Energy Conference, Uppsala, Sweden*, 416–420.

White, F. M. (2009). *Fluid Mechanics* (Seventh Edition). McGraw-Hill.

Xie, J., & Zuo, L. (2013). Dynamics and control of ocean wave energy converters. *International Journal of Dynamics and Control*, *1*(3), 262–276. https://doi.org/10.1007/s40435-013-0025-x

Zuini, P., & Cepellos, M. (2015, July 28). *Startup uses ocean waves to generate energy*. https://revistapegn.globo.com/Banco-de-ideias/noticia/2015/07/startup-usa-ondas-do-mar-para-gerar-energia.html